MEIZI WANG

Morphological and biomechanical effects of high heel shoes on the lower limbs during gait

Supervisor: Dr. habil. Fekete Gusztáv

Complex Exam Committee:

President:

Prof. Dr. Zoltán RAJNAI

Members:

Dr. Endre JÁNOSI

Dr. Anikó KELEMEN-ERDŐS

Public Defence Committee:

President:

Prof. Dr. László POKORÁDY

Secretary:

Dr. István BARÁNYI

Internal member(s):

Dr. István NAGY

External member(s):

Dr. Endre JÁNOSI

Dr. Tej SINGH

Reviewers:

Prof. Dr. István BÍRÓ

Dr. Ildikó MOLNÁR

DECLARATION AGAINST PLAGIARISM AND CORRECT REFERENCING

I, Meizi WANG, declare that the dissertation entitled: Morphological and biomechanical effects of high heel shoes on the lower limbs during gait is my original work where the references given in the Reference list are used. All sections, which are transcribed or rewritten from some publications, they are correctly referenced.

Date: 2022.10.05

Meizi Wang

(Signature)

Content

The motivation for the work

The potential impact of high heel shoes (HHS) on women's health has been concerned over 50 years in medical circles. Despite widespread warnings from public health institutions and international medical societies [1], there is still a large proportion of the population wearing HHS in their daily life. Regarding why women choose to wear HHS, Broega et al. surveyed 574 females, between the age of 24 to 45, who indicated that beauty and femininity were the key drivers of women's behavior [2]. However, the pursuit of beauty also comes with the risk of injury. According to the latest reported data on injury related to HHS wearing among the women in America from 2016-to 2020, it was recorded 6,290 HHS related emergency cases in 2020 involving ages from 15 to 69 years old [3]. More interestingly, the number of cases in 2020 was significantly lower than the 16,000 cases per year in 2016-2019. This decline in HHS-related injury cases began after the implementation of Coronavirus disease 2019 (COVID-19) shutdowns and quarantine regulations, which caused a restriction on mobility and socializing and more work from home, leading to women wearing HHS less, and eventually decreasing the HHS-related injury rate.

From the biomechanics perspective, it has been demonstrated that HHS resulted in a lower self-selected walking speed, shorter step length, and smaller stance phase duration, while it increased ankle plantar flexion, knee plantar flexion, anterior pelvic tilt, and trunk extension [4-10]. Redistributing the plantar pressure, higher ground reaction forces (GRF), larger loading rate, higher peak knee external adduction moments, and higher peak patellofemoral joint stress have been detected during walking in HHS [5, 9-11]. It is worthy to note that substantial bodily adjustments have been observed in HHS gait, such as altered neuromuscular activation pattern, shortening of the gastrocnemius fascicle, increased Achilles tendon stiffness, and increased muscle activity of the soleus, tibialis anterior, medial gastrocnemius [12-14]. These alterations have been identified as negatively affecting the musculoskeletal system, leading to a variety of pathologies including metatarsalgia, hallux valgus, Achilles' tendon tightness, knee osteoarthritis (OA), plantar fasciitis, and lower back pain, as well as instability and imbalance of body posture in HHS gait, which may lead to a greater risk of falling and slipping [3, 15-18].

As mentioned above, the biomechanical characteristic of the lower extremities in HHS gait have been extensively studied, mainly focusing on kinematic and dynamic changes in the lower extremities (ankle, knee, and hip joint) and muscle activation patterns. However, several limitations still exist in the previous literatures. Firstly, the foot as a multi-segmental structure plays a crucial role in human locomotion, but information on multi-segmental movement of the foot in HHS gait is limited. In particular, the study of biomechanical variation in the hallux segment could provide valuable details for understanding the potential mechanism of hallux valgus development related to HHS wearing. Secondly, the research on the morphological characteristics of foot structure under HHS condition is still blank, which could provide an important clue for exploring functional adaptation and pathology of the HHS-related foot injuries. Thirdly, the biomechanical response of plantar fascia in HHS gait is still unclear, and traditional methods have limitations in studying the in vivo structure of the foot under HHS conditions. In this case, the finite element model (FEM) and musculoskeletal modeling (MSM) analysis could provide an efficient and fidelity way to simulate the internal variation of the foot in HHS.

Research Objectives

The first objective: To reveal the mechanism of hallux valgus development related to HHS wearing during gait. This aim is to be accomplished by investigating the biomechanical characteristics of the hallux, forefoot, and hindfoot segments under HHS conditions by using a multi-segment model (Oxford foot model).

The second objective: To determine how the foot morphology is modified by HHS wearing as a function of different heel heights. This aim is to be accomplished by investigating the angular variation of the multi-bone structure of the foot, where a three-dimensional model reconstruction method will be adapted to create the high-fidelity 3D foot model in four different heel heights (0cm, 3cm, 5cm, 7cm) respectively.

The third objective: To reveal the plantar fascia biomechanical response in HHS gait. This aim is to be accomplished by investigating the strain distribution on the plantar fascia in HHS gait, where a methodology workflow of FEM combined with MSM derived force will

be used to predict the internal strain distribution of the plantar fascia strain variation in three different heel height (3cm, 5cm, 7cm) respectively.

Methodology of the dissertation

In this doctoral work, the complex method is used to address problems involving experimental measurement, 3D model reconstruction, and numerical methods. Firstly, the thesis begins with the experimental measurement to describe the kinematics characteristic of the foot multi-segments in HHS gait. A Vicon motion system with 8 cameras (Oxford Metrics Ltd., Oxford, UK) was used to capture kinematic data, the oxford foot model (OFM) was utilized in this measurement to estimate the hallux, forefoot, and hindfoot movement in HHS gait.

Secondly, reconstruction technique is used to establish a high-fidelity 3D foot model under HHS conditions with different heel heights. The reconstruction of the foot model is based on computed tomography (CT) images, which can scan the foot shape of the subject under the HHS wearing. Therefore, foot models with high reliability and fidelity will be created, and foot morphometry conducts using different angle descriptions at different heel heights (0cm, 3cm, 5cm, 7cm). Also, foot model is provided for finite element analysis.

Thirdly, the MSM analysis is used to estimate the major muscle force in HHS gait with different heel heights, the analysis is carried out in Opensim software to establish a specific model to provide optimal loading conditions for finite element analysis.

Fourthly, the FEM is used to evaluate the biomechanical response of the plantar fascia under HHS condition with different heel heights, and the major muscle forces obtained from MSM analysis as loading condition is combined. In this part, the workflow of FEM and MSM analysis is established.

1 Literature review

1.1 Musculoskeletal system of the human foot

1.1.1 Structure build-up of bone and major joint of the foot

The foot has been considered one of the most dynamic structures in the human body, it acts in coordination with the rest of the body segment during various movements. The vivid interplay of internal forces makes its multiple functions possible, but it is easily neglected and that it is often seen as a static and sculpted graph of the whole structure. From the anatomical and clinical viewpoints, the foot structure is one of the most complex structures. The foot comprises 26 individual bones, made up of 42 muscles, and controlled by numerous ligaments to provide support, balance, and mobility [19]. The whole foot can be transversely divided into three segments which include the hindfoot, midfoot, and forefoot (metatarsus and phalanx) (Fig. 1.1). The ankle joint complex is the most complex structure, which comprises three joints, namely tibiotalar joint, subtalar joint, and transverse-tarsal joint, all those joints assembly shaped the stable kinetic linkage meet a key requirement for daily movement. Despite sustaining high compressive and bone-to-bone pressure occurring on the ankle joint in weight-bearing, the special bony structure, muscles, and ligamentous facilitate it to function with a high degree of flexibility and stability [20, 21].
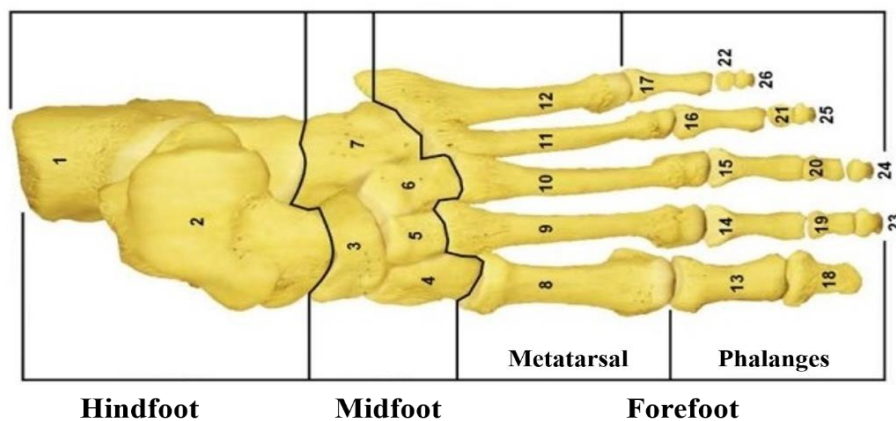

Fig 1.1. Regions of foot

The tibiotalar joint (talocrural joint)

The tibiotalar joint (TJ) is made up of the distal end of the tibial and fibula, and the superior of the talus (Fig 1.2). The tibial-talus interface is a major part of load-bearing, the force is

transferred from the tibial to the trochlea superior until the talus [22]. The trochlea surface of the talus fits well into the mortise of the tibial and fibula, then both malleoli of the tibial and fibula are positioned to constrain the talus, such hinge shape primarily determines the plane in which plantarflexion and dorsiflexion movements occur [23].

There are three major groups of ligaments that provide the stability of TJ, the tibiofibular syndesmosis acts to restrict motion between the tibia and fibula in tri-plantar, the deltoid ligament conjuncts movement of the tibial, talar, navicular, and calcaneus, and the lateral collateral ligaments limit the inversion and rotation of the joint [20, 24, 25].
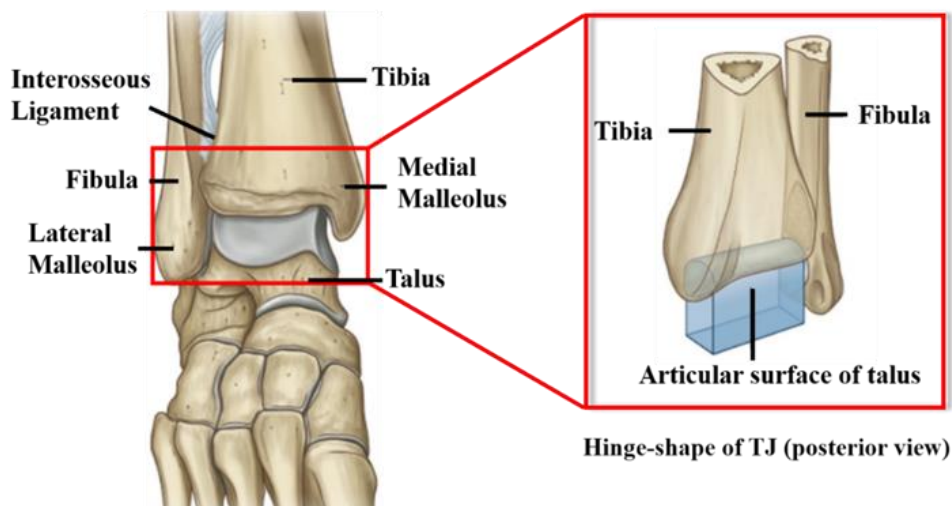

Fig 1.2. The tibiotalar joint.

The subtalar joint

The subtalar joint consists of two independent chambers consisting of talus and calcaneus. The inferior convex facet of the talus matches the superior concave facet of the calcaneus as the anterior talocalcaneal joint (TCJ), and the superior convex aspect of the talus fits with the inferior concave aspect of the calcaneus as the posterior TCJ (Fig. 1.3 (A)). Due to the subtalar joint being enclosed by articular cartilage, it is considered a synovial joint structurally and plane synovial joint functionally [26]. This joint is supported by the talocalcaneal ligament which distributes in the posterior, medial, and lateral respectively [27]. The subtalar joint is located on an oblique axis and is, therefore, the main part of

eversion and inversion movement in the foot, it is likely to be an important contributor to the mechanical change of foot function [28]. The subtalar joint axis view showed in Fig. 1.3 (B/C).
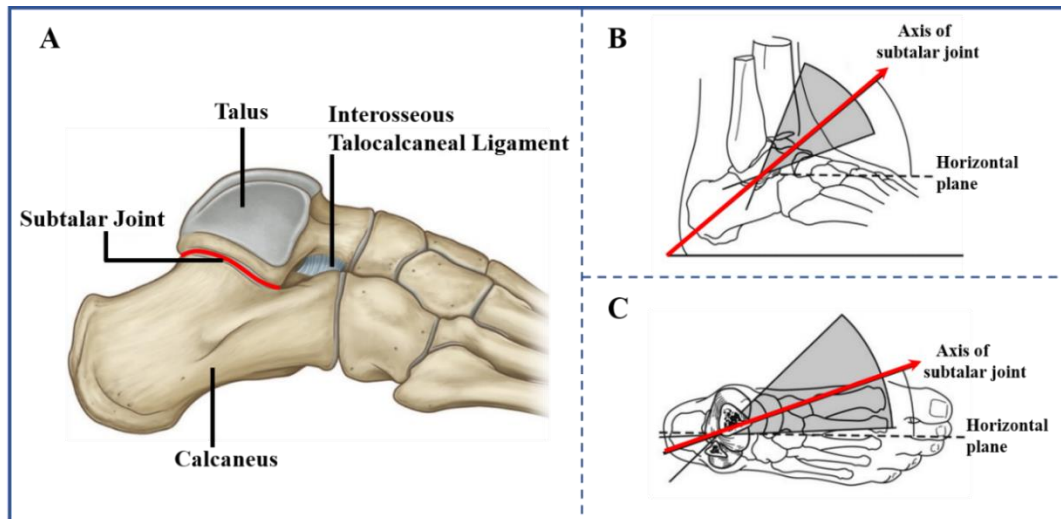

Fig 1.3. A is the subtalar joint; B is the subtalar joint axis in the anterior-posterior view demonstrating deviation; C is the subtalar joint axis in the lateral view demonstrating inclination.

The transverse tarsal joint (TTJ)

The TTJ also known as the midtarsal joint or Chopart's joint, horizontally crosses the foot, combining the two segments of the hindfoot and midfoot [29], as a composite joint consisting of two synovial joints: talonavicular and calcaneocuboid joint. The talonavicular joint, which is more mobile out of the two, is an articulation between the talus and the navicular, the calcaneocuboid joint is formed of cuboid and calcaneus. The surrounding ligamentous reinforcements TTJ exhibited unique motion patterns and multiple functions [30]. The movement of TTJ is biaxial and tri-plantar, TTJ moves around the longitudinal and oblique axis in three planes, which involves supination and pronation movement, the detail of supination and pronation movement see below. Additionally, the TTJ motion is mechanically accompanied by that of the subtalar joint, especially when TTJ performs inversion and eversion movement, which require the synchronous participation of the subtalar joint [31].

1.1.2 Structure build-up of foot arch

There are three arches in the human foot, including the transverse arch, medial longitudinal arch, and lateral longitudinal arch (Fig 1.4). These arches are formed by the metatarsal and tarsal bones, supported by tendons and ligaments of the foot, in which the medial longitudinal arch is the highest. The arch could play as an elastic and adaptive base to sustain the entire body.

The medial longitudinal arch is shaped by the metatarsals (first to third metatarsals), navicular, three cuneiforms, talus, and calcaneus of the foot. It is supported by the calcaneonavicular ligament, deltoid ligament, medial talocalcaneal ligament, talotalocalcaneal interosseous ligament, posterior tibial tendon, and plantar fascia. Particularly, the calcaneonavicular ligament supports the head of the talus, and the plantar fascia plays a supporting function between the two pillars of the medial arch. In addition, the medial longitudinal arch acts as an important function in shock absorption during weight-bearing, and foot propulsion during the gait [32].

The lateral longitudinal arch is formed by the calcaneus, cuboid, fifth and fourth metatarsal. The height of the lateral arch is lower than the medial longitudinal arch and closing contact with the support surface in the weight-bearing foot. It also plays an important role in supporting the body's weight during locomotion [33, 34]. The transverse arch travels from the medial to the lateral side of the tarsometatarsal portion of the foot. It is shaped by three cuneiforms, cuboid proximally, and five metatarsals distally [35]. Clinically, the transverse arch comprises the complex capsuloligamentous structures that maintain stability in the midfoot and forefoot [36].

The height of the medial longitudinal arch is often used to define the foot morphology, such as normal foot, pes planus (flatfoot), and pes cavus (high-ached foot). The medial longitudinal arch is directly associated with flatfoot and high-arched foot. Those abnormal arch structures could display the disturbed biomechanical parameters of lower limbs during the movement, and predispose an individual more vulnerable to injury [37].
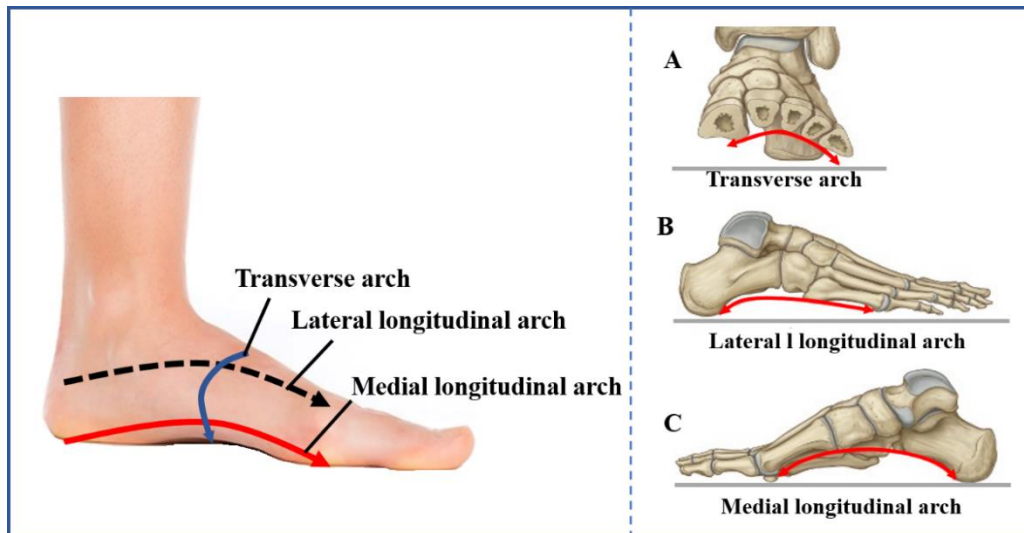
Fig 1.4. Three arches of the foot, represent by the right foot, A is a view of the transverse arch from the distal row of tarsals and metatarsals; B is a lateral view of the lateral longitudinal arch; C is a medial view of the medial longitudinal arch.

1.1.3 Major muscle and plantar fascia structure

Major muscle anatomy

During the movement, the integrated function of joints, ligaments, and muscles facilitates the foot with the capability to support the weight-bearing, absorb the impact, and propel the body move [38]. The majority of foot movement is dominated by the 12 extrinsic muscles, which originate in the leg and extend to the foot, and these muscles are classified into four compartments based on EMG evidence [39]. Firstly, the anterior compartment contains four muscle groups: the anterior tibialis (AT), the extensor digitorum longus (EDL), the extensor hallucis longus (EHL), and the peroneus tertius (PT). The AT and the EHL perform dorsiflexion and inversion motion of the foot, and the AT has been described as the most active and also supports the movement of the forefoot. The PT dominates the dorsiflexion and eversion movement of the foot, the EDL only manages the dorsiflexion of the foot. Secondly, the posterior compartment composes of three muscles known as triceps surae which involve the gastrocnemius, the soleus, and the plantaris, primarily producing the plantar flexing of the foot. Thirdly, the lateral compartment is combined with two muscles: the peroneus longus and brevis, which conducts the foot motion of plantarflexion and eversion. Lastly, the deep posterior compartment includes three muscles: the posterior

8

tibialis, the flexor digitorum longus, and the flexor hallucis longus, which perform the plantarflexion and inversion movement (Fig 1.5).
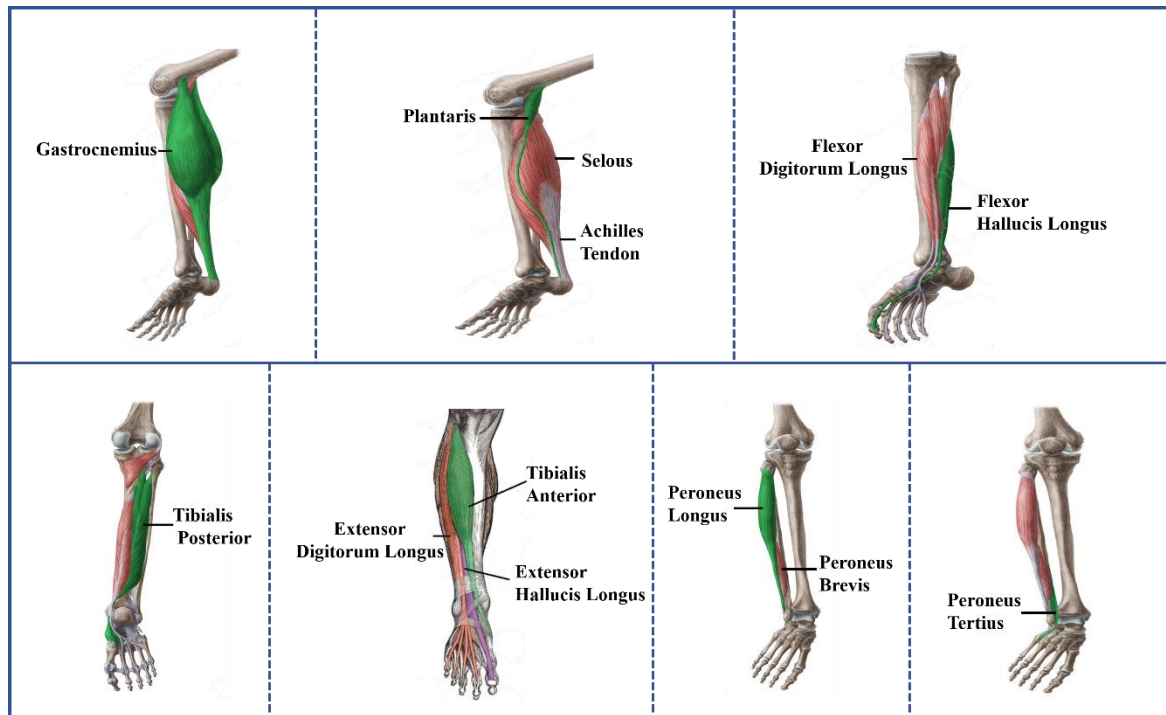

Fig 1.5. The major group of muscles in the lower extremities.

Plantar fascia structure

The plantar fascia (plantar aponeurosis) originates from the medial tubercle of the calcaneus and inserts into the plantar forefoot creating a complex network of connective and adipose tissue. It acts mainly static and occasionally dynamic function, serving the role of stretching or constraining the motion of musculoskeletal segments beyond their anatomical restriction [40-42]. The complete structure of plantar fascia consists of three main areas, such as central, lateral, and medial, in which the central portion is the major component [43, 44].

The central component body is divided into five superficial longitudinal tracts that extend to the five toes, end up inserting into the overlying subcutaneous tissues and skin (Fig 1.6). At the level of the proximal metatarsophalangeal joint (MPJ), the superficial longitudinal tracts are interconnected and oriented transversely forming the superficial transverse tracts. At the distal level of the MPJ joints, the transversely directed fibers generated from the central superficial longitudinal tracts to contribute the natatory ligament [45-47].
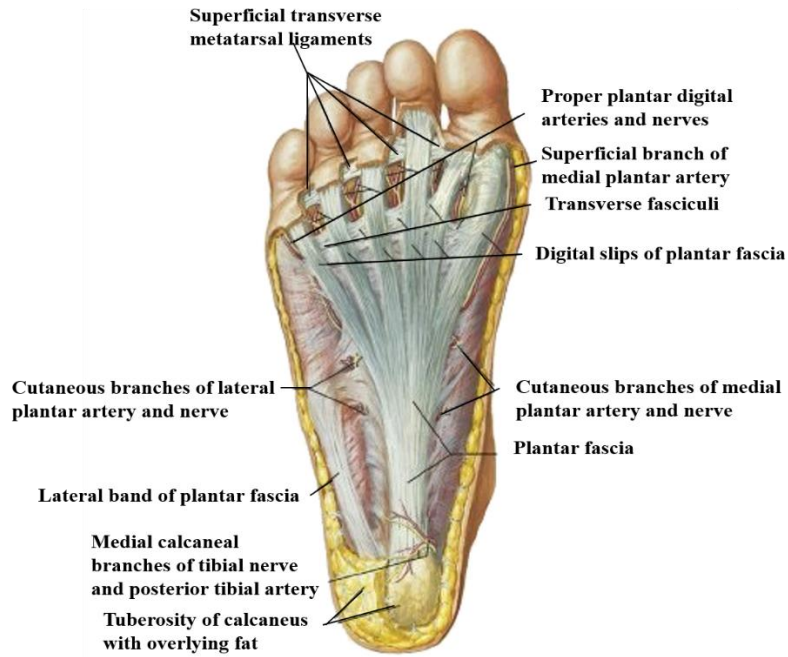
9

Fig 1.6. The figure depicting the anatomy of the plantar fascia is from [48].

The biomechanical function of plantar fascia has been well demonstrated in previous studies. According to Hicks' detailed description that the plantar fascia can be analogous to a "windlass mechanism" [49]. Functionally, the distal end of the plantar fascia is blended with the plantar pads of the metatarso-phalangeal joints, the plantar pads are pulled forward and lie anterior to the metatarsal head while toe extending, and this movement ended up pulling the attachment process of the plantar fascia, causing distance between the metatarsal bone and the calcaneus became shorter, eventually causing the elevation of the arch, this whole process is defined as "windlass mechanism" [49] (Fig 1.7). Additionally, the loading on plantar fascia caused by the windlass acting during the push off phase of gait contributes to stabilizing the longitudinal arches, transforming the foot into the rigid lever for effective propulsion [50-52]. Also, the plantar facia provides an energy storage function in the foot and cushioning against the GRF occurring in gait [53, 54].
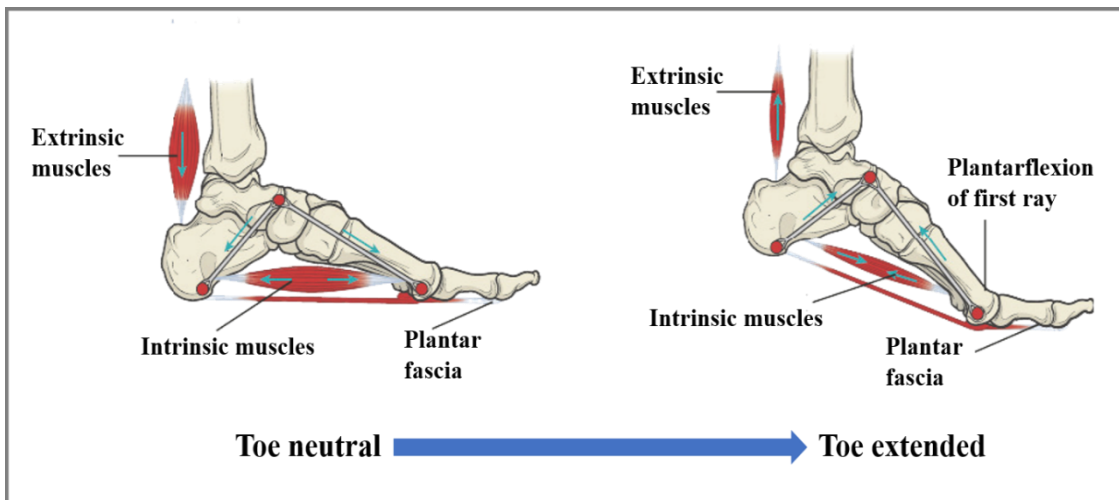
Fig 1.7. The windlass mechanism of the plantar fascia, extracted from [55].

1.1.4 Biomechanical characteristics of lower limbs during gait

Basic characteristic of foot movement

Foot movement is a complex action involving six degrees of freedom in three planes, the sagittal plane presents dorsiflexion and plantarflexion, the frontal plane shows adduction and abduction movement, and the transverse plane exhibits inversion and eversion [56] (Fig 1.8). The combination of these motions produces the interdependence movement throughout the foot known as supination and pronation [20].

Supination is defined as the tri-plantar movement including the plantarflexion, inversion, and adduction. There two mechanisms are thought to cause supination movement of the foot, firstly, it is intrigued by extrinsic muscle during the midstance to toe-off phase. The electromyography (EMG) studies reported that muscle activity increased in gastrocnemius, soleus, posterior tibialis, FDL, and FHL at end of the stance phase of gait, this enables the muscles to function more efficiently and plays a rigid lever to propel the body moving forward [57, 58]. The second contributor to the supination of the foot is the external rotation of the lower limb ankle joint [59].

Pronation is a normal foot movement that happens at the heel strike to toe strike phase while running or walking. It is also composed of three plantar motions: eversion, dorsiflexion, and abduction, which occur simultaneously. Normal pronation of the foot is a very important

postural for attenuating multiple forces during the heel strike to toe strike period since four types of general force occurred during gait, which includes compression, torque moment, anterior-posterior shear, and medial-lateral shear. Unlike the moment when supination occurs, pronation is initiated at the heel strike phase, and dominated by the eccentric supinator. The three muscles that show high activity during the pronation movement are the anterior tibialis, extensor digitorum longus, and extensor hallucis longus.
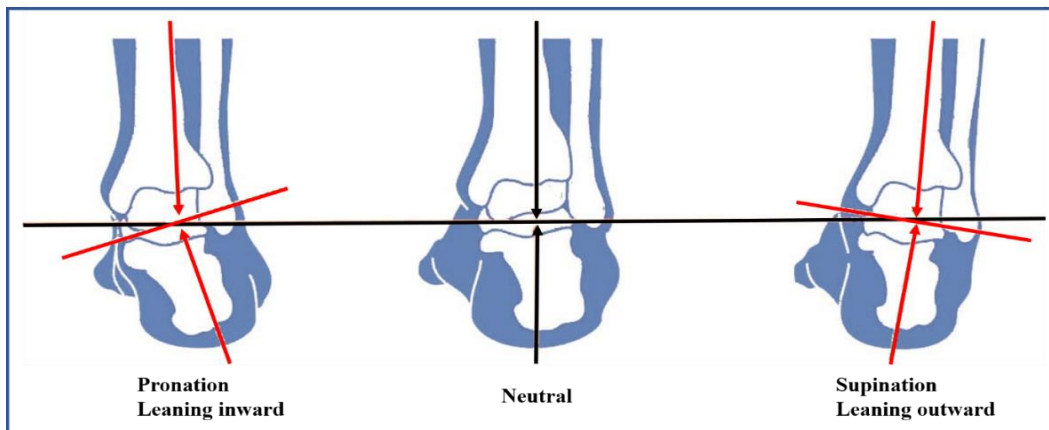

Fig 1.8. The pronation and supination position of the foot.

Foot movement during gait cycle

Gait analysis is an effective objective tool to quantify kinematic and dynamic changes in foot motion. The gait cycle was suggested to be divided into two different phases, which involved stance and swing phase. Specifically, standing phase accounts for 62% of a complete gait cycle and can be subdivided into the three phases: i) the heel contact; ii) the stance phase; iii) the toe-off. The swing phase constitutes 38% of a complete gait cycle, which is classified into three phases: acceleration, toe clearance, and deceleration [20]. During the stance phase, starting with heel contact ground to whole plantar contact ground, the subtalar joint is everted, because of the pivot between heel and ground being shifted laterally from ankle joint central. At the same time, the tibia segment is internally rotated and foot is pronated. Then, during the heel rise to toe off phase, the subtalar joint eversion combined with tibia extension rotation can be observed. This movement provides the foot with enough rigidity which is required to propel the body moving forward [60].

In terms of the range of motion (ROM) of the ankle joint, previous studies have shown that the sagittal ROM of the ankle is 65-75° during the gait, ranging from 10-20° dorsiflexion to 40-55° plantarflexion, and an overall ROM in the frontal plane is approximately 35° [61]. Indeed, the ankle joint position, muscles, and the surrounding ligaments determine the loading distribution on the talus. During the weight-bearing, 77 to 90% loading is transferred from the ankle to the dome of the talus, with the rest carried by the medial and lateral talar facets [62]. When the ankle joint moves from the plantarflexion to dorsiflexion, the talar contact area shifts from the posterior to the anterior and reaches its maximum at the dorsiflexion angle [63]. When the ankle moves inversion to eversion, the loading on the talar facet moves laterally. The kinematic characteristic of the ankle joint during the gait is shown in (Fig 1.9)
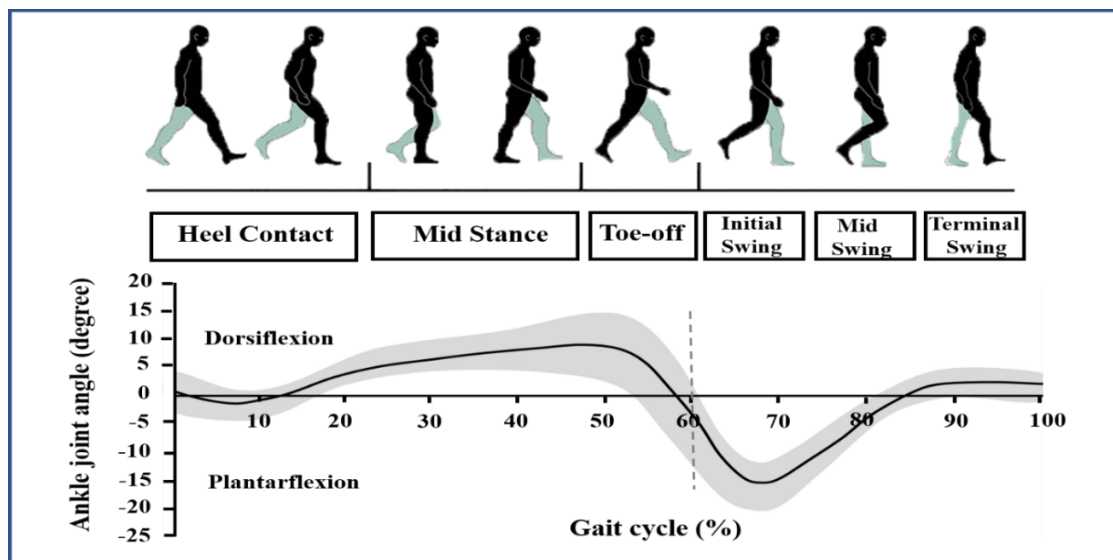

Fig 1.9. The ankle joint angle in the sagittal plane during gait by Deanna and Nielsen [63].

1.2 High heel shoe gait biomechanics

1.2.1 Introduction of high heel shoes

HHS is designed as shoes in which the heel is higher than the forefoot region, shaped by a narrow toe box, a rigid heel cap, and a curved plantar region, all of those characteristics disturb the natural foot function. On the other hand, HHS is considered one of the most important fashion accessories and could achieve a slender and taller body shape in female wearers. Many women wear HHS regularly in their daily life in attempt to increase their

attractiveness. The American Podiatric Medical Association (APMA) has reported that 72% of women wore HHS in America and 39% of them wore HHS daily, representing a larger proportion of the female population [18].

It has been revealed that HHS shoes pose a high prevalence of injury in the female population. A survey conducted on the 3000 HHS wearers, reported that 10% of females had to receive medical treatment or even be hospitalized due to the HHS use and near half of the subjects had the experience of ankle sprain, and the most prevalent injuries were ankle and knee joint twisted, infected blisters, bunions and tendon pains [64]. However, despite the numerous medical cautions against HHS use, it remains popular among females. What's more, previous studies demonstrated that, postural control, plantar pressure, impact force, muscular activities and gait kinematics and kinetics can be changed by HHS [65].

Heel elevation is also related to an increased risk of falling. Studies indicated that wearing HHS led to a backward rotation of the pelvic and a decrease in the distance between the ankle and keen joint, creating an unstable posture that disturbs the human balance system [66]. In addition, recently, relative research demonstrated that the consequence of posture change caused by HHS regarding posture control balance, gait, and general well-being is not only localized on the foot but instead there is a chain reaction traveling up the lower extremities at least as far as the spine [7].

1.2.2 Biomechanical characteristic of lower limbs in HHS gait
Center of pressure (COP) trajectory and plantar pressure distribution
Walking stability and tilting foot movement during HHS gait can be analyzed based on the COP trajectory in the anterior-posterior and medial-lateral direction, which is calculated by summing the product of the pressure which is measured by each sensor with its insole coordinates system. Earlier studies compared the gait and standing balance among the various heel heights of HHS by investigating the COP oscillation, indicating that both gait and standing balance were significantly worse with COP trajectory shifted medially, and anteriorly as heel height increased [67-71] (Fig 1.10). What's more, Wan et al. pointed out the effect of heel height (1cm, 5cm, 8cm, and 10cm) on standing stability, in addition to

finding consistent results, they also indicated that the main effect of heel height on COP oscillation was found in the medial-lateral direction increased by 129.5% at 10cm than 1cm, and only increased by 66.9% in the anterior-lateral direction. Meanwhile, the plantar pressure distribution showed a similar trend with increasing heel height in HHS gait [72].

The distribution characteristics of plantar pressure in gait of HHS can be reflected by the insole measurement system [73-75]. It has been demonstrated that plantar pressure was anteriorly shifted from the hindfoot to the forefoot, and medially shifted from the lateral forefoot to the medial forefoot under HHS condition, the peak pressure increased by 30%-40% in the center of the forefoot (2nd-4th metatarsals), the pressure time-integral increased by 12% on the hindfoot region, 48% on the center forefoot, 47% on the medial forefoot (1st metatarsal), and 20% on the hallux region, respectively. In addition, the magnitude of peak pressure and pressure time-integral in the medial forefoot was linearly correlated with the heel height [75]. The anteriorly and medially shifted plantar pressure under HHS condition has been considered as an adverse factor leading to forefoot deformities such as hallux valgus [76-78].
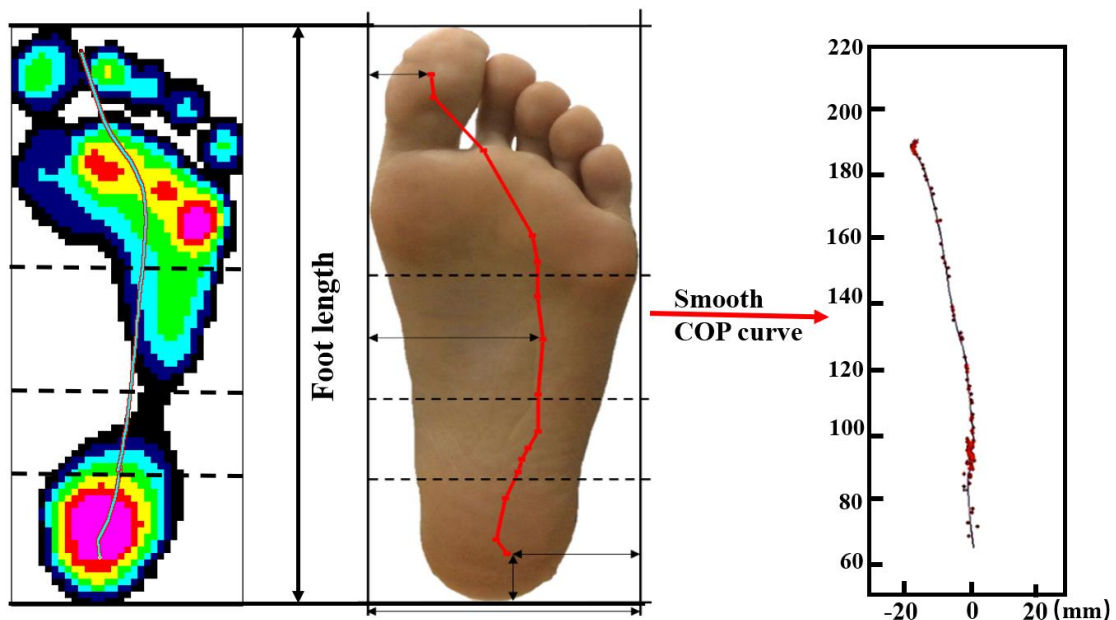

Fig 1.10. COP trajectory on the insole measurement system [79].

The GRF

The time history of GRF reflects information about the magnitude, direction in the three planes, and point of application of the impact force (Fig 1.11). Studies have demonstrated that the time history variation of GRF is dependent upon numerous factors, such as gait speed, subject's body mass, gait style, loading rate, foot contact area, shoe type, etc. During HHS gait, a significant change has been found in GRF with its magnitude increased in the vertical, anteroposterior, and mediolateral direction as heel height elevation [80].
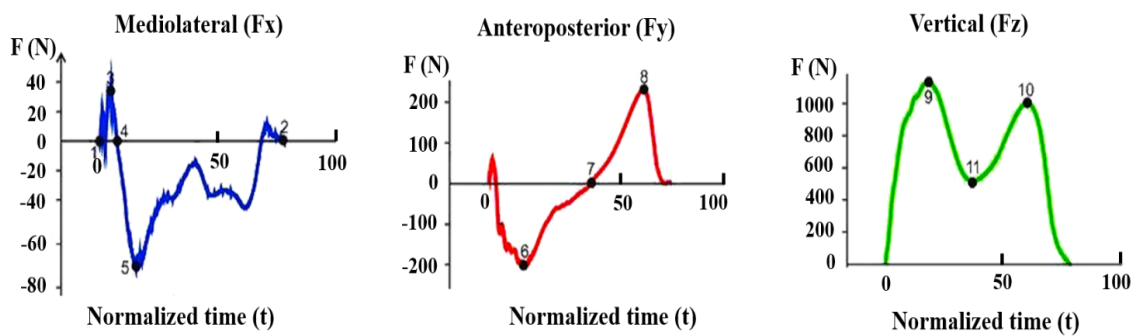

Fig 1.11. The ground reaction force during the stance phase of one step.

In terms of different shoe types and heel heights, Wang et al. investigate the GRF changes during normal gait by comparing three different types of shoes (running shoes, 2.5cm; leather shoes, 1.3cm; HHS, 7.5cm) using the Kistler force platform. The major findings indicated that the greater impact force in the vertical and anterior-posterior direction was found in the toe-off phase compared to the heel contact phase under both HHS and leather shoe conditions. The explanation of smaller vertical GRF in heel strike phase and larger vertical GRF at the toe-off phase can be related to the 1) HHS causes an unstable postural leading to a conservative strategy with a softer heel strike pattern; 2) The larger braking force causes a significant deceleration of center of mass (COM), which need to be counteracted by increasing the peak propulsive force to accelerate the COM at toe-off phase, thus propelling body move forward during gait [76].

Kinematics, kinetic and muscle activity of lower limbs in HHS gait

The ankle joint: The foot can automatically adapt to various shoe surface structures by adjusting the function of muscle, ligament, tendon, and inner foot segments. Especially, during HHS gait, the foot mechanical function has experienced a dramatic change. For instance, the ankle joint axis displaces anteriorly and the line of gravity displaces posteriorly relative to the ankle joint [77]. More significantly, HHS leads to a higher and shorter foot length [78]. This deformation even continuously remains after a day of wearing HHS, that heel heights of no more than 2.1cm resulting in a 0.3cm reduction in arch height; and the heel height range from 6.2cm to 7.1cm contributes to a 0.4cm higher arch height [79].

There is a consistent result that a larger plantarflexion and a smaller peak plantar flexor moment in the ankle joint were found during HHS gait. [6, 8, 14, 81]. Previous evidences suggested that the smaller moment of ankle plantar flexor was an inevitable reaction to the shorter length of triceps surae fascicle and Achilles tendon moment arm caused by HHS with the foot at a more plantar flexed angle [6, 15, 81].

In the frontal plane, ankle eversion moment progressively increased as heel height gradually elevated [4, 81]. This may be due to the medial displacement of the ankle joint center caused by supinated foot posture HHS condition, which leads the ankle to locate in an inversion biased direction, and this needs to be counteracted by an eversion moment to provide a stable gait. In addition, the ROM of subtalar joint and tibial internal rotation movement is restricted at the heel strike phase due to the more plantar flexed foot posture, these kinetic limitations may adversely affect the ability of the foot to absorb impact loads early in heel contact phase [82].

Additionally, the muscle activation pattern of lower extremities can be changed by HHS wearing, previous studies found higher muscle force in the soleus, anterior tibialis, medial gastrocnemius, and peroneus longus during HHS gait [6, 8, 83]. And the increased muscle force around the ankle joint promotes higher joint stiffness and presumably contributes to HHS gait stability [7, 83]. However, considering the adverse aspect that the increased muscle activity leads to higher transport energy costing and fatigue is easily appeared in

17

higher activated muscle than lower activated [84].

Csapo et al. showed that the length of gastrocnemius muscle fascicles was decreased and Achilles tension size and stiffness size were increased after long-term wearing HHS, thoes changes contributed to a reduction in the sagittal ROM of ankle joint, and relatively increased frontal ROM of ankle joint, which was thought to be a major factor for ankle sprain [3]. The consistent results were also found by Cronin et al. the strain value of gastrocnemius muscle fascicles in experienced HHS wearers showed 3 times higher than barefoot condition [6]. Normally, the muscle-tendon unit (MTU) undergoes adaptive changes during movement. When the muscle tendons are passively stretched and upon a higher tension, the MTU is forced away from the tendon tissue and transfer to muscle fascicles. This change may interfere with the neural activation pattern, resulting in reduced MTU efficiency and increased energy expenditure [85, 86].

The knee joint: In the sagittal plane, the plantarflexion angle of knee joint has been significantly increased with heel height elevation in HHS gait [12, 15, 87]. Accordingly, knee extensor moment increased which is thought to be a compensation mechanism of decreased ankle plantarflexion moment to maintain a stable body posture [7, 14, 88]. Although, a few inconsistent results showed that there was no difference in peak keen extensor moment among the varied heel heights [81, 82], which may be caused by different walking speeds and wearing experience. As mentioned above, the spatiotemporal characteristics of HHS gait tend to manifest as a decrease in walking speed and an increase in strike length with increasing heel height to achieve gait balance. The similar gait strategy has also been found in inexperienced HHS wearers of HHS compared to experience wearers [89, 90]. According to previous research, the influence factors of walking speed and wearing experience on HHS gait are easily neglected.

In the frontal plane, the significant effect of heel height on the keen moment has been confirmed. Kerrigan et al. found the peak external knee varus moment was 23-24% larger in 6cm heels than in barefoot walking [81]. Similarly, Esenyel et al. indicated a 25% greater peak external knee varus moment in 6cm wide-heeled shoes compared with a sports shoe

[8]. Also, Barkema et al. reported the frontal plane knee net joint moment increased as heel height elevated (1cm, 5cm, 9cm) [4]. There was no significant difference in the transverse plane motion of knee joint under different heel height.

On the other hand, the increased knee moment in the frontal plane corresponds with higher quadriceps muscle activity [14, 91], leading to an increase in the patella tendon tension, patellofemoral joint pressure, and tibia-femoral compressive force in the medial compartment, which eventually causes knee degenerative and development of knee OA [92, 93]. This has been confirmed by Kerrigan et al. in a 1998's publication, which investigated the potential relationship between OA and HHS wearing, and found that the normal varus torque at the knee was exaggerated by 23% during the stance period at 6cm heel height when compared with the barefoot condition [81]. The increased varus torque imposes greater ligament stretching force and muscle force through the knee joint, leading to degenerative development in the medial compartment, which has been demonstrated in animal experiments [94].

The hip joint: The increased internal hip abduction moment has been found during HHS gait, Stefanyshyn et al. reported a 25% increase in hip varus moment in HHS gait compared to barefoot [16]. Esenyel et al. observed an 11% increase in the hip abductors which was thought as a mechanism to counter higher hip varus moment induced by HHS [8]. As well as the greater gluteus medius activity was observed during the HHS gait, which was thought to be a response to reduced varus torque at the hip or knee [95]. The biomechanical difference in the hip joint under HHS condition receives less attention when compared with knee and ankle joint, it seems the changes in hip joint generally small throughout the previous findings, and most pathologies development caused by HHS wearing occurs in foot, ankle, and knee joint. The comparisons of the angle and moment variation in ankle, knee, and the hip joint between the flat shoes (1cm) and HHS (6cm) are shown in Fig 1.12.
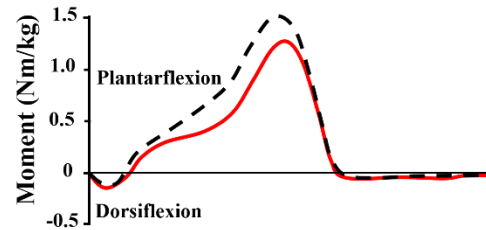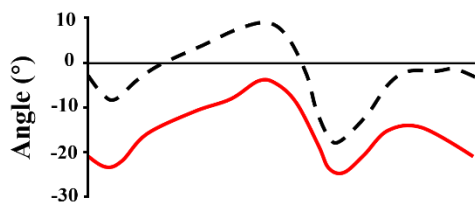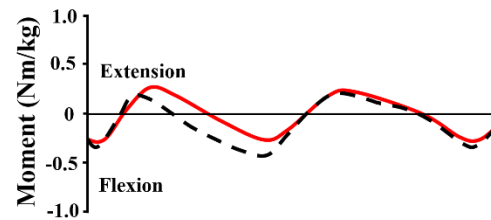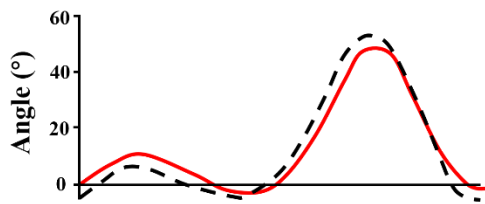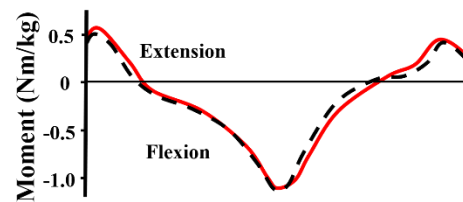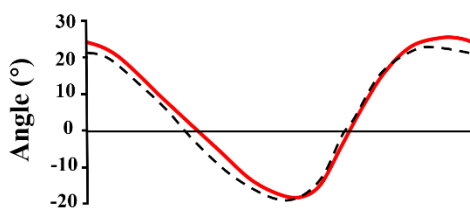
Fig 1.12. The angle and moment variation of lower limbs in the sagittal plane during gait, the red solid line represents HHS with 6cm, and black dash line represents flat shoes with 1cm. The data was extracted from Esenyel et al. [8].

1.2.3 HHS biomechanics in experience and inexperience wearer

According to previous literature, the experience of HHS wearing is another aspect that has attracted the attention of researchers, while most previous studies have ignored its possible importance. Opila-Correia et al. indicated that the biomechanical adaptations varied between the experience wearers (EW) and inexperience wearers (IEW) in HHS gait, which demonstrated a higher knee extension and greater upper trunk rotation in the IEW group than in EW [87]. There more differences were found in the previous research, such as increased abductor and decreased internal rotator moment of the hip joint; decreased knee joint ROM in both sagittal and frontal plane; increased internal rotation and external rotator

moment of ankle joint in EW when compared to IEW during HHS gait with self-selected speed [11, 90]. Furthermore, Gefen et al. reported that EMG activity of gastrocnemius in two heads were unbalanced in EW, the muscles of peroneus longus and gastrocnemius lateralis were more easily prone to fatigue in IEW groups than EW, negatively affecting gait stability [96]. In contrast, Simonsen et al. noted that there was no different in the kinetic features muscle activity between the EW and IEW groups [14]. Similar results have also been previously reported by Ebbeling et al. suggesting that HHS wearing experience did not affect lower limb mechanisms, or even heart rate and oxygen consumption [7].

In terms this controversy, there are several factors needed to be concerned about. The age of participants can be a potential contributor since the various aspect of neuromuscular function and balance control can be directly affected by age. Additionally, the capacity of chronical adaptation for foot structural and soft tissue induced by HHS is also different with age [6, 97]. Furthermore, the height of heels also needs to take into account, the habitual wearer of lower heel height such as 2-3cm may not present a chronic adaptation of neuromuscular function.

1.2.4 Pathologies associated with increased HHS wearing

Clinical presentation of the potential foot disease related to HHS wearing range from commonly discomfort to foot pathologies, such as foot deformity, hallux valgus, plantar fasciitis, plantar calluses, ankle inversion sprain, Morton's neuroma, Achilles tendon pain, and knee osteoarthritis have been presented in the previous studies (Fig 1.13) [6]. In addition, the foot pain generally appeared in the toes, ball of the forefoot, heel, as well as arch. The difference in foot pathology happens over time courses, can also be affected by individual foot structure and shoe structure such as heel height, the based support size, and shoe materials.

Fig. 1.13. The common foot disease induced by HHS wearing.

In conclusion. Gait biomechanics is a comprehensive system, therefore, a sing change, like elevating heel height in HHS gait, modifies the whole movement pattern. We can see from this brief review that the movement performance, balance, and musculoskeletal system control are compromised during HHS gait. The most significant change is observed in the ankle and knee joints, the references show that the biomechanical changes induced by HHS wear are in good agreement. In further research, the long-term neuromuscular adaptations in HHS wearing should be investigated, as well as the biomechanical mechanism responsible for such neuromuscular adaptations. Three major factors seem to play a determinant role in the occurrence of adaptation, such as the heel height, duration, and frequency of HHS wearing. These factors are needed to be investigated in a comprehensive and long-term way. Once the main factor affecting high heel gait are identified, along with musculoskeletal adaptations, we can give more suggestions to counteract the negative effects of high heels.

1.3 Musculoskeletal modeling of human movement

1.3.1 Introduction of Opensim application

The neuromusculoskeletal system is made up of a variety of elements, each of which interacted functionally, efficiently enables coordinated movement, facilitating a wide range of human movements. The relationships between muscles and joint motions during static movements have been extensively characterized by an abundance of data [98]. However, it remains a major challenge to integrate a detailed description of the neuromusculoskeletal system elements with movement measurements to develop a comprehensive understanding of extensive movement and to create a scientific fundamental for modifying abnormal movement [98]. A dynamic simulation of movement involves multiple aspects, including element of the anatomy, physiology, and multi-joint motions that must be combined coordinately to provide an integrated neuromusculoskeletal system. Therefore, a muscle-driven dynamic simulation is needed to estimate muscle and joint force which are difficult to record by experimental measurement.

OpenSim as an open-source software, provides a musculoskeletal modeling environment that allows users to create dynamics simulations of various movements based on the motion capture data. The OpenSim Software has plug-in architecture that enables user to establish individual's muscle models according to their needs, and a dozen plug-in analysis models developed by different users can be utilized by the public.

The musculoskeletal system in OpenSim is described by sets of differential equations that enable to the analysis of muscle contraction dynamics, musculoskeletal geometry, and body segment dynamics [99]. Neuromuscular excitation properties based on the time-dependent behavior are defined by differential equations. Once a dynamics model is described, it is necessary to find a pattern of muscle excitation to construct a coordinated movement of the musculoskeletal system. Simulation is usually verified by the degree of consistency of kinematic, kinetic, and EMG activities in experimental measurements. Once the simulation is performed and validated, it can be analyzed to assess the muscle contributions to body movement and the outcome of the simulated treatment. In terms of developing a dynamic simulation to generate a coordinated movement, the important challenge is to identify a set

of muscle excitations. Now, with the development of computer science, robotic computed muscle control technology can quickly determine the level of muscle excitation.

Operate steps in OpenSim software

There are four steps to establish a dynamic simulation model. In Step 1, MSM scaling is used to match the anthropometry of specific individual. Each body part is scaled according to the location of the marker captured from a 3D motion capture system. The mass characteristics of each body part are scaled to reproduce the individual's total measured mass, and the length of muscle-tendon actuators is also scaled.

In Step 2, inverse kinematics (IK) is used to identify the generalized coordinate values of the model to regenerate the original data of markers. This step is processed by a least-squares formulation that minimizes the marker array deformation between the measured marker positions and the model's virtual markers position, along with joint constraints [100]. If the experimental measurement includes the joint angle of the body segment generated by the motion capture system, can also be involved in the formulation. Therefore, the inverse kinematics is used to reduce the weighted squared error for each frame of kinematics variables obtained from experimental measurement [101].

In step 3, differences exist between the modeling assumptions and experimental error, such as values of the GRF and joint moment measured in the experiment are often differing from those in the MSM. In this step, a residual reduction algorithm (RRA) is utilized to promote the generalized coordinates of a model that made in step 2 more in accordance with the GRF and joint movement obtained from experimental measurement.

In Step 4, the computed muscle control (CMC) algorithm is utilized to generate a muscle-driven simulation. CMC distributes forces across synergistic muscles by using a static optimization criterion to produce a dynamic simulation [102]. The activation and contraction dynamic of muscles are represented by the full state equations, to be incorporated into the dynamic simulation.

1.3.2 MSM establishment for muscle-drive simulation of human gait in OpenSim

Rajagopal et al. provide a complete process for creating a generic open-source 3D musculoskeletal dynamic model in OpenSim and describe a reliable method for verifying the model using reference value [103]. The purpose of their study is to establish a highly validated musculoskeletal dynamics model of lower limb muscles in healthy young subjects for gait simulation, and computationally efficient enough to be used for conducting muscle-driven simulation in the OpenSim. In their study, the muscle architecture of lower limbs was created by combining the cadaver-based evaluation of muscle length and MRI (magnetic resonance imaging) muscle volume data [100]. The generic musculoskeletal modeling was created by following several steps: (1) rigid body geometry construction, the model's skeleton structure was created by 22 articulating rigid bones, containing 20 degrees of freedom (DOF) in the lower extremities and 17 DOF in the upper body. The coordinated system was aligned in each rigid structure, with the X-direction assigned as anteriorly, the Y-direction assigned as superiorly, and the Z-direction assigned as the right. all joints and the segments were modeled with motion range and DOF; (2) muscle and torque actuators establishment, 80 muscle-tendon units and 17 torque actuators were used in the lower extremities to drive the model. Each muscle unit was defined by a Hill-type muscle model (Fig 1.14), based on the description of Millard et al [104]. Each of the muscle-tendon force-length functions and joint angles was scaled by experimentally measured values according to previous research. In their study, the software of OpenSim (3.3 version) was used to produce muscle-driven simulations in a single gait cycle of a healthy subject.
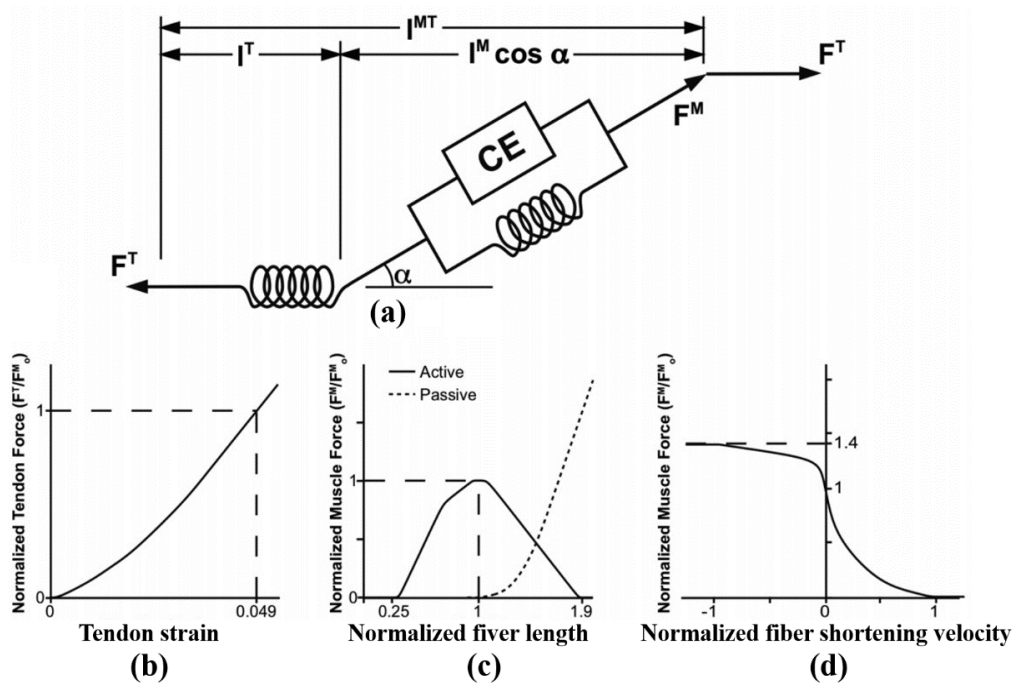
Fig 1.14. A computational model of muscle-tendon. (a): total muscle-tendon length is presented by the geometric pose function of the model, α represents muscle pennation angle; (b): function of tendon strain; (c): muscle fiber is designed as a contractile element; (d): muscle fiber velocity [103].

The four simulation steps have also been used. Firstly, the scaled version of the generic model was created using Scale Tool in OpenSim to match subject anthropometry. Secondly, joint kinematics of lower extremities during gait was calculated based on motion capture data in OpenSim using an inverse kinematic tool. The subtalar and metatarsal-phalangeal joints in lower limbs, as well as DOF of the wrist and ulnar, were constrained due to lower accuracy. Thirdly, the RRA was utilized to create smoothed kinematics that minimizes the inconsistency between the measured kinematic and kinetic data. Finally, the smoothed kinematics obtained in step 3 were input into the CMC algorithm to compute muscle excitations, activations, as well as muscle force.

For simulated model validation, fidelity and speed criteria of the model were tested, i) the musculoskeletal geometry in the simulation and experimental parameter were compared; ii) muscle activities in simulation and EMG data were compared; iii) joint moment in muscle-

driven simulation and inverse dynamics calculated were compared; iv) time for simulating a single gait cycle was computed. The final result of relative muscles is presented in Fig 1.15. The muscle architecture, which includes muscle-fiber length and muscle volume, is well consistent with experimental data, and the simulation timing of lower limb muscles in a single gait cycle was well-matched with EMG measurement.
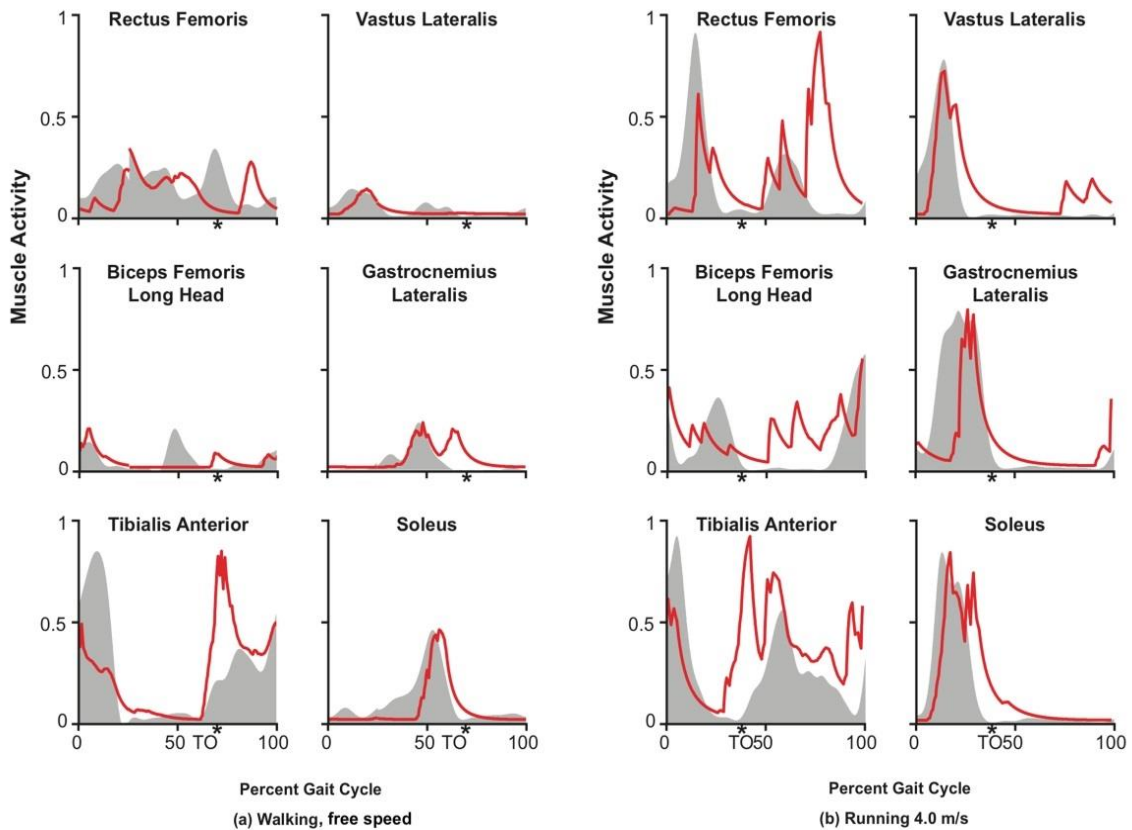

Fig. 1.15. Muscle activities compared between the simulation and measurement during walking and running, (a) is walking and (b) is running. The Red line represents the simulation result, and the gray shadow represents the EMG measurement result [103].

Personalized ability is currently one of the important trends in the development of MSM. The biological characteristics of individuals are complex and personalized, requiring more accurate and effective methods to diagnose and treat musculoskeletal diseases. Current MSM development involves personalized 3D body segments, intrinsic properties of muscles, activation patterns of muscles, and comprehensive process of individual kinematics and dynamics [104-107].

27

The combination of medical imaging and 3D motion analysis allows exploration of the relationship between external kinematic properties and internal joint behavior. Although 3D motion capture systems are widely used to measure the kinematic variation of body segment, 3D capture technology has certain limitations when applied to specific body systems due to the complex anatomical nature of individuals. Recently, new imaging techniques such as dynamic MRI have been used to measure more accurate and enriched kinematic parameters. Additionally, the fluoroscopic application of lower limb joint kinematics also provides a useful and efficient way to study human biomechanics in various sports [108-110]. These new imaging models open a new perspective for biomechanical research and provide accurate kinematic parameter support for personalized MSM construction. Compared with other calculation methods such as finite element modeling, the calculation efficiency of multi-rigid body segment is higher. In addition, the use of generic MSM in Opensim can provide an efficient solution, especially in clinical applications where decisions need to be made in a short period of time with minimal computational effort [111, 112].

1.4. Finite element model application of human foot

1.4.1. Introduction of finite element model analysis

The complexity of foot anatomy and function, along with the difficulty of making in vivo measurements to explore the physiological strain-stress that occurs in response to loading, prompted researchers to computational methods to model its behavior. In the early 1970s, with the development of computer technology, FEM analysis was introduced into the analysis of human musculoskeletal mechanisms. The fundamental advantage of finite element analysis in foot mechanical simulation is its ability to simulate irregular geometry, complex material properties, and create a variety of load and boundary conditions, which play an important role in biomechanical evaluation of foot and ankle composite joints. Furthermore, the biomechanical investigation of the foot and ankle complex based on the FEM analysis has been used to conduct a wide range of foot biomechanical investigations, which include foot pathologies analysis, prosthetic designs, rehabilitation evaluation, shoe, and insole design, and soft tissue evaluation (muscle-tendon, skin, ligament, and plantar fascia).

Creating a comprehensive fidelity foot model to explore the specific mechanical characteristic of the foot in its specific condition is one of the excellent hallmarks of a scientific investigation. Neither the foot model should not be so complex that the results cannot be predicted, nor should it so simple that results deviate from reality. Establishing a model that balances these aspects needs knowledge of creating processes and how they can meet the optimal condition.

Naturally, judgment based on previous research and experience in processing molding is needed. To provide insight into foot FEM analysis, three simple but concrete viewpoints can be concluded, which will be applied in our further research:

1. The model should be determined by the purpose of the investigation. Depending on the study's aim, specific foot regions can be modeled, and scanning a smaller area of the foot can help reduce computational costs.

2. Given the complex nature of the foot model, extensive validation of the modeling

process, the final integrated system, and the prediction results is required to ensure the accuracy of the model.

3. The FEM analysis of the foot can combine the MSM approach which provides loading and boundary conditions for foot model prediction, creating a realistic simulation environment.

Even though there is no integrated foot modeling could be directly applied in the clinic, there are considerable progress still needed, based on the current research that the comprehensive toolbox of foot FEM creating for future work towards clinically application has been demonstrated. The major challenge is to collect information about geometry construction, the material properties assignment and loading requirement on a specific basis, and computational cost-effectiveness.

1.4.2 The procedure of the finite element model performed on the human foot
Geometry reconstruction

A complete 3D foot model is generally reconstructed from computed tomography (CT) and MRI by image segmentation [113-115]. The surface scanning of a specific dissected part of cadavers also has been utilized [116]. If the soft tissues (muscle-tendon, ligament, plantar fascia) are included in the model, the insertion location of soft tissues needs to be determined by imaging data or anatomical reference [117]. Previous research has generated a highly detailed foot model which involved multiple components such as bones, cartilages, muscles, ligaments, and even plantar fascia (Fig 1. 16) [118]. While this detailed model exhibits a more realistic structure of the foot and assumedly should provide a more reliable result.
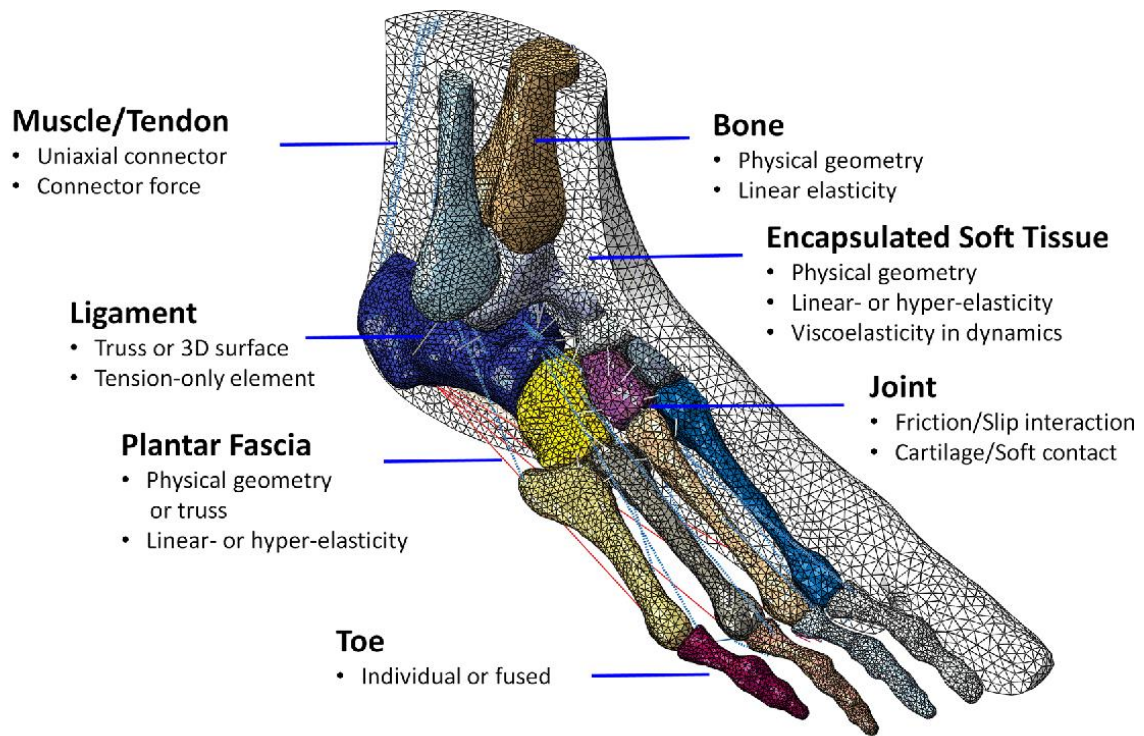
Fig 1.16. The foot component reconstruction [118].

Normally, in terms of constructing a complexity foot model, a significant amount of time for both development and solution is needed. Therefore, a simplified model with a specific part of the foot is also used in an attempt to provide a useful evaluation in shorter timeframes and improve the efficiency of the solution [119]. In a systematic review of FEM clinical application, Behforootan et al. reported that 64% of the 96 collected studies showed a detailed 3D model of the entire foot, and while 10% of these researches focused on a specific part of the foot, then 14% of reviewed researches generated two-dimensional (2D) foot model based on an X-ray/CT/MRI image [120]. Additionally, Actis et al. performed a simplified simulation on a 2D foot model that was based on the sagittal plane of the X-ray images to evaluate the effects of removing anatomy on foot function, the results indicated that even a small part of phalange could lead to a negligible influence on the model result [121].

Assignment of material properties

Regarding the foot structure, multiple components including bones, cartilages, ligaments, tendons, and soft tissues are having different material behavior. Particularly, the soft tissue

of the foot has been assigned as non-linear viscoelastic behavior [73, 122, 123], some studies also simplified soft tissue as a linearly elastic mechanical behavior to minimize the model solution time [124]. According to previous studies reported, bones and cartilages were usually modeled as homogenous linearly elastic material ranging from 7000 to 15,000 MPa [125-127], and ligaments and tendons were defined as linearly elastic with Young's modulus ranging from 11.5 to 1500MPa, the fiber-reinforces, viscohyperelastic model also was used on ligament simulation [128]. The material properties are crucial in the simulation process for realistic simulation of the mechanical behavior of ligaments and tendons [129]. It has been suggested that considering the increased computational costs and complexity of simulations, the optimal material model selection in each case should be rigorously validated according to the specific objectives and level of accuracy of the study [129, 130].

Interactions, boundary, and loading condition

Depending on the model characteristic, it is necessary to define the interaction between different tissues, interfaces, and connector elements. For example, to create a realistic simulation of the foot interacting with the insole, the contact mechanical behavior between the foot and insole is defined by friction coefficients ranging from 0.3 to 0.6. Behforootan et al. reported that 43% of the 96 reviewed studies assigned loading force on the model as a percentage of body weight (BW), in which 50% of BW loading condition is mostly applied on the static standing simulation, and the muscle force usually assigned 25% to the Achilles tendon [120]. Besides, the magnitude of the imposed loading can also be obtained by Vivo measurement, the GRF as an important loading parameter can be directly measured using force plates, or insole pressure sensors. The amount of GRF applied load from measurements appears to be more relevant for studies that focus on specific gait stages and foot regions to provide reliable and accurate plantar pressure estimates. For example, Budhabhatti et al. imposed a measured GRF at the toe-off phase on a specific individual 3D foot model [131].

Indeed, all FEM analyses compute the foot inner strain and stress distribution according to the assumed and measured loading force. This fundamental feature of FEM simulation

indicates that FEM method cannot directly predict and calculate the gait adaptation and even internal tissue loading. To overcome this limitation, FEM foot simulation can be performed in combination with the MSM. More specifically, Scarton et al. created a workflow estimating the effect of gait modification on strain and stress in the diabetic foot by integrating MSM and FEM, in which MSM model was used to evaluate the forces in muscles, ligaments, and joint contact during the modeled movement, and FEM was used to establish the foot model of a specific individual, the calculated muscle and ligament forces were assigned as loading and boundary condition on the FEM foot model to improve the prediction of internal strain and stress on the foot [132]. Despite the high computational cost, this approach enables to performance of the non-invasion estimation of the tissue's strain and stress characteristic on diabetic foot using optimal loading control.

Meshing

Individual component needs to be meshed into discrete elements which connected by nodes. According to the complexity and geometry of the parts, a series of element geometry can be used for discrete solid parts, such as triangles, quadrilaterals, tetrahedra, hexahedral elements, etc. (Fig 1.17). The various behavior options of these basic element shapes can be assigned to meet model requirements, such as, hybrid elements can be used on one component to reduce the solution time at the expense of accuracy. Tadepalli et al. used a hybrid element that combined the hexahedral, quadratic, and tetrahedral to model incompressible materials of soft tissue [133].

Additionally, mesh density is another important factor that distinctly affects the simulation results. Fontanella et al. conducted a mesh convergence analysis on a foot model and showed that more than 10,000 hexahedral elements are required to achieve an optimal mesh density for simulating the peak plantar pressure at the push-off phase [134]. While Chokhandre et al. [135] used 30,576 hexahedral elements for their heel model. In terms of how to conduct a convergence test of mesh, according to Li et al, the sizes of the elements were gradually reduced until the variation of force-displacement is less than 3% between the two size meshes [136].
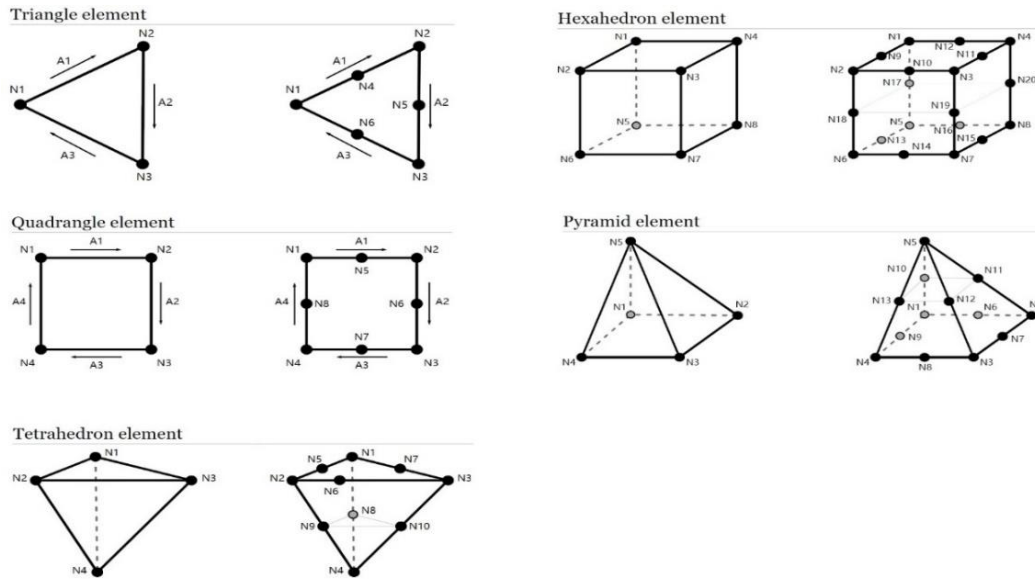
Fig 1.17. Diagram of mesh element types.

FEM validation

The validation of FEM analysis is paramount important for FEM application, also this is one of the most challenging aspects of biomechanical simulation. According statistic data reported by Behforootan et al. indicated that 56% of studies of 96 reviewed articles validated the computational foot model by comparing prediction results with in vivo or in-vitro experimental data or with previously published data [120]. In terms of experimental data comparison, the plantar pressure distribution or the peak value of plantar pressure was compared between prediction and experimental measurement [137, 138]; as for comparing data to literature, the numerically predicted plantar pressures, or strain-stress mechanical behavior of specific tissues was being used to compare the published data [127, 139-141].

1.4.3 Summary

The application of FEM analysis on human musculoskeletal structure, provides an invented insight into evaluating the internal biomechanical mechanism of human multi-segment. However, creating a geometrically and kinematically accurate model is still a challenge in conducting a fundamental investigation for pathology feature simulation and prediction in clinical application. Besides, the several challenges of foot FEM analysis need to be carefully concerned in further investigation:

1. The first challenge is that reconstructing the foot geometry in a non-invasive way is a time-consuming and laborious step, due to the foot structure being rebuilt based on the images of CT scanning and MRI.

2. The second challenge is that the material properties of soft tissue increase the difficulty of simulation because of the complex nonlinear mechanical behavior of soft tissue.

3. The third challenge is to assign boundary and loading conditions for the foot model that can apply clinically relevant loading without using time consuming measurement.

4. The fourth challenge is to determine the threshold of mesh density for each foot component, which is time-consuming progress needed to do progressive mesh testing.

2 The foot multi-segment biomechanics in HHS gait

2.1 Introduction

Kinematic details regarding the effects of HHS on foot movement and structure are limited. Yu et al. have suggested that the force distribution in the foot can be changed by HHS and contributes to hallux valgus [139]. Theoretically, foot posture consists of an alignment of the foot skeleton, and any abnormal landings or misalignments will change posture and directly affect the function of the foot. Therefore, a more reliable and objective classification method is needed to study the details of foot kinematics in HHS gait.

The OFM is a multi-segment model and provides comprehensive foot movement details that can be analyzed to reveal the kinematic characteristic of the hallux, forefoot, and hindfoot during gait [142, 143]. The repeatability and reliability of the Oxford foot model have been outlined, it has been widely used in the biomechanical filed and in a range of populations to observe both normal and pathological foot in the children and adult [144, 145, 146]. Levinger et al. investigated the kinematic difference in foot segment between normal and flat-arched feet during walking by using OFM, demonstrated a significant difference in forefoot and hindfoot movement in the sagittal and transverse plane between two comparison groups, revealing the flat-arched feet had a greater pronation than normal feet during walking, then it was suggested that this altered biomechanical mechanism could pose a high injury risk on flat-arched feet population [147]. Alonso-Vázquez et al. assessed the kinematic characteristic of forefoot varus during gait among the children who age ranged from 7 to 13 years, demonstrated the specific kinematic chain and movement pattern of lower extremities in subjects with forefoot varus [148].

In terms of foot movement in HHS gait, the foot structure has been changed dramatically as hindfoot passively elevated by heel along with COM shifted toward to the forefoot which becomes the major support. Despite this special foot structure attracted massive researchers' attention with biomechanical research centered around topics of the HHS gait which manly investigated the kinematical and kinetic of lower limbs including ankle, knee, and hip joint, the foot movement still unclear in HHS gait. Therefore, in order to provide insight into the

biomechanical function of foot and acquire the possible kinematic evidence to explain the pathology of foot related to HHS wearing, such as hallux valgus, the hallux, forefoot, and hindfoot movement in HHS gait was assessed using OFM.

2.2 Method

Fifteen healthy women (23 ± 2.5 years, 1.65 ± 0.3 m, 51 ± 3.6 kg) were recruited. A Vicon motion system with 8 cameras (Oxford Metrics Ltd., Oxford, UK) was used to capture kinematic data of the hallux, forefoot, and hindfoot using a frequency at 100 HZ. This trial was conducted under two different experimental conditions, barefoot walking (BF) and HHS with heel height of 5 cm. The size of experimental shoes ranged from 36 to 38. Data was collected right foot. To evaluate the three-dimensional movement of left foot, the reflective markers were placed according to guidelines outlined in Plug-in Gait as defined in previous study [145]. The OFM markers attached to the right leg were based on a previous definition (Fig 2.1).

Following warm up, the subjects with markers were asked to stand in a suitable data capture position in front of the camera for static data collection. Once dynamic testing was performed, the three markers (RMMA, RPCA, RD1M) were removed [142]. Participants were asked to walk through the data capture area at a normal speed. The subjects were tested five times to ensure gait stability and to reduce experimental data collection error.
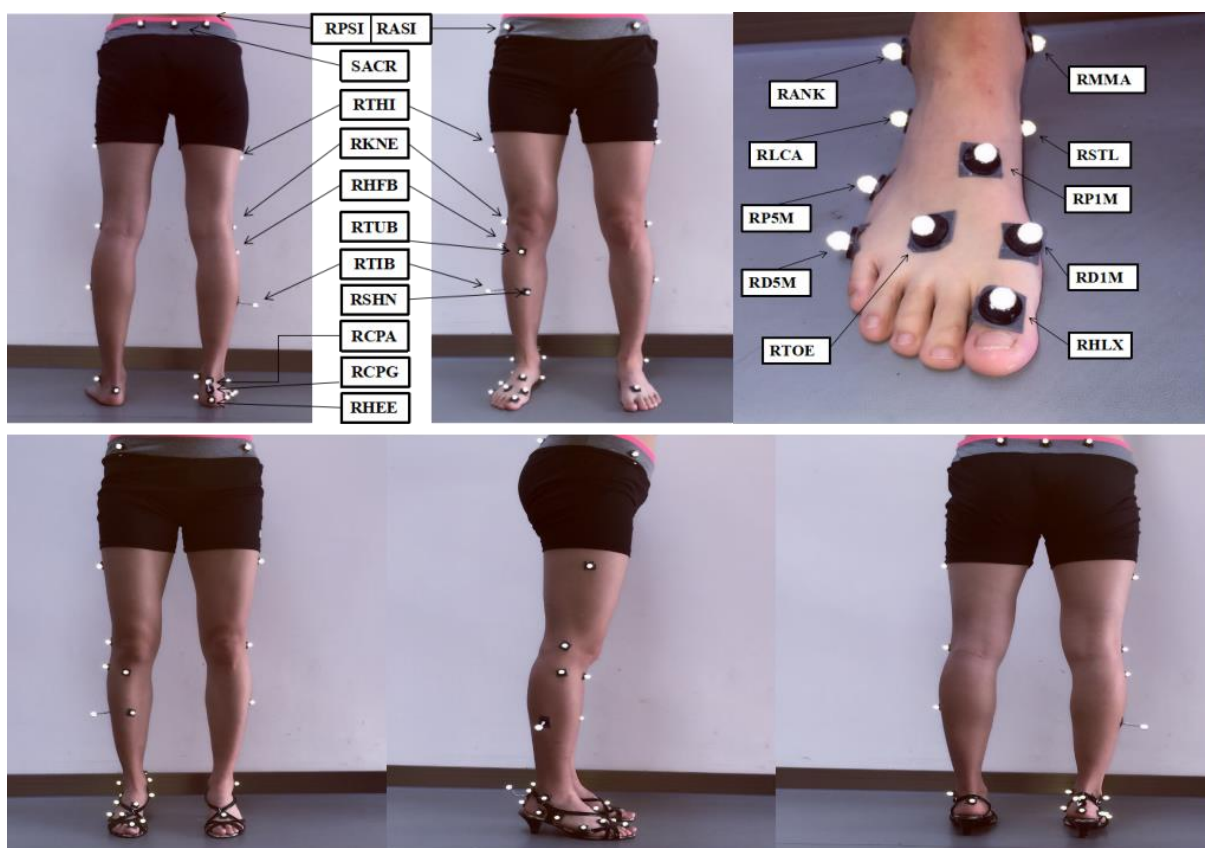
Fig 2.1. Oxford markers position on lower limbs under barefoot and HHS condition. The maker description: RASI- Anterior Superior illiac Spine; RPSI- Posterior Superior iliac Spine; SACR- Posterior Superior iliac Spine; RKNE- Standard lateral knee; RTIB- Tibia marker; RHFB- Later head of fibula; RTUB- Tibia tuberosity; RSHN- Anterior aspect of the skin; RANK- Ankle; RMMA- Medial Malleoli; RCPG- Posterior end of the calcaneus; RHEE- Heel; RACA- Posterior calcaneus proximal; RLCA- Lateral calcaneus; RSTL- Sustaniculum tail; RP1M-1st metatarsal, proximal dorsal; RD1M-1st metatarsal, distal medial; RP5M-5st metatarsal, proximal lateral; RD5M-5st metatarsal, distal lateral; RTOE- Toe; RHLX- Hallux.

Data analysis

The timing and magnitude of angular movement of the hallux with respect to forefoot, forefoot with respect to hindfoot, and hindfoot with respect to the tibia during a complete gait cycle were compared between barefoot and HHS gait in a sagittal plane, a frontal plane, and a transverse plane respectively. Statistical analysis was performed using statistical

software SPSS 19.0 (SPSS Inc, Chicago, IL, USA). Independent sample t-tests were used to assess any differences in kinematic parameters between the barefoot and HHS gait. For all analyses the significance level was set at 0.05.

2.3 Results and Discussion

Kinematic variations of hallux, forefoot, and hindfoot in both HHS and barefoot gait are shown in the Figure 2.2. The findings demonstrated significantly greater hallux dorsiflexion in HHS gait than barefoot during the last stance phase (22.55º ± 1.62º VS 26.6º ± 2.33º; P = 0.001). There is smaller hallux plantarflexion in HHS than barefoot during the initial stance phase (−4.86º ± 2.32º VS −8.68º ± 1.13; P < 0.001) (Table 2.1)

In terms of forefoot movement relative to the hindfoot. HHS significantly increased forefoot abduction compared to barefoot during the late stance (16.15º ± 1.37º VS 13.18º ± 0.79º; P < 0.001). However, there was no statistical different in forefoot adduction between HHS and barefoot. Also, no difference was found in the sagittal and transverse plane movement of foot between HHS and barefoot (Table 2.1).

In term of hindfoot movement respective with tibia. There was a greater value of dorsiflexion angle during the terminal stance phase in HHS compared to barefoot (16.59º ± 1.69º VS 12.08º ± 0.9º; P < 0.001), but no difference was found in plantarflexion. Additionally, in the frontal plane, subject with HHS showed a greater internal rotation angle barefoot during the initial stance phase (16.72º ± 0.48º VS 7.97º ± 0.55º; P < 0.001). Also, HHS indicated a significantly decreased in the extension rotation compared to barefoot during the mid-stance phase (−5.49º ± 0.69º VS −10.73º ± 0.42º), but there was no significant difference observed in the transverse plane (Table 2.1).

Table 2.1. The peak value of angular motion for hallux relative to the forefoot, forefoot relative to hindfoot, and hindfoot relative to the tibia in the barefoot and high heels shoes (0cm vs 5cm).

| Variable	BF (deg) (Mean ± SD)	HHS (deg) (Mean ± SD)	P Value
Hallux relative to the forefoot			
Dorsiflexion	22.55 ± 1.62	26.6 ± 2.33	**0.001**
Plantar- flexion	-8.68 ± 1.13	-4.86 ± 2.32	**< 0.001**
Forefoot relative to hindfoot			
Dorsiflexion	12.49 ± 0.45	11.46 ± 2.49	0.7
Plantar- flexion	-4.04 ± 1.04	-1.7 ± 1.79	0.05
Adduction	13.18 ± 0.79	16.15 ± 1.37	**< 0.001**
Abduction	8.42 ± 2.81	7.19 ± 0.41	0.15
Inversion	4.16 ± 1.67	4.45 ± 1.06	0.11
Eversion	-4.47 ± 0.64	-5.12 ± 0.7	0.86
Hindfoot relative to the tibia			
Dorsiflexion	12.08 ± 0.9	16.59 ±1.69	**< 0.001**
Plantar- flexion	-16.26 ± 1.93	-18.1 ± 2.29	0.16
Inversion	6.88 ± 0.9	8.16 ± 1.16	0.07
Eversion	-14.4 ± 1.69	-15.92 ± 0.41	0.19
Internal rotation	7.97 ± 0.55	16.72 ± 0.48	**< 0.001**
External rotation	-10.73 ± 0.42	-5.49 ± 0.69	**0.001**

Note: the significance at $P < 0.05$.
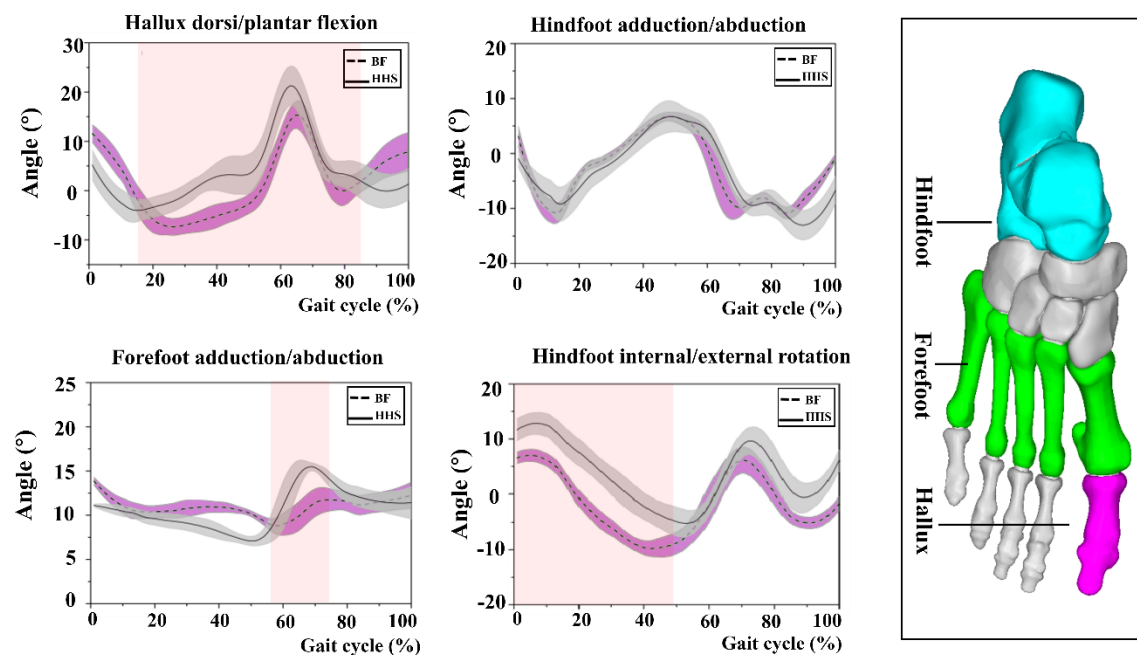
Fig 2.2. The comparison of foot kinematics in three different planes between the HHS and BF. The red region indicated the significant differences between HHS and BF.

Discussion

The kinematic characteristics of the hallux, forefoot and hindfoot in HHS gait were studied by using OFM technique. The major results showed that the hallux sagittal plane changed significantly in HHS than barefoot.

It is widely accepted that wearing high heels can lead to adverse loading conditions and negatively affect the structure of the foot [149]. Healey and Chen [150] pointed out that the hallux dorsiflexion is significantly increased due to the elevation of the hind foot, which will lead to shortening of the metatarsal fascia and elevation of the medial longitudinal arch. To maintain a stable gait, larger sagittal dorsiflexion can be compensated by increasing the duration and amplitude of ankle extensor moments, which may increase ankle load, pose greater risk of an ankle injury. In addition, high heels were associated with hallux valgus which was defined as a common foot abnormality structure [151]. The movement of the hallux dorsiflexion causes the sesamoid to move to the distal segment, and a significant increase in hallux dorsiflexion may result in a high risk of sesamoid dislocation. The sesamoid has the function of limiting hallux toward eversion and can alleviate most of the

load bearing force in the first metatarsal head [152].

Regarding movement of forefoot relative to the hindfoot, the forefoot showed an increased value of adduction during the last stance (toe-off) and it was found to be higher in HHS gait compared to barefoot. HHS could cause foot to slide towards the head of the shoe, contributing to squeeze between the shoe and the forefoot. Particularly, the squeezing can be more intense when the head of the high heel shoes was narrower than the forefoot. Inevitably, the hallux is squeezed toward abduction direction, as a compensate reaction the forefoot increases adduction angle during HHS gait to maintain the foot stability. However, the increased forefoot adduction movement are usually accompanied by foot supination motion, and potentially increase the risk of the overuse injury [147]. Adduction movement of the first metastatic is considered to be a serious underlying cause of bunions [153]. On the other hand, the stress of the foot would be correspondingly changed as forefoot adduction angle increased. Cavanagh et al. [149] pointed out that compared with barefoot, HHS can transfer larger GRF to the first metatarsal bone, and then the loading rate, shear stress and force concentration can be significantly increased.

In addition, a significant increase in the hindfoot dorsiflexion and a significant decrease in hindfoot plantarflexion were observed. Those changes induced by HHS could constraint the ankle ROM during gait. Cronin et al. demonstrated that HHS increased Achilles tendon force, resulting in a stiffer Achilles tendon condition, which leads to a reduction in ankle range of motion [154]. Therefore, wearing HHS for long periods may lead to Achilles pain and increases the risk of ankle sprain. Furthermore, a greater internal rotation of hindfoot was found HHS gait compared to the BF condition. Anatomically, the hindfoot segment is connected to the tibia by the talus, and we hypothesized that increased rotation of the hindfoot may also lead to increased rotation of the tibia. Meanwhile, there is a coupling relationship between subtalar joint movement and lower limb [155]. If the movement of the hindfoot is abnormally altered, this may affect the movement of the tibia and therefore have an adversely impact on the function of the proximal joint such as the knee joint [156 157].

Several limitations need to be taken consideration. In previous studies, the OFM has been used to evaluate different populations which can prove valid repeatability measures for the hallux, the forefoot, and hindfoot segment [142]. However, kinematic models of the foot and classification methods of postures vary greatly from study to study, which makes it difficult to compare the results with other studies [158]. The midfoot has a very important role in loading transfer from the forefoot to the hindfoot, but in this study, movement in the midfoot was unable to investigate due to the OFM's limitation that midfoot segment is not involved. Another limitation in this study is that only inexperienced wearers were involved, the experienced participators may show an appropriate walking pattern which could lead to different results.

2.4 Conclusion

Based on this experimental, the major findings indicated that significantly higher dorsiflexed movement occurred on the hallux and higher adduction movement occurred on the forefoot segment during HHS gait compared to barefoot gait. The combined effect of cyclic bending and the high rate of change will result that the hallux will be twisting outwardly, while the forefoot will be twisting inwardly. This mechanism will create a propagating, long term trauma that eventually ends in hallux valgus or "bunion". Meanwhile, the hindfoot internal rotation becomes significantly higher during HHS gait, in the stance phase (between 0% and 50% of the complete gait cycle). Higher movement of the hindfoot in the transverse plane leads to an unstable posture during stance phase that could increase the risk of the ankle sprain.

3 Foot model reconstruction and the foot morphology measurement under HHS condition

3.1 Introduction

Footwear has been implicated as being responsible for the majority of foot pathologies and deformities. The adverse effect of footwear has been proposed by previous literature, ill-fitting shoes pose deforming effect on the foot leading to various foot pathologies, such as hammertoes, hallux valgus, corns [159]. Frey et al. indicated that footwear is the essential extrinsic factor leading to foot deformities, especially, for the development of forefoot pathologies in women, and they showed that 80% of the healthy women in 356 subjects have sort of foot deformity. However, there is a fact remained in their study that 20% of the investigated women who did not suffer foot deformities and developed foot pains, even for those who wear HHS. There must be some intrinsic factors that resist foot deformation in HHS wearing.

From a biomechanical point of view, the foot as a multi-segment structure can be dramatically changed by ill-fitting shoes, such as HHS with heel elevated, small support base areas, narrow forefoot box. What's more, the HHS leads to a dramatic change on the foot morphology, with arch passively raised and shorten as heel elevated, and the forefoot becomes a major support segment, as well as the internal multiple-bone position, has been modified. The biomechanical characteristic of lower extremities under HHS conditions is increasingly being investigated in the complex 3D kinematics and kinetics. These and many other researchers led to a tremendous increase in our knowledge, and in vivo function of the foot on HHS gait is being more and more appreciated. However, Anthropometric in 3D foot shape under HHS conditions has not been proposed yet.

Traditionally, the X-ray image is frequently used to analyze the skeletal morphology by obtaining weight-bearing radiographs of the specific segment of the body, but these are intrinsically limited due to the single plane projection view. Nowadays, most of the restrictions of traditional radiographic measurement can be addressed by current MRI and

CT technology, which provide the 3D volume of the skeletal structure with high spatial resolution. As such, the image of CT and MRI can also support more precise assessment and diagnoses of various musculoskeletal pathologies [160]. Foot morphology is, therefore, of tantamount importance to understanding foot functional adaption, and provides a reference for further work to address the relationship between foot function and foot morphology.

3.2 Methods

CT examination: one healthy female subject was recruited to conduct a CT scan. Prior to the measurement, the foot condition of the subject has been checked without any foot deformity or foot pathologies. Then subject with high heels of different heel heights (0cm, 3cm, 5cm, 7cm) conducted CT scanning. The subject was supine on the CT scanning bed, and the ankle joint was kept in a neutral position. Thin layer scanning was performed on the tibiofibular and the whole foot. Scanning parameters were assigned as: the voltage was 120 kV, the current intensity was 240 mA, and the scanning layer thickness was 0.600 mm. A total of 8232d tomography images' interval thickness was 2 mm interval, and resolution quality was 512×512. Then CT scanning images were saved in DICOM (Digital Imaging and Communications in Medicine) format.

Data import: The obtained DICOM file is imported into the software of Mimics Medical 20.0 (Materialise, Belgium). The image orientation is determined in Mimics software to complete the CT data import. Regarding the foot reconstruction in Mimics, firstly, the thresholding option was used for varying grayscale values, with a minimum threshold of 213 and a maximum of 3 071; Secondly, the regional growth option was used to separate the bony structure from each other; thirdly, calculate 3D from Mask was used to reconstruct bony one by one (Fig 3.1); fourthly, all 3D models are saved in Stereolithography (STL) file format, input Geomagic Wrap 2017(Raindrop, America) software to smooth surface model of optimizing bone, curved surface reconstruction function was used to establish the foot bone, then each part of the proceeds to the STL format file, import into 3-MATC software for angle measurement. The final reconstruction foot model is presented in Fig 3.2.
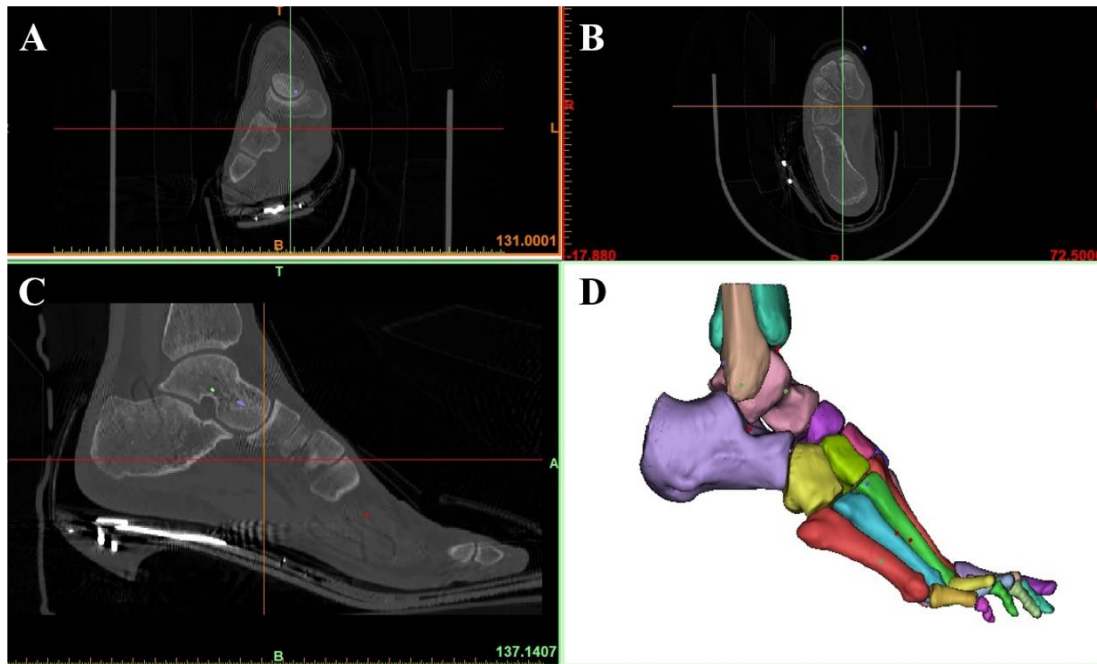
Fig 3.1. The foot image is in three planes; A is in the frontal plane; B is in the transverse plane; C is in the sagittal plane; D is a reconstructed bony involving 24 bones.
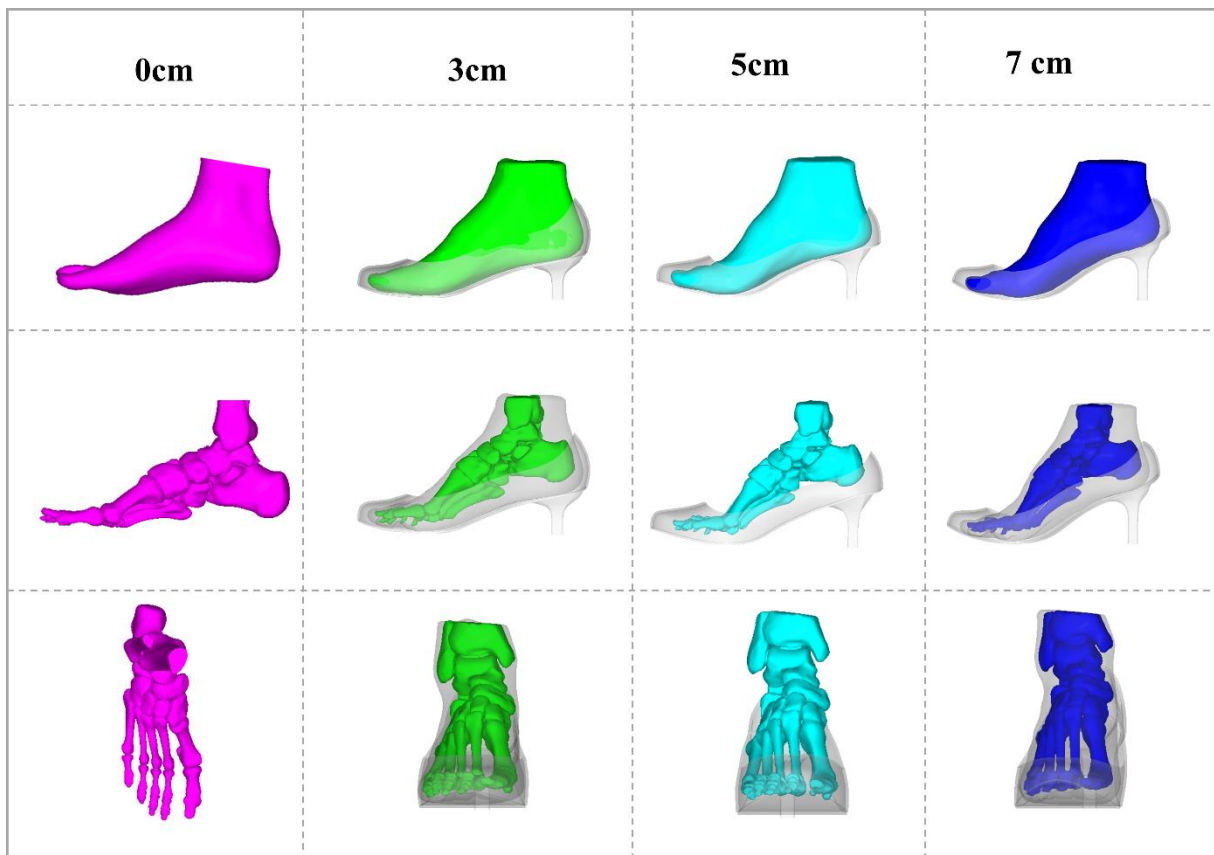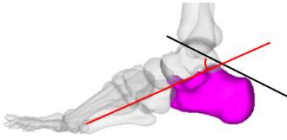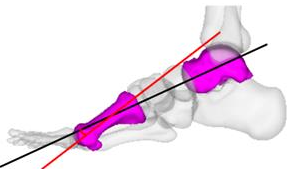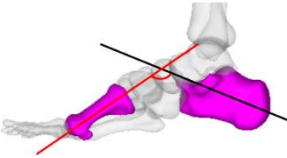

Fig 3.2. The final reconstruction 3D foot model under HHS condition with four different heel heights.

3.3 Results and Discussion

Foot morphology in different heel height conditions (0cm, 3cm, 5cm, 7cm) was quantified by using angle measurement, which included Böhler angle, Gissane angle, the talus-first metatarsal (TFM) angle, the Calcaneal-1st metatarsal (C1M) angle, the hallux valgus (HV) angle, the metatarsal break (MB) angle, the first metatarsal declination (1MD) angle, the First intermetatarsal (FIM) angle. The angle description is presented in table 3.1.

Table 3.1. The description of measured angle [160][167].

Angle	Description	Image
Böhler angle	The angle between the tangents of the anterior-dorsal aspect and the posterior-dorsal aspect of the calcaneus	
Gissane angle	The angle between the downward and upward slopes of the calcaneal anterior-superior surface	
TFM angle/ Meary's angle	The angle between the long axis of talus and the long axis of the first metatarsal	
C1M angle	The angle between the axis of the first metatarsal and the long axis of calcaneus	
1MD angle	The angle between the long axis of the first metatarsal bone and the supporting surface	
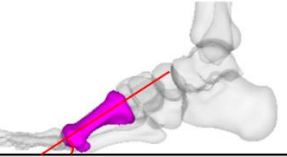
HV angle	The angle between the long axis of the first metatarsal and the long axis of the hallux proximal phalanx	
FIM angle	The angle between the long axis of the first metatarsal and the long axis of the second metatarsal	
MB angle	The angle between two lines segment through the most anterior aspect of the head of the 1st, 2nd, and 5th metatarsal bones	

As shown in Fig 3.3, the Böhler angle is an angle between the tangents of the anterior-dorsal aspect and the posterior-dorsal aspect of the calcaneus [161-163]. More specifically, is the angle on a lateral foot view between a line from the highest anterior process of the calcaneus to the highest point of the posterior calcaneus articular facet, and the line from the highest posterior calcaneus articular to the highest location of the calcaneus tuberosity [164]. The normal range value of the Böhler angle is from 25° to 40°. Although there is a wide difference between the individuals, also a little variation is apparent in the left and right feet of a single individual. According to the angle measurement, the Böhler angle in the five different foot conditions showed a significant difference. The largest value of the Böhler angle is shown at 0cm heel height, and gradually decreased from $36.62°$ to $29.36°$ with heel height increased from 0cm to 5cm, presented the smallest angle at 5cm. Following the slightly increased from $29.36°$ to $30.34°$ as heel height raised from 5cm to 7cm. Although the heel height posed an important influence on the Böhler angle under HHS conditions, all

those angle magnitudes are within the normal range, even the heel raised from 0cm to 7cm. The calcaneus segment has a relatively higher ROM in the sagittal plane among the multiple segments of the foot, thus the acceptable ROM activities are relatively large. The Böhler angle is correlated with the calcaneal function, and a reduction value in the Böhler angle can be considered an indicator of the severity of the calcaneal injury. Under HHS conditions, with heel height elevated from 0cm to 7cm, the Böhler angle varied by 7.26° from the largest value of 36.62° in 0cm to the lowest value of 29.36° in 5cm. This slight change of Böhler angle under dramatically increased heel height may indicate that the calcaneus position in the sagittal plane is not changed with heel height elevation to provide a stability function on the subtalar joint and ankle joint.
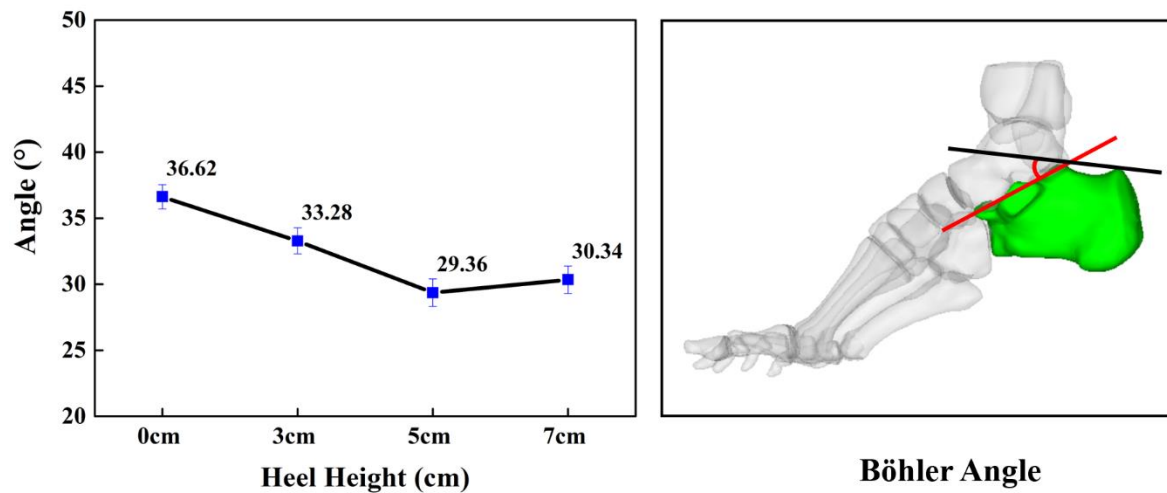

Fig 3.3. The Böhler angle variation among the four different heel heights.

As shown in Fig 3.4, the Gissane angle in five different foot conditions is displayed. Gissane angle is measured by 2 lines in lateral view: one line is along the anterosuperior facet of the calcaneus and joins another line along the posterosuperior facet of the calcaneus, which is used to estimate the severity of calcaneal fractures [164]. The normal value of the Gissane angle is between 120° and 145°, and a wide variation in the value of the Gissane angle has existed between the individuals, as well as a relative difference between the right and left foot [164]. According to the angle measurement among the five different heel heights, the whole angle varies by 7.94° from 0cm to 7cm, the highest angle (150.34°) was found at 5cm,

and the smallest angle (142.4°) was observed in 7cm. Normally, the Gissane angle and together with the Böhler angle is utilized to diagnose the severity of the calcaneal fractures and stability, and these angles can provide the restored reference for surgical treatment of calcaneal fractures [165]. The Gissane angle and the Böhler angle varied by 7.94° and 7.26°, the similar variation range from 0cm to 7cm could highlight that the subtalar joint is relatively stable in the sagittal plane since calcaneal segment position is only slightly disturbed by heel height.
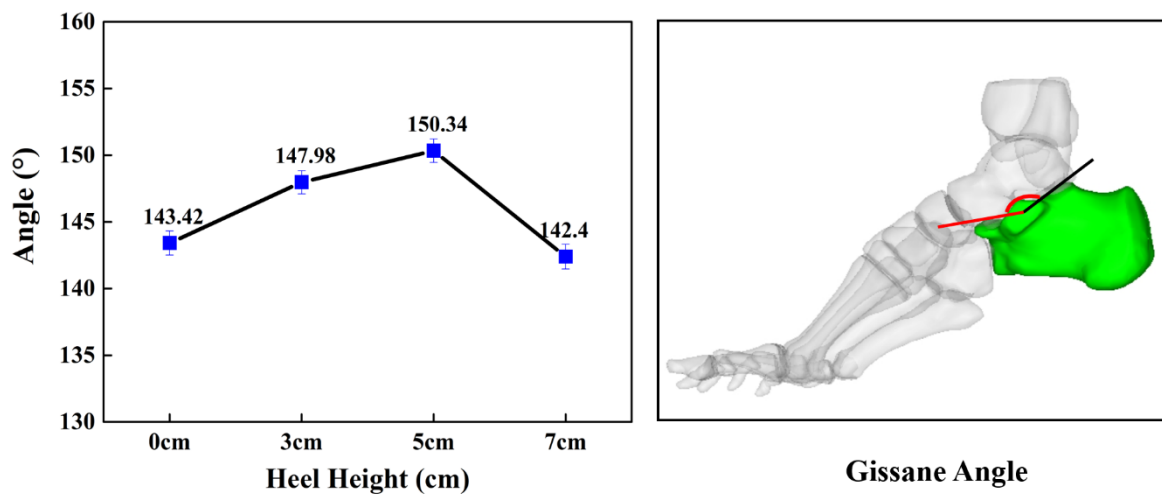
Fig 3.4. The Gissane angle variation among the four different heel heights.

As shown at Fig 3.5, the TFM angle is formed by the midline of the talus axis and the longitudinal line of the first metatarsal, also known as Meary's angle has been used to determine the apex deformity in individuals with pes cavus. The positive value of the TFM angle indicated the angle apex is in the dorsal direction and represents a greater talar declination; while the negative value is directed in a plantar direction and represents a greater first metatarsal inclination [165-167]. The normal angle value of TFM is 0° which means the extension lines of the midline axis between the first metatarsal and talus are parallel. And the severity of pes cavus can be classified into three conditions based on the TFM angle which include mild: < 15°; moderate: 15-30°; severe: > 30° [168-170]. According to measurement, the TFM angle increased as heel height elevated from 0cm to 7cm, and there is a dramatic increase of 87.67% as heel height raised from 0cm to 3cm, and the angle increased by 22.1% from 3cm to 7cm. The HHS forces the foot into a pes cavus with

moderate deformation, and the severity of the pes cavus would develop further with heel height increasing. Under HHS condition, the medial and longitudinal arch is passively raised as the heel increasing, which tighten the Achilles tendon and plantar fascia producing claw toes due to the windlass mechanism influence [171]. Furthermore, the high rigidity arch lacks shock absorption and is prone to heel pain and plantar fasciitis. In here, the heel height we measured is limited to 7cm, and if a heel height of HHS more than 7cm is chosen, which could force the foot into a more severe condition of pes cavus, causing severe damage to the musculoskeletal system.
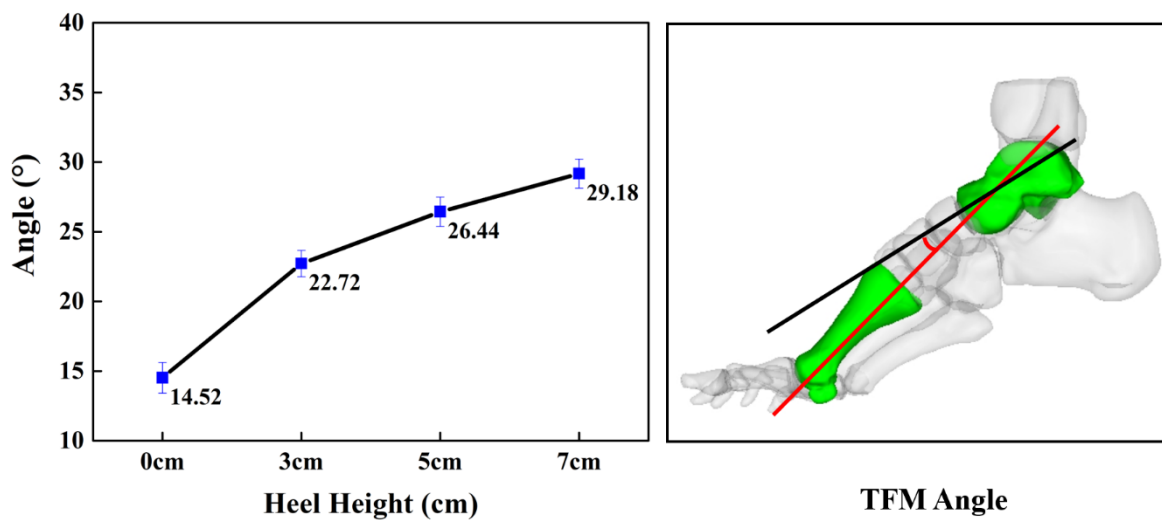

Fig 3.5. The TFM angle variation among the four different heel heights.

As shown in Fig 3.6, the C1M angle also known as the Hibbs angle, is defined as the angle between the line from the inferior surface of the calcaneus and joined a line of the longitudinal axis of the first metatarsal. C1M angle measured as lateral view reflecting the sagittal alignment of the hindfoot and forefoot, there is a strong relationship between the arch height, the normal angle of it is 150°, and it decreases as the signal of cavus deformity and high longitudinal arch. Cavus deformity can result in a loss of arch shock absorption function in gait due to the inability of the hindfoot to bear a valgus alignment. What more's, the Cavus deformity also leads to an unstable tripod weight-bearing structure of the foot, which causes ankle instability or painful calluses of the plantar [172-175]. According to the measurement, the magnitude of C1M angle decreased as heel height elevated from 0cm to 7cm, a sharp decrease of 17.2% occurred on 3cm compared with 0cm. The angle variation

significantly exceeds the normal range from 3cm to 7cm, which indicates a cavus deformity induced by HHS. The results are consistent with Meary's angle which describe above.
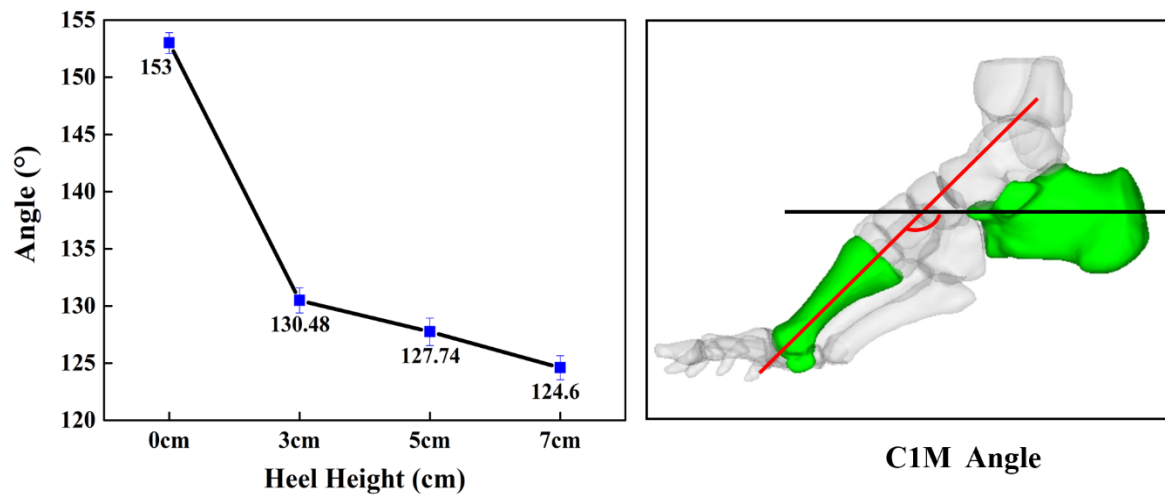

Fig 3.6. The C1M angle variation among the four different heel heights.

The hallux valgus (HV) angle in five different foot conditions is presented at 3.7. The HV is the angle defined between the longitudinal axis of the first metatarsal and the longitudinal axis of the first proximal phalanx [176-179]. HV malformation is considered to be one of the most common foot disorders, particularly among women who regularly wear HHS, and previous studies have shown that the prevalence of HV is significantly higher in those who are habitual HHS wearers than those with unshod or flat-shoes feet [180]. The index of HV angle is used to evaluate the severity of the deformity, which is classified into three groups: mild (15º - 20º); moderate (20º - 40º); severe (> 40º). According to the angle measurement, the HV angle increased as heel height elevated from 0cm to 7cm. There is a significant increase of 65.27% found at 3cm when compared with 0cm, and a slight increase from 3cm to 5cm, and the largest HV angle of 35.1 º was found at 7cm. Therefore, the HHS could pose a high risk of HV development on the foot. As Gu et al. demonstrated that a subject with mild HV resulted in an increased pressure under the first metatarsal head compared to healthy control groups [181]. Additionally, the COP oscillation medially shifted to the first head metatarsal was found in the mild HV group, which may adversely affect the first ray and lead to a greater susceptibility to HV deformity [82].
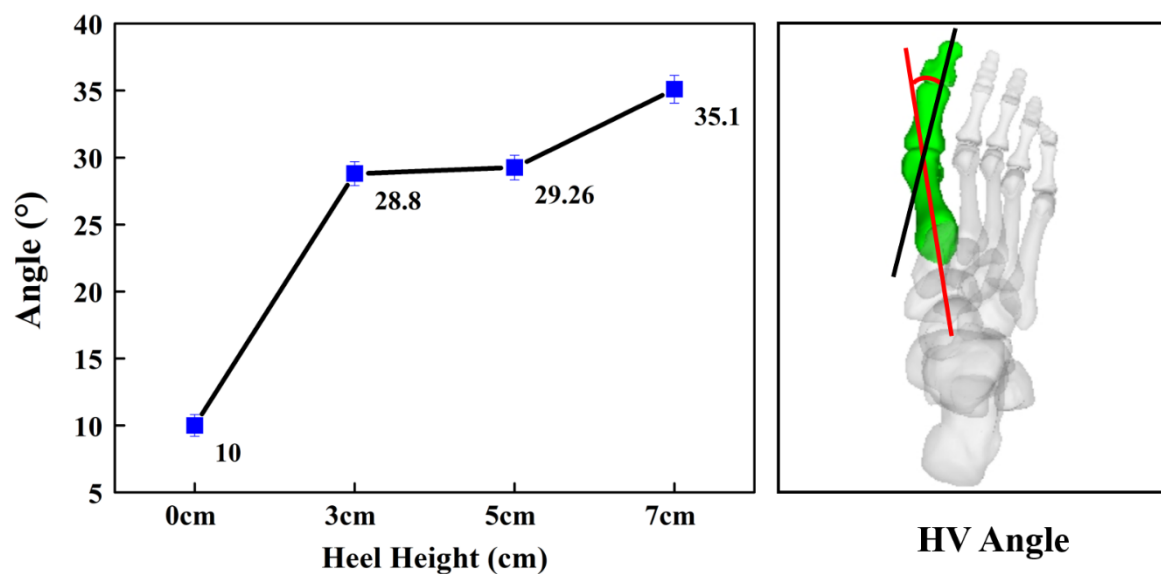
Fig 3.7. The HV angle variation among the four different heel heights.

As shown in Fig 3.8, the first intermetatarsal (FIM) angle is formed between the line of the longitudinal axis of the first metatarsal and the line of the second metatarsal [177, 181-183]. The identification and measurement of the FIM angle indicate the HA deformity severity degree [176, 178, 184, 185]. It has been reported that the normal angle of FIM angle is no more than 9°, the increased FIM angle implicates the hallux valgus deformity [184]. The correlates with HV severity following: mild (9°-11°), moderate (12°-17°), and severe ($\geq$ 18°). According to the measurement, the FIM angle increased with heel height elevation, and the tendency of increased angle is consistent with HV angle characteristic that has been described above. Additionally, there is a sharply increase of 23.9% found from 3cm to 5cm, and from 5cm to 7cm only increased by 3.2%. The FIM angle provides obvious evidence that there is at least a moderate risk of HV development in HHS population. The prevalence of HV in HHS population may continuously increase to the severity level when heel height is raised more than 7cm.
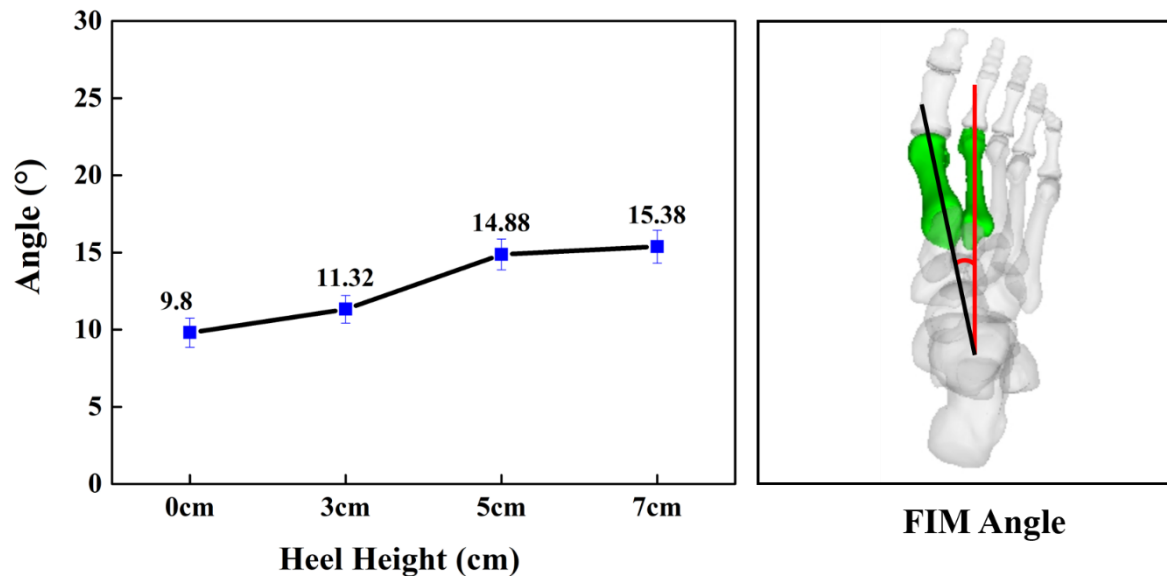
Fig. 3.8. The FIM angle variation among the four different heel height.

Fig 3.9 presents the metatarsal break (MB) angle, also known as metatarsal index, which is formed by the line from the most anterior point of the first metatarsal head to the most anterior point of second metatarsal head and another line from the most anterior point of second metatarsal head to the most anterior point of the fifth metatarsal head [183, 186, 187]. The MB angle is used to evaluate the length relationship between the first metatarsal and the rest of metatarsals, and has been classified into three categories: plus index indicates that the first metatarsal is at the distal end of the arc; plus-minus indicates that the distal end of the first metatarsal contact with the arc; minus index indicates that the first metatarsal head approaches the arc. Additionally, a minus index indicates increased bunion and (related) metatarsal pain due to increased load on the second and third metatarsal bones [186]. Also, the magnitude of the MB angle increases with relatively longer first and five metatarsals, and decreases with relatively shorten first and five metatarsals [187]. According to measurement, the angle variation of MB among different conditions is consistent with the changes of foot structure under HHS, that is, the arch height raised and forefoot segment shortened as heel height elevation. Therefore, the MB angle is reduced as heel height increased from 0cm to 7cm, but there was only a 4.5% difference between 7cm and 5cm.
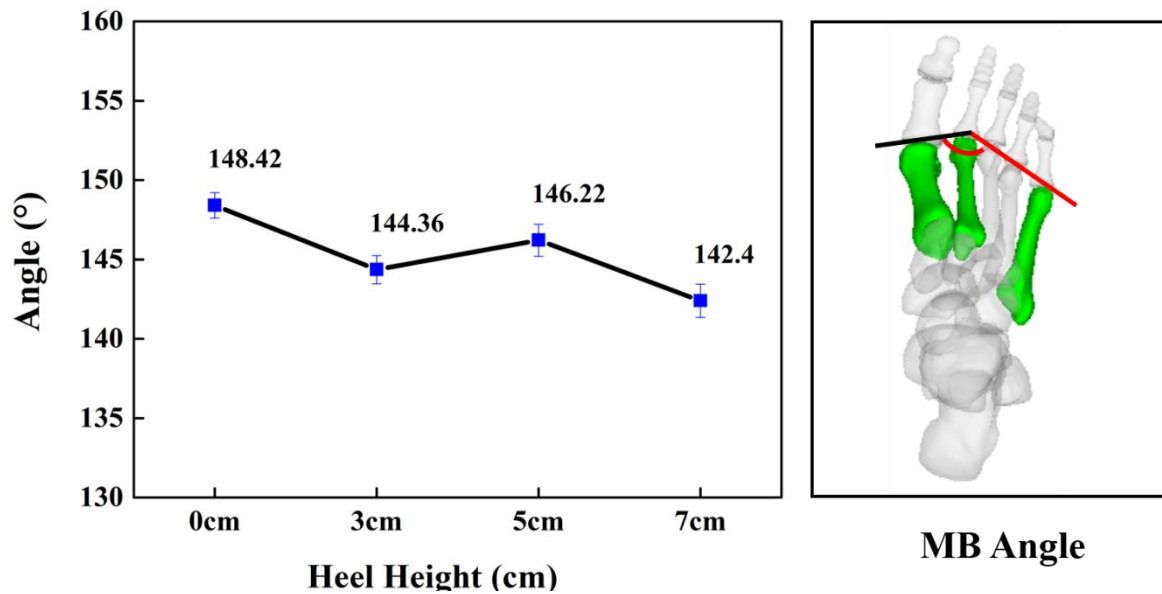
Fig 3.9. The MB angle variation among the four different heel height.

Fig 3.10 shows the first metatarsal declination (1MD) angle, which is defined as the angle formed by the longitudinal axis of the first metatarsal with respect to the supporting plane [163, 177, 183, 188]. The 1MDA is normally utilized to evaluate the primary metatarsal of hallux rigidus associated with the metatarsus primus elevatus [189], which is considered to be induced by wear and tear of the first metatarsophalangeal joint [190-193]. In terms of the patient with hallux rigidus, the most common surgical approach for treating the severity hallux rigidus is reducing the elevation of the proximal end of the first metatarsal [194, 195]. The normal 1MD angle has been defined as 20°-21° in the previous research [184, 196, 197]. Regarding the influence of the heel height on the magnitude of the 1MD angle, the results indicate an increased tendency of 1MD angle as heel height elevated from 0cm to 7cm. Additionally, there a sharply increased value of 57.0% is found from 0cm to 3cm heel height, 12.3% increase is found from 3cm to 5cm heel height, and 6.5% increase is found between 5cm and 7cm. The increase rate of 1MDA is decreased with heel height gradually elevated from 0cm to 7cm, this may be caused by the limitation of metatarsophalangeal joint motion range. The rigid metatarsophalangeal joint increased under HHS conditions, to provide a stable support on the lower extremity, its strength increases as heel height elevation.
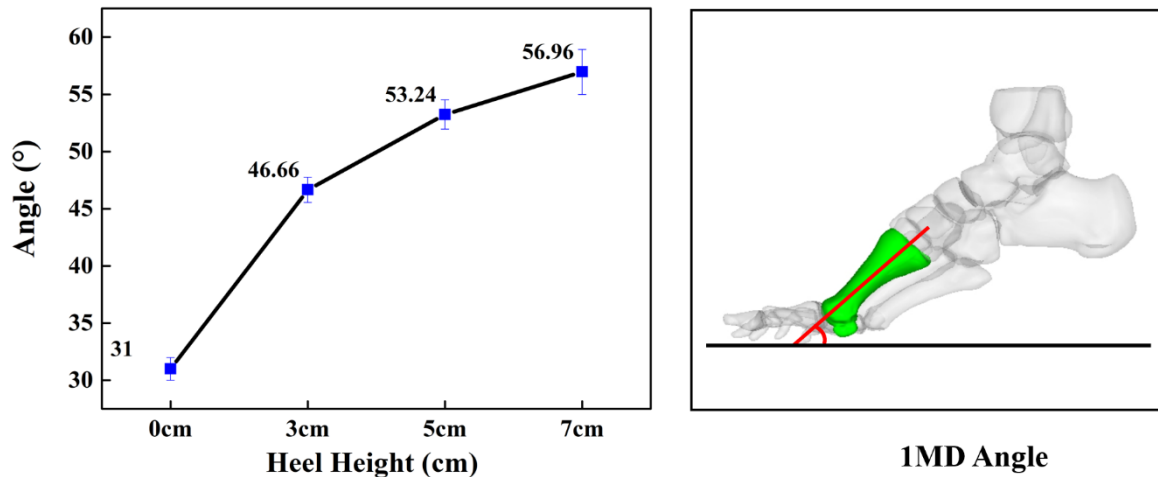
Fig 3.10. The 1MD angle variation among the four different heel heights.

3.4 Conclusion

Based on the 3D model reconstruction method, the high-fidelity 3D foot model in four different heel heights (0cm, 3cm, 5cm, and 7cm) has been built respectively, as a new perspective to provide the foot morphological details under HHS condition. According to the measured angle, the morphology of the longitudinal arch and the hallux valgus experience a dramatically modified by HHS as heel height elevation from 0cm to 7cm (average difference of 89.71% in the TFM angle; average difference of 18.56 % in the C1M angle; average difference of 71.5% in the HV angle; average difference of 36.28% in the FIM angle; average difference of 63.13% in the IMD angle), which result in a loss of the arch shock absorption ability and increase the risk of hallux valgus development. In addition, it seems that general foot deformity induced by HHS reaches a limitation level at the heel height of 5cm since there only a slight difference in the measured angles are observed from 5cm to 7cm when compared to other heel heights (average difference of 6.5% in the1MD angle; average difference of 3.2% in the MB angle; average difference of 2.4% in the C1M angle; average difference of 9.3% in the TFM angle).

4 MSM and FEM analysis on plantar fascia strain under HHS condition

4.1 Introduction

The plantar fascia is a rather complex and important structure, which has different biomechanical functions in gait, such as supporting transverse and longitudinal arch, facilitating force transmission between foot and ground, balancing weight-bearing distribution on foot, cushioning ground reaction force, preventing the foot from injury [47, 198-201]. However, any injury to plantar fascia inevitably affects the biomechanical function of the foot. In the United States, approximately 2 million people experience symptoms of heel and plantar pain due to plantar fascia injury yearly [198]. Known as plantar fasciitis, which is caused by excessive repetitive loading of the plantar fascia leading to microtears and inflammation of the calcaneal adhesions [202, 203], and it is a common complaint among women, especially those wearing HHS regularly [204].

It is evidence that wearing HHS adversely affects the musculoskeletal system, altering ankle-foot complex function, changing the force transmission pattern of a muscle tendon, interfering load distribution of the foot [72, 205, 206]. The length of the calcaneus to metatarsals is shortened in accompanied by arch rising under HHS conditions, leading to a change in arch morphology, transferring a greater portion of weight-bearing to the forefoot, reducing the plantar contact area of midfoot, leading to increased contraction and tension force on plantar fascia [207]. Khodair and Younes investigated the relationship between the plantar fasciitis pathology and HHS wearing in 40 female patients with resulting heel pain, they reported that 30 patients had fascial edema at calcaneal insertion and plantar fascia thickened; signal intensity in plantar fascia increased in 21 patients, which are characteristic signals of plantar fasciitis [208].

On the contrary, there are different opinions about the effect of HHS on plantar fascia strain. Some investigators have suggested that the appropriate heel elevation was beneficial in the treatment of plantar fasciitis on account of the plantar fascia tension could be temporarily reduced by heel raising [209, 210]. It was believed that the angle discrepancy between the hindfoot and metatarsus decreased under HHS, which allowed more movement of the

forefoot in the plantar-flexion position, and reduced fascia tension [209]. Recently, Yu et al. investigated the effect of heel height on strain-stress on the plantar fascia using FEM, its total tension force was reduced by 77.3% as heel height raised from 0 to 5.08 cm during balanced standing [18]. However, the plantar fascia in this research was simply represented by a one-dimensional (1D) linear truss element, which may overestimate its elastic modulus resulting in an inaccurate plantar fascia strain [198, 211].

Accordingly, to address the controversial views of the tension force in plantar fascia as the main crucial biomechanical concern in foot pathological in HHS population, to further understand the influence of heel height on plantar fascia tension, a solid 3D plantar fascia modeling is established. In this experimental, the effects of HHS with three different heel heights (3cm, 5cm, 7cm) on the strain-stress variation of 3D plantar fascia by using a combination of FEM and MSM analysis. Comparison of 3D and 1D digitization of plantar fascia, with 1D of plantar fascia created by linear truss elements that simply connect the heel and five proximal phalanxes was carried out.

4.2 Methods

In this study, a healthy female (age: 26 years old; height: 165cm; weight: 53kg) with no sign of musculoskeletal pathology and lower limbs injury was recruited. For data acquisition, gait capturing 3D motions of the subject wearing HHS in three different heel heights (3cm, 5cm,7cm), and each gait corresponding to relevant muscle forces and strain distribution in plantar fascia were computed using MSM and FEM, respectively.

4.2.1 MSM analysis during HHS gait with different heel height
Gait analysis

The gait analysis was used to drive MSM. A Vicon motion capture system (Oxford Metrics Ltd., Oxford, UK) consisting of 8 cameras and two AMTI force platforms (Watertown, MA, United States) was utilized to capture the kinematic and kinetic of lower extremities during HHS gait. The kinematic and kinetic data were measured synchronously at frequencies of 100 Hz and 1000 Hz respectively (Fig 4.1). The marker set was placed on the subject's various lower extremities key points according to generic GaitModel 2392 in Opensim. One

static standing trial and 6 successful walking trials were captured on each heel height condition. For walking trail data acquisition, the subject walked through the motion capture area in a straight direction at self-selected speed with both feet stepping entirely at the force platforms. The captured representative data of 6 trials of each heel height were selected for musculoskeletal modeling analysis.
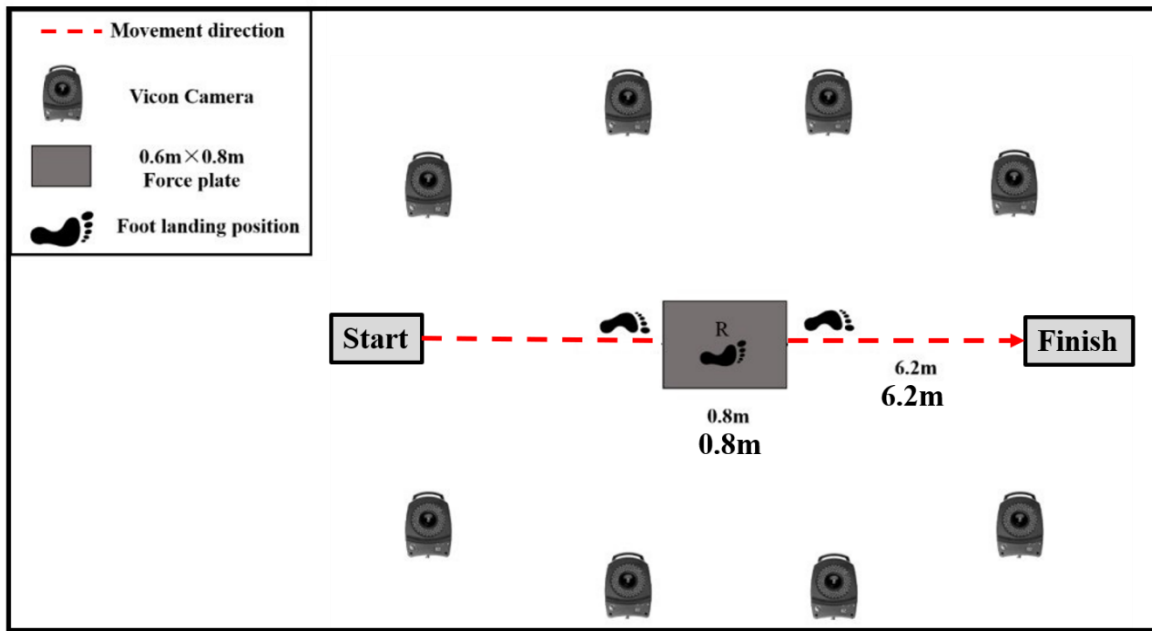

Fig 4.1. Experimental set-up.

EMG measurement

In this experimental, the muscle activity was acquired from EMG signals that were captured by Delsys system (Delsys, Boston, MA, United States), involving gastrocnemius (GC), tibial anterior (TA), and soleus (SL), these three muscles play an important function on ankle joint control under HHS condition. The EMG was conducted at a frequency of 100Hz, band-pass filtered between 16 to 380Hz. In addition, a low-pass filter with a 10 Hz frequency was utilized to smooth EMG signals (Fig 4.2). The amplified EMG signals obtained from experimental measurement can be used to compare with simulated muscle variation in the OpenSim, which serves as efficient validation for MSM model.

Fig 4.2. The Delsys surface electromyography devices.

MSM simulation in OpenSim

To calculate the relevant muscle forces in the lower lime, GaitModel 2392 as a generic MSM was selected in Opensim. The GaitModel 2392 has 10 main rigid body segments, 23 degrees of freedom, and 92 musculotendon actuators to represent 76 muscles in the lower limbs and torso [211]. Three major extrinsic muscle groups of lower extremities: -GC, SL, and TA for foot movement were digitized. GC and SL play important roles in ankle plantarflexor and TA produces major dorsiflexion moment to the ankle during gait [212].

The kinematic data and GRF in 3cm, 5cm, and 7cm heel height condition was converted into Opensim from the Visual 3D (V3D) to calculate the muscle forces. The following process was performed in Opensim: the selected musculoskeletal modeling was scaled to accommodate the height and mass of the test subject with adjusting muscle attachments and length. The scaling process is performed as follows: the model anthropometry is adjusted by a scale tool to match a particular subject. Scaling is typically performed by comparing the position between the experimental makers and virtual markers on a model. Then, the residual reduction algorithm was applied to match the coordinates of the model which drives the generalized coordination of the dynamic musculoskeletal model toward the desired kinematic trajectory. The workflow of the MSM establishment is shown in Fig 4.3.
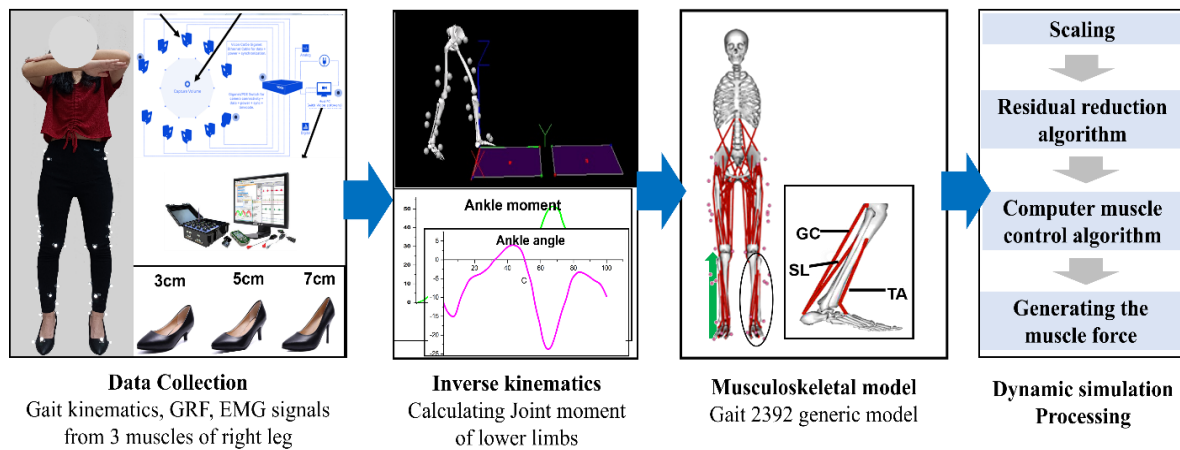
Fig 4.3. The workflow of MSM establishment using OpenSim.

4.2.2 Development of the FEM

Geometry model construction

CT scan was performed on one subject using a 3.0-T SIEMENS MR system, and the images of the sagittal, coronal, and transverse planes were collected (repetition time:4.11s; slice thickness:1mm; and matrix:320x260). Before CT scanning, the foot health of the participant has been carefully checked by an experienced physician and it was found that the participant is free from any disease and injury. To place the foot in a neutral position during CT scanning, a custom-made ankle foot orthosis was utilized to fix the foot (Fig 4.4).

Fig 4.4. CT scanning was performed on the right foot with a custom-made ankle foot orthosis fixed in an HHS shoe.

The geometrical shapes of the right foot model were segmented based on the CT scanning pictures of the participant using Mimics 18.0 (Materialise, Leuven, Belgium). The boundary of each boney and soft tissue was obtained by Mimics tool and a 3D surface model of each bony and soft tissue was created including 28 bones and 1 encapsulated soft tissue (Fig 4.5).

The distal phalanx is merged with the middle phalanx, and the sesamoids were merged with the first metatarsal. The bony and soft tissue model was imported into the software of Geomagic Studio (Geomagic Studio) which is a reverse engineering and scanning software, that provides a series of options to modify and smooth model, then create the solid model. The solid model of bone and soft tissue was imported into SolidWorks 2016 (SolidWorks Corporation, Massachusetts) to construct cartilage, encapsulated soft tissue, and 3D plantar fascia, in which cartilage was generated based on areas of 2 adjacent segmented bones, encapsulated soft tissue was generated by subtracting the bony and cartilage, and plantar fascia was generated according to the anatomical atlas [213], starting from the calcaneus tubercle, separating into five branches extend to the five proximal phalanges.

In addition, the major muscle, tendon, ligamentous structures were also involved, the insertion position of these structures were based on the Interactive Foot and Ankle (Primal Picture Ltd., London, UK, 1999), and three muscle groups GC, TA, SL, and 20 ligaments and Achilles tendon together with the plantar fascia connecting the corresponding points, were modeled as 1D linear truss elements (Fig 4.5). All the ligamentous, tendon, cartilage, and bony structures were embedded in the bulk volume of the encapsulated soft tissue.
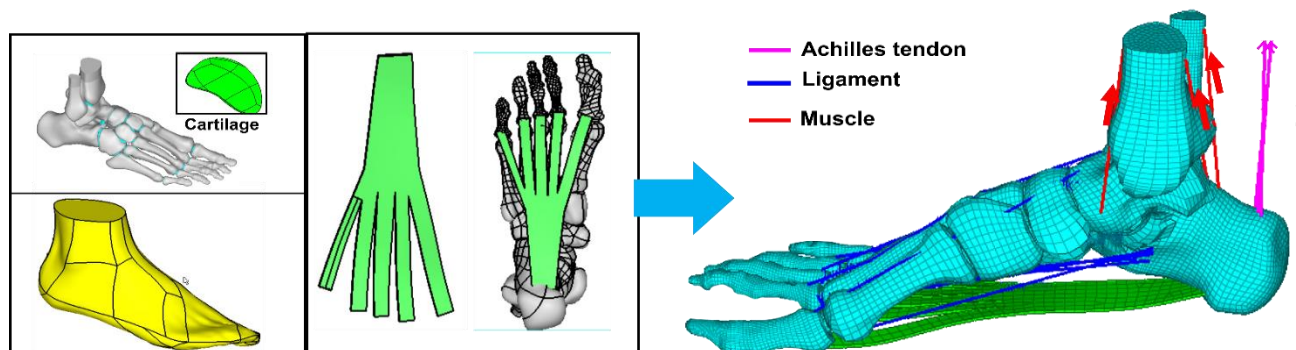

Fig 4.5. The solid components include bone, soft skin, cartilage, and the 3D plantar fascia, while the 1D linear truss elements include the Achilles tendon, ligaments, and muscles.

Then the HHS was also created in SolidWorks, three different heel height was generated. The shoe size was 37 EU properly fitted participant foot. To simplify the simulation, only the shoe sole was included, which is comprised of two components: heel and sole (Fig 4.6).
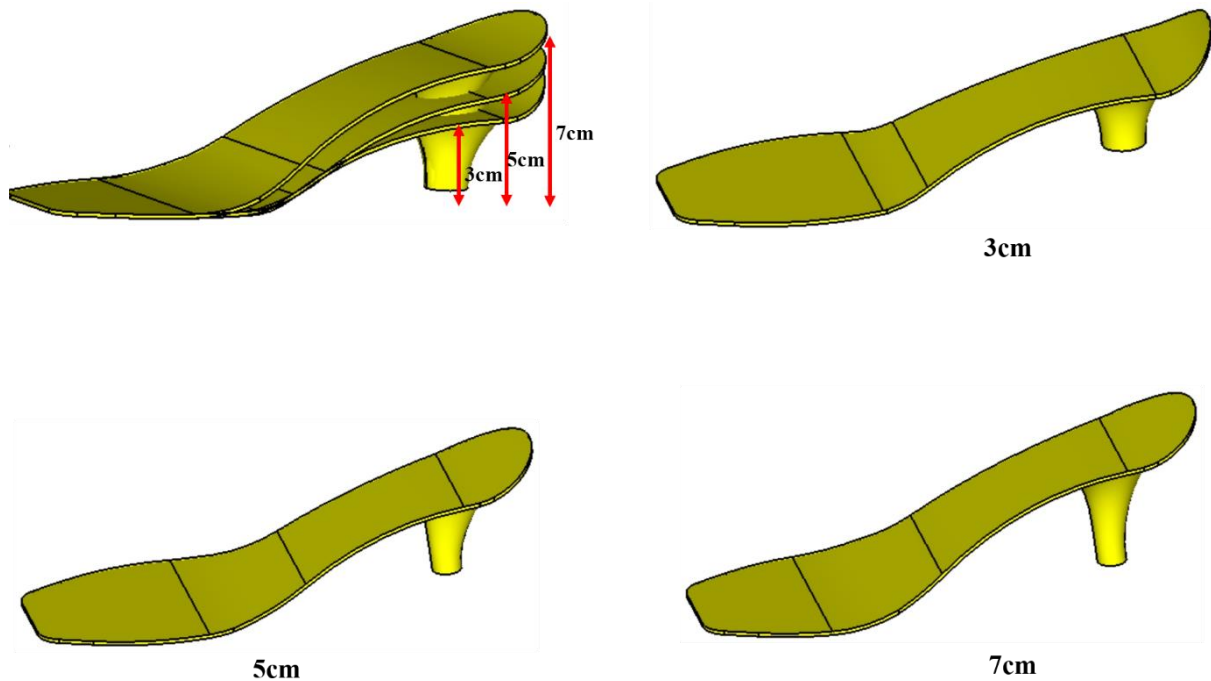

Fig 4.6. HHS model in three different heel height.

Geometry mesh and element assignment

The foot model predominately meshed with hexahedral elements with less than 5% of tetrahedral elements in Hypermesh (14.0). Hexahedral elements usually provide an equivalently accurate and efficient solution with less computational cost. However, it is difficult to automatically generate the hexahedral due to the irregular shape of bony and encapsulated soft tissue. Thus, the irregular bony and encapsulated components were sectioned and re-meshed manually to improve the quality of the mesh with an aspect ratio of 3D element close to 1, and a Jacobi ratio of 0.6 [136]. The mesh size of the bone and encapsulated structure referred to previous literature, which was assigned as 8mm [136].

The mesh size of 3D plantar fascia was determined by a sensitivity test, and the sizes of the elements were gradually reduced until the variation of force-displacement is less than 3% between the two size meshes [136]. The second-order element was assigned to the plantar

fascia structure since plantar fascia is mainly targeted for simulation, and the first-order element was assigned to the bone, cartilage, and encapsulated structure to reduce the computational cost. The element of ligament, muscle, and Achilles' tendon were defined by bar using a 186 solid element with lineally property, the sectional width was assigned to 2mm in the Hypermesh.

Material properties assignments

To simplify the complexity of the model, the components including bone, ligament, cartilage, muscle, and Achilles' tendon was idealized as homogenous, isotropic, and linearly elastic material (Table 4.1). Additionally, the encapsulate soft tissue was defined as nonlinearly elastic based on the uniaxial stress-strain curve measured by Lemmon et al.1997 shown in Fig 4.7 [214].
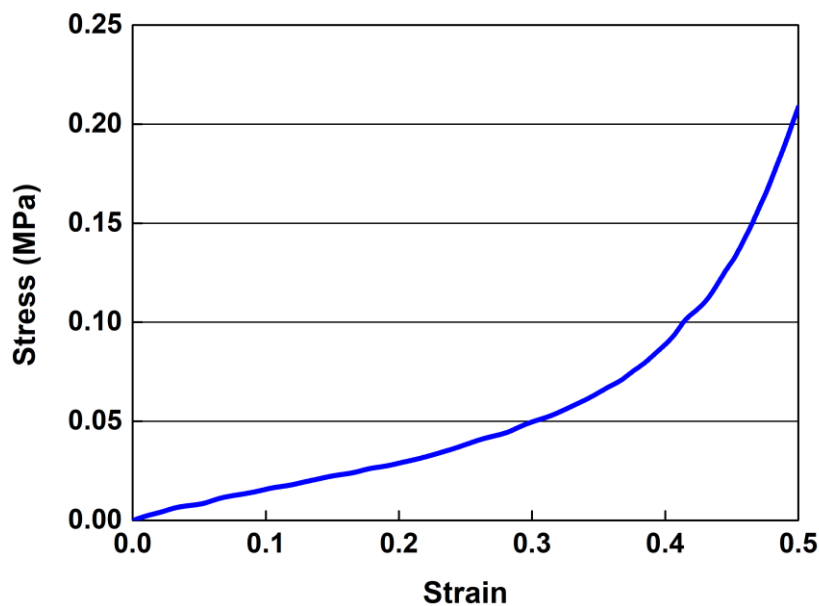

Fig 4.7. Stress-strain curve for bulk soft tissue [214].

To quantitively describe the nonlinear material, the hyperplastic material model was used in Ansys (ANSYS, Inc., Canonsburg, USA), and the coefficients of the hyperplastic material model of the second-order polynomial were obtained from a previous study. Table 1 shows the material property of shoes, bone, muscle, plantar fascia, cartilage, ligament, Achilles tendon, and encapsulated soft tissue, as previously reported [214-217].

Table 4.1. Material properties of the components in the finite element model.

	Elastic modules (Mpa)	Poisson ratio	Cross-section (mm^2)	Mass density ρ (kg/m^3)
Bulk soft tissue	second-order polynomial strain hyperelastic model (C_{10}=0.8556, C_{01}=0.05841, C_{20}=0.03900, C_{11}=0.02319, C_{02}=0.00851, D_1=3.65273)			-
Bone	7300	0.30	-	1500
Sole	200000	0.42	-	7800
Ligaments	260	-	18.4	-
Cartilage	1	0.40	-	1050
3D plantar fascia	350	0.45	-	-
1D plantar fascia	350	-	58.6	-

Boundary and loading condition

The loading condition during walking in FEM simulation was determined from the experimental data of the participant. Three instants (GRF first peak (25% stance phase), the GRF valley, (45% stance phase), and the GRF second peak (60% stance phase)) of the stance phase were used to drive the foot model.

Before the simulation runs, with the sole of shoes fully restrained, the foot model was paced as heel strike position with an angle between the plantar and sole set at 20º, which was the angle acquired experimental data between the sole of the shoe and the ground. With the tibia set as the axis of rotation defined by the load joint option in Ansys, an inclination angle of the tibia relative to the ground of 0º was set as the initial first peak stance condition. The tibia was further rotated about the X-axis from 0º to 25º relative to the vertical ground axis (Figure 3(a)) to define the mid-standing stance and second-peak stance conditions, and the

rotation moment function described by the ankle moment in the sagittal plane. In the analysis, the foot FEM model translation and rotation in coronal and transverse planes were not considered. For the surface between the sole and the forefoot, a friction coefficient of 0.6 was defined [218], and the respective GC, SL, and TA forces acquired from the MSM at three stances were applied, with Achilles tendon forces obtained from previous research applied [218]. The Transient Solver was selected in Ansys to avoid convergence problems. The loading and boundary conditions of the foot simulation was shown in Fig 4.8.
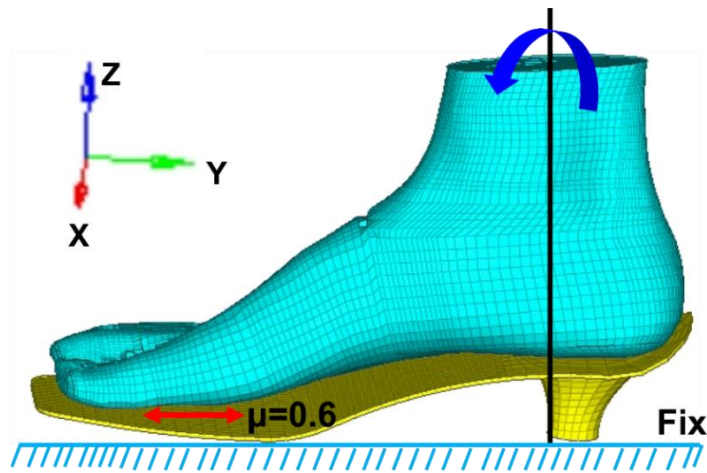
Fig 4.8. Loading and boundary condition of the foot on the high heel sole (present in 3cm heel height).

FEM validation

The validation was conducted by comparing the plantar pressure of the experimental measurements and FEM predictions in three different stances phase of three different heel height conditions. Firstly, the plantar pressure was measured by an in-shoe system (Novel Pedar System, Novel GmbH, Munich, Germany) during the HHS gait in each heel height condition with each corresponding peak contact pressure recorded. Secondly, both experimental and predicted maximum contact pressure in 9 plantar regions (big toe, other toes, 3 equally divided regions in the forefoot, lateral and medial of midfoot and hindfoot) were collected. Then by applying Pearson correlation, $|r|$, the agreement between predictions and experimental measurements of 18 data pairs were compared. Value of $|r| \leq 0.35$, $0.36 \leq |r| \leq 0.67$, and $0.68 \leq |r| \leq 1.0$ represent weak, moderate, and strong correlation, respectively

[219]. The predicted tension of 1D plantar fascia was compared with existing research, as well as muscle force in GC, SL, and TA.

4.3 Results and Discussion

Muscle activation validation between the EMG and MSM

The muscle force measured by EMG was qualitatively compared with MSM-based muscle activations to validate the simulation model. The three-muscle force during HHS gait cycle with different heel heights (0cm, 3cm, 5mc, 7cm) was presented, and the comparison results are shown in Fig 4.9. The simulated muscle activation shows a good agreement with EMG recording during a gait cycle.
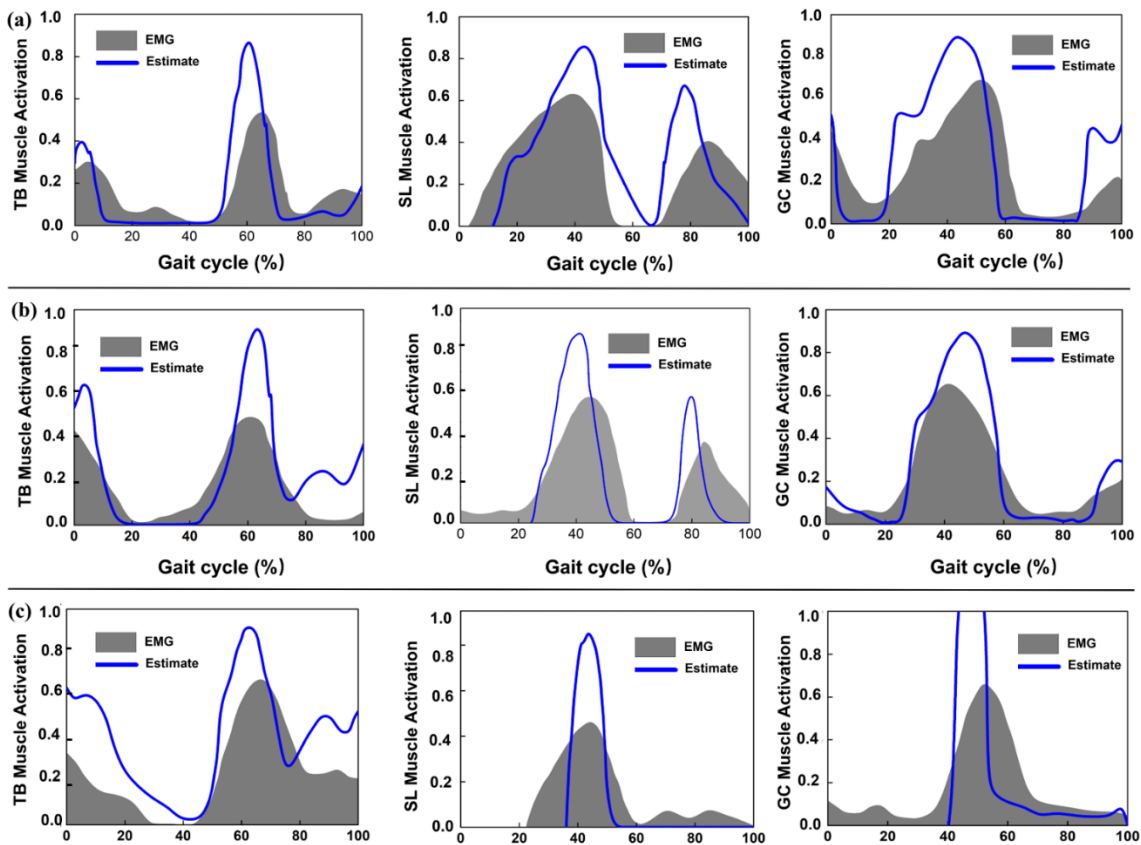
Fig 4.9. Muscle activation between an estimate and EMG signals during HHS gait in different heel heights; (a) shows 3cm heel height gait; (b) shows the 5cm heel height gait; (c) shows the 7cm heel height gait.

FEM Validation

Fig 4.9 (b and c) showed the plantar pressure distribution of 3-cm heel heights condition obtained from the FEM prediction and the experimental measurement in three stance phases. Correlation analysis showed a high linear relationship between the FEM prediction and measurement ($r=0.83$; confidence interval:95%, 0.57-0.90; $P<0.002$). The difference between experimentally measured and computationally estimated is 14% in first-peak, 13.8% in mid-standing, and 28.6% in second-peak. Fig 4.10 showed the muscle forces calculated by Opensim compared with previous studies, the graphs show similar corridor trends [212, 220]. Lastly, the variation range of predicted strain in 3D and 1D plantar fascia models at mid-standing is 3%-5.7%, which was consistent with previous measurements [209]. Based on these validations results, our simulation results are considered to be reliable.
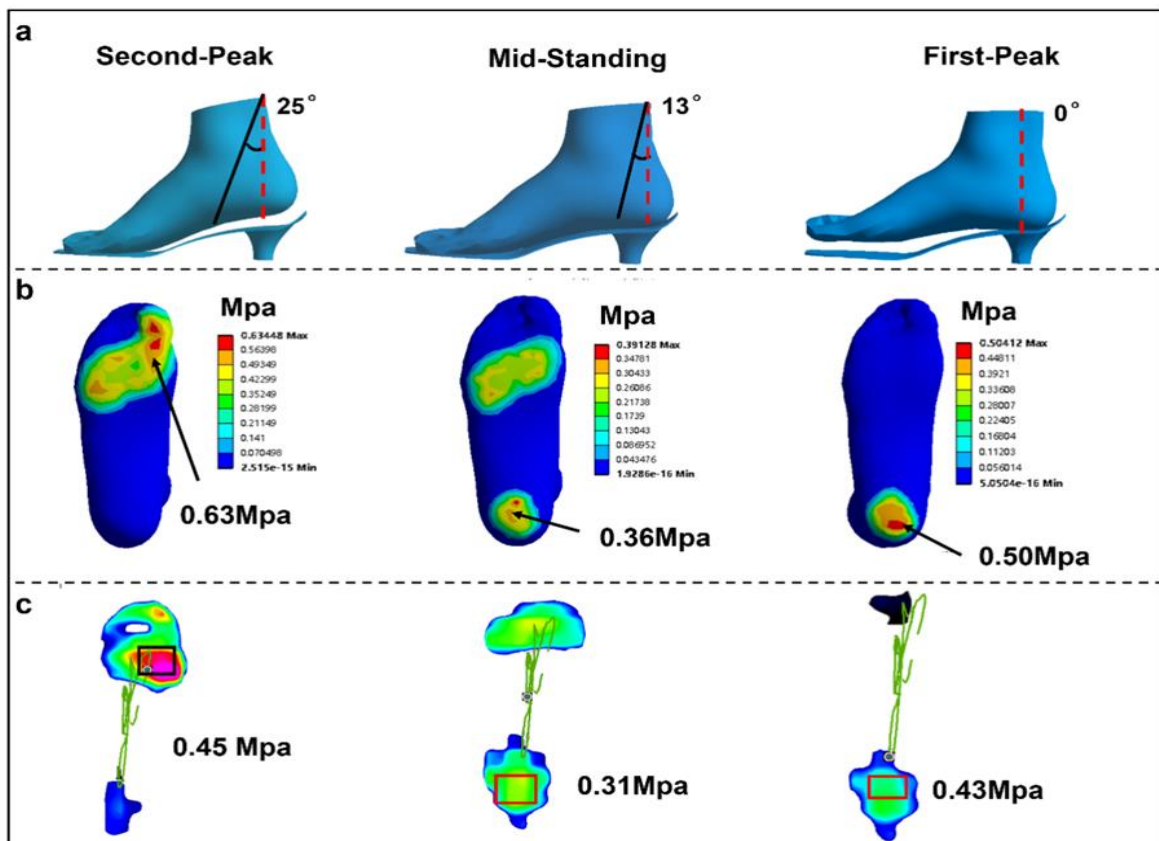

Fig 4.10. (a) the different stance phase of HHS gait, (b) FEM predicted, (c) plantar contact pressure in experimental measurement.

The muscle activation pattern in HHS gait with a different heel height

The major activity of GC force appeared in the mid-stance phase, the peak muscle activation of GC occurred in the post midstance, and the second greatest level of GC activity occurred in the terminal swing phase. The peak amplitude was significantly increased with heel height elevation, the highest GC amplitude occurred at 7cm heel height. Furthermore, in comparison with barefoot, GC force is increased by 56.5% in 7 cm heel height. Then, compared with the heel height of 3cm and 5cm, GC force in 7cm heel height was increased by 35.7% and 17.3%, respectively.

The SL presents a similar trend with GC amplitude from the midstance to toe-off phase. The major SL activation occurred on the midstance, reached the maximum value at post midstance in all gait conditions, then gradually decreased at toe-off phase. During mid-swing phase, SL reached to the second greatest level. And all gait conditions exhibit the same activation pattern in SL muscle. In addition, there is a dramatic increase of SL force as heel height increased, 88.7% of the increase in 7cm when compared with 0cm. Followingly, decreased by 77.5% and 48.5% in 7cm when compared with 3cm and 5cm respectively. On the other hand, the maximum amplified of SL is significantly higher than that of GC muscle force, it seems that the SL muscle plays a more important role in propelling the body move forward then GC muscle.

The major muscle activity of TA occurred around the time of toe-off, the maximum magnitude of TA force in all gait conditions appeared at 60% of stance phase, fell away rapidly at pre-swing phase, then increased lightly at 80% of stance between the mid swing and terminal swing phase. In contrast to GC and SL activation pattern, TB amplified is gradually increased as heel height elevated from 0cm to 7cm, and the highest TA muscle force is occurred on 7cm heel height during heel contact and swing phase. However, there no significant difference was found in peak TA force among four gait conditions.

The findings in present study are consistent with the report of Stefanyshyn et al. evaluated the biomechanical response of kinematics, kinetics, and EMG in HHS gait with various heel height (1.4cm, 3.7cm, 5,4cm, and 8.5cm) [16]. It was reported a systematically increased in

the GRF, ankle joint flexion, and knee joint flexion angle, then SL muscle activation showed a graded response as heel height elevated.

During HHS walking, the body's COM is elevated and shifts toward, this may impose the plantarflexors to produce greater torques to take off during movement, possibly, to offset the destabilizing influence induced by the altered GRF vector, this could explain the consequence of the GC and SL muscle force reached to peak at pre-toe-off phase during HHS gait. Furthermore, both the GC and SL is activated in a plantarflexed position under HHS condition, and it plays an important role to generate the push-off force propelling the body to move forward. Also, as a result of the plantarflexion increase caused by HHS wearing, the length of the moment arm of the AT is decreased, then muscle of SL and GC tends to increase stabilizing the ankle joint.

The muscle force is considered to be affected by the physiological cross-sectional area that reflects the amount of sarcomere, and fascicle length that defines the length-force relationship of the muscle [221, 222]. Csapo et al. investigated the effects of HHS wearing on the anatomical function of calf muscle MTU, and indicated that muscle fascicles can be shortened by HHS wearing in a long term, and accompanied by increased Achilles tendon (AT) size and stiffness [3]. They also observed that the length ratio between the tendon to fascicle is 14% greater in HHS group compared to the control group. The length ratio is widely used to measure fascicles shortening during isometric contraction [223], it shows the compliance extent of the MTU, as well as the sarcomere variation [224]. Consequently, the shortened length ratio of tendon to fascicles reflects the contacted calf muscle under HHS conditions. In additional, the length of the calf MTU is decreased by the ankle plantarflexion under HHS conditions, which could be further decreased as heel height elevation. Previous studies have shown that the reduction in sarcomere number caused by shorter MTU length represents the muscle's chronically adaption [225]. Indeed, hindfoot is lifted by HHS wearing and posing the plantarflexor MTU at a relatively shorter length, which also could increase the tension around the GC and SL muscle, and an adequate level of tension in the MTU is needed for force transmission and proprioception control.

Changing of strain value on plantar fascia among different heel height

As predicted strain distributions of plantar fascia from FEM simulations showed similar patterns for three different heel heights in three different stances, Fig 4.11a showed the typical strain distribution pattern on plantar fascia in 5-cm heel height condition. The two end portions of 3D plantar fascia tied to the bones at the proximal and distal regions were excluded to avoid excessive deformation, and the remaining region of the 3D fascia was divided equally into proximal, medial, and distal regions. FEM prediction results showed heel height had a significant effect on the strain level of fascia in the three stances phase.

For the strain level of the plantar fascia, irrespective of heel heights, at the first peak and mid-standing phases, the middle and proximal regions experience a similar level of higher peak strain on fascia than in the distal region. At the second-peak phase, the plantar fascia strain presents the highest value in proximal region, followed by distal region with the lowest strain in the middle region.

For different heel heights, the simulations predicted different plantar fascia strain distributions at different regions irrespective of stances phases. Fig 4.11d showed highest plantar fascia strain occurred in the second peak stance phase. In this stance phase, in the proximal region, the peak strain increased by 102% for heel heights of 3cm to 7cm. For heel height raised from 3cm to 5cm, the fascia strain increased by 26.1 %, and there is a sharp increase of 60.3% from 5cm to 7cm of heel height.

However, for the model with fascia modeled as 1D truss elements, there are no distinct three regions as defined for 3D fascia. The peak strain in 1D fascia is smaller than 3D fascia in all three different heel heights in all different stance phases.
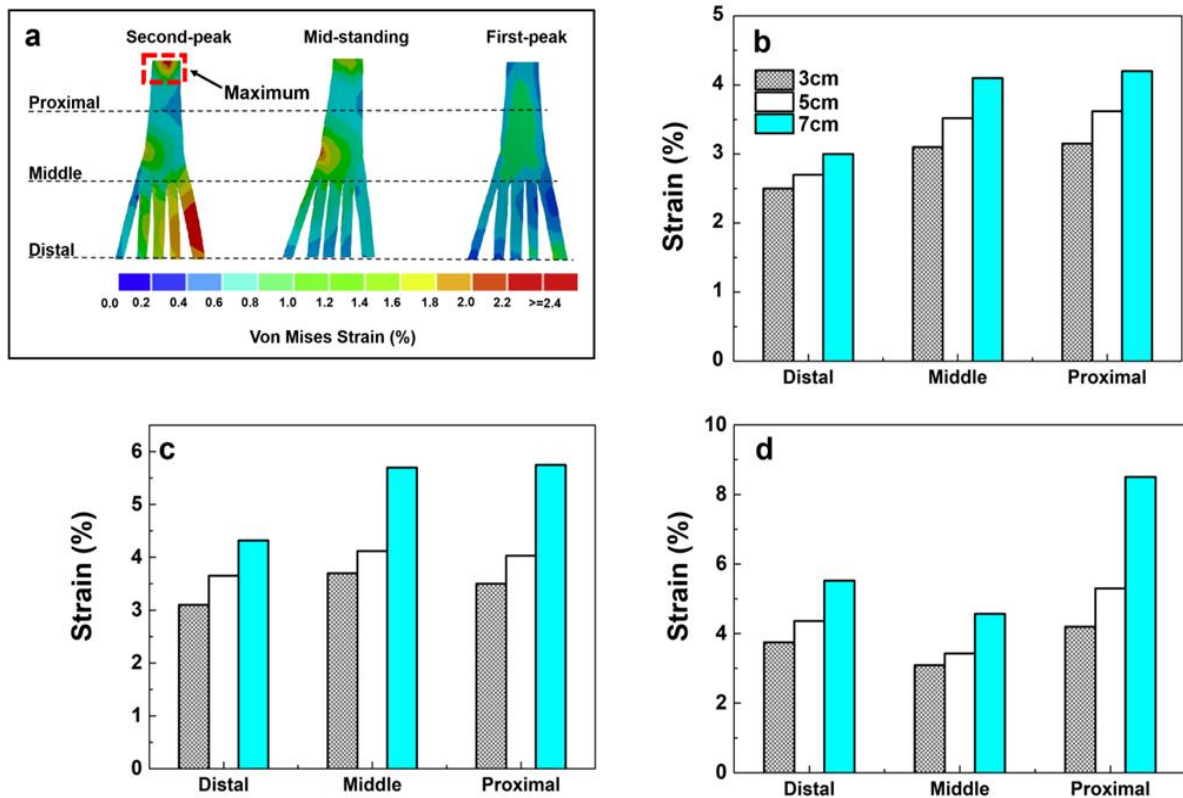
Fig 4.11. The peak 3D fascia strain for three heel heights in three gait events, (b) First-peak phase, (c) mid-standing phase, (d) second-peak phase.

Discussion

Due to the complex interaction between foot movement and internal components, it is difficult to investigate the biomechanical mechanism of plantar fascia from vitro measurements. Therefore, establishing a realistic plantar fascia simulation method is the premise to understand the biomechanical response of plantar fascia under HHS conditions. In this study, a combination method of FEM and MSM was used to evaluate the strain characteristics of plantar fascia during HHS walking in three different heel heights.

The opinions on heel elevation as a treatment approach for plantar fasciitis is questionable based on the results of this study. The plantar fascia strain progressively increased in both 3D and 1D modeling when heel height elevated from 3cm to 7cm. The highest strain was found at the 7cm heel height, the lowest was found at 3cm heel height, and there was a sharp increase of 60.3% from 5cm to 7cm of heel height. However, the findings differ from previous reports [18]. Yu et al. indicated that the average tension force and strain on plantar

fascia decreased from 151.0 N (strain: 0.74%) to 59.6 N (strain: 0.28%), which was reduced by 60.5% and 62.2% respectively when the heel height elevated from 0 cm to 5.08cm during balanced standing with HHS, then there was a remarkably increased from 5.08cm to 7.62cm of heel height. They suggested that the strain of plantar fascia could be decreased by an appropriate heel height. According to Yu et al., the 1D element of plantar fascia was used in their simulation, this simplification did not take into account the complex relationship between ligaments and articular surfaces. In terms of foot structural complexity, the biomechanical response of plantar fascia under loading is different in the lateral and medial aspects, and it may be responsible for limiting the predicted loading result in an abnormal plantar fascia strain when it is depicted as a 1D truss [213]. Therefore, a more comprehensive 3D modeling could provide insight into the biomechanical response of the plantar fascia variation under HHS conditions. In our study, 3D fascia modeling shows a higher average strain than that of 1D fascia at all heel heights, and strain variation of the entire 3D fascia structure can be demonstrated. The peak strain of plantar fascia in the proximal region was larger than that of the middle and distal portion in three different heel heights, especially at the second peak phase. The results were consistent with previous reports that stress and strain were concentrated on the medial calcaneus tubercle, close to the site of heel pain [226]. However, this strain response does not appear in the current1D fascia model or the previous linear fascia model.

Meanwhile, the predicted results of this study are different from previous cadaver experiments, in which plantar fascia strain decreased gradually from heel height of 2cm to 6cm [209]. According to the cadaver investigation, the heel elevation was achieved by a contoured platform with a shank profile located in the mid-region, which simulates the inner weight-bearing surface of shoes, and provides complete support for the foot arch. The decreased plantar fascia strain was induced by an extended shank profile from under the calcaneus to the cuboid, this may be enough to relieve severe symptoms of plantar fasciitis [209]. Researchers have suggested that the load transmission pattern could be changed by shoe interface configuration, further affecting the strain response of plantar fascia [75, 209, 227]. Differently, in our study, stilettos shoes with narrow base support were used which

could lead to plantar pressure concentrating on the hindfoot and forefoot as well as reduce the contact area on the mid-foot [228]. Furthermore, the arch is raised passively and reached its limit of flattening with toes flexion that requires greater muscle force to keep body posture stability under stilettos shoe condition. However, maintaining the posture under HHS condition demands a higher-level activity on intrinsic muscles that becomes inadequate, especially in terms of a long period using HHS that muscles are easily prone to fatigue [229]. Thus, plantar fascia is more likely to experience tightness and obtain higher tension force. The appropriate heel elevation may contribute to strain relief on the plantar fascia, but it certainly does not refer to HHS with narrow heel base support. In further research, the influence of different sole structures of shoes on plantar fascia strain and tension force should be investigated.

On the other hand, the peak strain on plantar fascia reaches the maximum at second peak stance compared with the first peak and valley stance phase. Under HHS conditions, the MPJ keep in a dorsiflexion angle progressively increased with heel elevation. Healey and Chen, demonstrated that the increased MPJ dorsiflexion as a result of the elevated hindfoot is a compensation mechanism to stabilize body posture [150]. However, the larger dorsiflexion angle of toes could increase tension force on plantar fascia due to the "windlass mechanism", which has been well described by Hicks in 1954 [50]. During the push-off phase, the toes are forced into an extended position as toe-standing, the plantar pad is pulled forward, then it moves the attached fascia anterior, contributing to a relatively shorter longitudinal arch. Therefore, plantar fascia will be subjected to greater tension force when the forefoot makes a push on the ground during the gait. In a cadaver model test, Erdemir et al. observed that plantar fascia tension gradually increased during stance, and reached the maximum at the late stance phase [230].

Certain limitations in this research should be discussed. Firstly, the realistic simulation of the mechanical behavior of plantar fascia is important for plantar fascia biomechanics response and the effect of pathological condition. But the material properties of ligament, cartilages, and plantar fascia were idealized as linearly elastic, to compare simulation results

with the previous one [218], thus the same material properties were adopted and the hyperelastic or viscoelastic behavior was ignored here. Although this consideration could reduce computational costs and complexity, the simplified material properties may negatively affect internal strain distribution on the plantar fascia. As for how different material models may affect the strain distribution of plantar fascia in specific applications, such as HHS conditions, further research is needed. Secondly, only extrinsic muscle forces were involved in this simulation, while other intrinsic muscles were not considered. Such as flexor digitorum brevis muscle that was longitudinally adhered by the central plantar fascia, its absence may adversely affect the accuracy of fascia strain value. Thirdly, FEM analysis is always limited to a specific subject and does not take into account differences in individual foot morphology. Lastly, the model gait 2392 we used here that limits DOFs at the ankle joint, the more detailed foot model should be used in future research to evaluate the foot function related to pathology.

4.4 Conclusion

For muscle activation pattern during HHS gait, there is a graded response in the GC and SL muscle activation pattern as heel height raised from 0cm to 7cm, but not found on TA muscle. The peak amplified of GC and SL muscle appeared at 40% of stance which is post midstance phase, plays a role in the push forward during HHS gait, as well as stabilizes the ankle joint. Additionally, the higher muscle activation pattern in GC and SL could beneficial for force transmission and proprioception control during HHS gait.

A 3D FEM model of plantar fascia has been established to explore the effect of heel elevation on plantar fascia internal loading during HHS walking, as well a 1D plantar fascia model was created for comparison. The results from the present research could reveal the strain variation on the plantar fascia and facilitate understanding of potential causes of plantar fasciitis induced by using HHS. According to this study, 3D plantar fascia could reflect the entire biomechanical change on plantar fascia than 1D, and provide a reliable strain distribution on plantar fascia under HHS conditions. The strain on the plantar fascia in this study was progressively increased instead of reducing as heel height raised from 3cm to 7cm. The trend of increased strain on plantar fascia under HHS conditions is more in line

with the "windlass mechanism". Meanwhile, the higher strain on the proximal region of fascia provides evidence for plantar fasciitis development in the HHS population. Proper heel elevation may help to relieve plantar fascia tension, but it certainly does not refer to HHS with narrow heel support. Therefore, the HHS as a treatment recommendation for plantar fasciitis is questionable. Considering the foot morphology as a determinant factor in load transmission patterns that can be shaped by footwear, the variation sole structure of shoes should be investigated in the future to quantify the effect of different force transmission patterns on the plantar fascia.

5 Conclusion and further work

Conclusion

It is unavoidable for most women to wear high heels in their daily lives in pursuit of beauty or to attend social events, despite widespread warnings from international medical associations about the adverse health effects of HHS wearing. Numerous studies have been conducted to explore the biomechanical change on the musculoskeletal system induced by HHS, to reveal the potential relationship between HHS wearing and injury/disease, to provide suggestions for HHS related pathological treatment. However, some limitations remain unsolved, such as how HHS affects the kinematic characteristic of foot multi-segment during gait, how HHS causes foot structure deformation in different heel height, how HHS affects plantar fascia biomechanical response in different heel height. Therefore, the purpose of this thesis is to address those questions using a comprehensive complex method.

Firstly, biomechanical characteristics of the hallux, forefoot, and hindfoot segments under HHS conditions has been investigated using a multi-segment model (Oxford foot model). The major findings revealed a significantly higher dorsiflexed movement in the hallux and higher adduction movement in the forefoot segment during HHS gait compared to barefoot gait. The combined effect will cause hallux being twisting outwardly, while the forefoot will be twisting inwardly during HHS. This mechanism could create a propagating, long term trauma that eventually ends in hallux valgus or "bunion".

Secondly, a high-fidelity 3D foot model under HHS condition with four different heel height (0 cm, 3 cm, 5 cm, and 7 cm) has been built respectively. Foot morphology has been described by 8 parameters, about the forefoot segment, the longitudinal arch height, and the calcaneus segment. These angle measurements provide an intuitive view and comprehensive understanding of foot morphological change caused by HHS. The major findings demonstrated that the calcaneus segment remained relatively stable as heel height increased from 0cm to 7cm, longitudinal arch height significantly increased and the hallux segment progressively raised as heel height elevation from 0 cm to 7cm.

Thirdly, a methodology workflow of finite element simulation combined with musculoskeletal modeling derived force has been used to predict the internal strain distribution of the plantar fascia in three different heel height (3cm, 5cm, 7cm) respectively. The major results showed that the highest plantar fascia strain occurred in the second peak stance phase, the plantar fascia strain increased by 26.1% from 3 to 5cm and increase sharply by 0.3% from 5 to 7 cm of heel height. Meanwhile, the higher strain was presented on the proximal region of fascia which could be a clue for plantar fasciitis development in the HHS population. Those findings can provide comprehensive biomechanical details and reference information for clinicians and physicians to develop an efficient rehabilitation program of HHS related foot injury or disease.

Direction for further studies

The human foot is a plantigrade pattern, its morphology can be changed by the support surface, mainly affected by footwear structure. As described, foot morphology experiences a dramatic change to the digitigrade pattern with the heel raised and forefoot contact with the ground in HHS gait. It is no doubt that enforced and unnatural foot morphological change would bring various injuries and risks to HHS wearers. However, despite widespread warnings from public health institutions and international medical societies, there is still a large proportion of the population wearing HHS in their daily life, it has been reported that beauty and femininity were the key drivers of women's behavior [21]. It seems HHS wearing is unavoidable for most women in their daily life. With numerous studies that have investigated HHS biomechanics and its relationship with injury risk occurring in the human musculoskeletal system, accurate suggestions must be provided about how to counter the adverse effects of HHS using, instead of only giving simple advice on not wearing it. Consequently, in the future, the design of HHS shoes must be associated with comfort and aesthetics to meet the requirements of beauty and health.

The animal bionic research could inspire designing more comfortable HHS or equipment that could relatively counter the adverse effect of HHS on the human musculoskeletal system. For example, Felines as typical digitigrade mammals, their distal limb segment

metacarpal /metapodials elevated off the ground, as a major support region contact with the ground. This special morphological structure allows felines to absorb two to three times their body weight while resting on their small distal joint. Interestingly, human foot morphology under HHS conditions is similar to the feline's metacarpal morphological. Therefore, the application of bionic design by investigating the internal biomechanical mechanism of felines' metacarpal /metapodials structure on the human foot could provide valuable information.

New scientific thesis points

1ˢᵗ thesis point: Based on my experimental results, significantly higher dorsiflexed movement occurred on the hallux and higher adduction movement occurred on the forefoot segment during HHS gait compared to barefoot gait. I derived the following conclusions:

- The HHS wearing does not affect the add/abduction of the hindfoot as it is seen on Figure 2.2. Only the last 10% of the movement shows some deviation.

- The hindfoot internal rotation becomes significantly higher during HHS gait, in the stance phase (between 0% and 50% of the complete gait cycle). Higher movement of the hindfoot in the transverse plane leads to an unstable posture during stance phase that could increase the risk of the ankle sprain.

- If Figure 2.2 is considered, it is obvious to see that the hallux dorsiflexion becomes significantly higher during HHS gait, in the majority of the motion (between 17% and 85% of the complete gait cycle). This result has particular physical effects as well. First, the higher hallux dorsiflexion leads also to greater change in forefoot adduction, as it is seen in the first 50% of the gait cycle (see Figure 2.2). Second, the higher peak, which is visible in the dorsiflexion function (see Figure 2.2, between 50 and 70% of the gait cycle), will cause an inflexion in the forefoot adduction in the "toe-off phase". The rapid change, with an approximately 11° of amplitude creates cyclic bending stress in the forefoot. The combined effect of cyclic bending and the high rate of change will result that the hallux will be twisting outwardly, while the forefoot will be twisting inwardly. This mechanism will create a propagating, long term trauma that eventually ends in hallux valgus or "bunion".
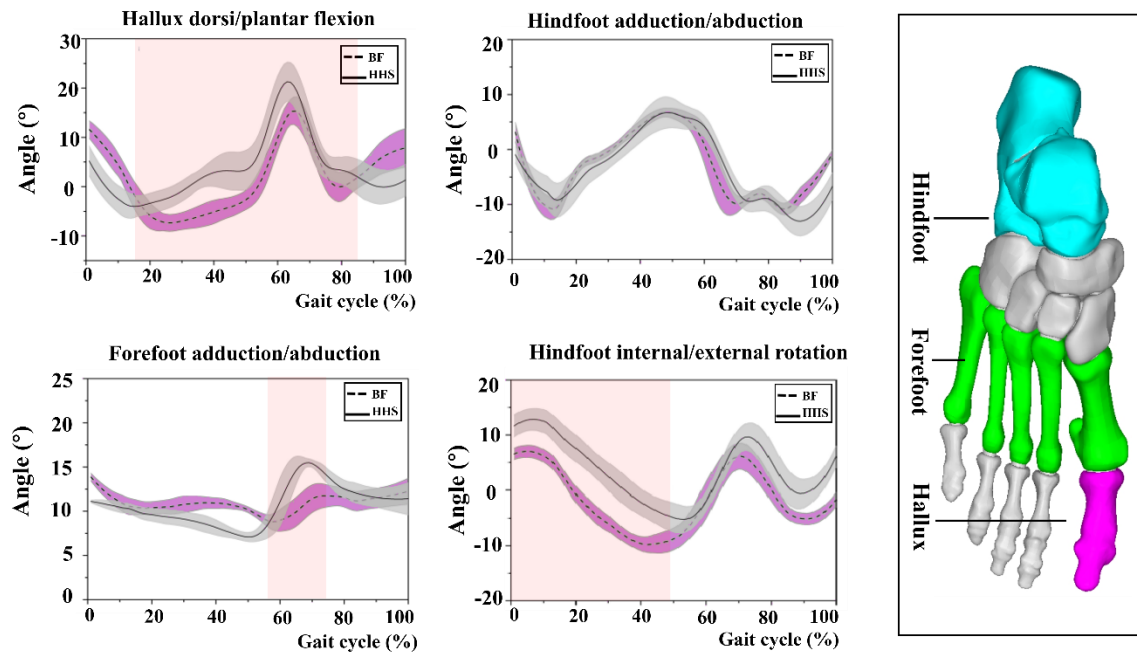
Fig 2.2. The comparison of foot kinematics in three different planes between the HHS and BF. The red region indicated the significant differences between HHS and BF.

Related articles to the first thesis point:

[1] **Wang, M.,** Gu, Y., & Baker, J. S. (2018). Analysis of foot kinematics wearing high heels using the Oxford foot model. Technology and health care, 26(5), 815-823. **IF:1.308, Q4**

[2] Zhang, Y., **Wang, M.,** Awrejcewicz, J., Fekete, G., Ren, F., Gu, Y. (2017). Using gold-standard gait analysis methods to assess experience effects on lower-limb mechanics during moderate high-heeled jogging and running. JoVE (Journal of Visualized Experiments), 127, e55714. **IF: 1.355, Q3**

2ˢᵗ thesis point: Based on 3D model reconstruction method, a high-fidelity 3D foot model, with four different heel height (0 cm, 3 cm, 5 cm, and 7 cm), has been built respectively, to provide a new perspective on foot morphological details under HHS condition. As a result, I provided a complete characterization, by the use of 8 parameters, about the forefoot segment (HV, FIM, MB, 1MD), the longitudinal arch height (TFM, C1M) and the calcaneus segment (Böhler, Gissane), the detail of the angle variation is shown in the Fig.5.1. I deduced the following scientific morphological trends:

- In case of the calcaneus segment, there a slight change is observed while the Böhler angle and the Gissane angle slowly progress as heel height increased. It is indicated that the position of the calcaneus segment remains relatively stable within the height range of 7cm.

- In the case of the longitudinal arch height, the talus-first metatarsal (TFM) angle shows a strongly progressive increasing trend (increased by 89.71% in 0-7 cm), while the calcaneus 1ˢᵗ metatarsal (C1M) angle shows a strongly progressive decreasing trend (decreased by 18.56% in 0-7 cm). It is indicated that the longitudinal arch height significantly increased as heel height elevation from 0 cm to 7cm, which could result in a loss of the arch shock absorption ability.

- In the case of the forefoot segment, the hallux valgus (HV) angle and 1ˢᵗ metatarsal declination (1MD) angle show a strongly progressive increasing trend (increased by 71.50% and 63.13% in 0-7 cm, respectively). In addition, the first intermetatarsal (FIM) angle shows a slow progressing trend (increased 36.28% in 0-7cm), while the metatarsal break (MB) angle shows a slight decreasing trend (increased 4.1% in 0-7 cm). Those progressively increased values of the angles indicate that the prevalence of the hallux valgus increased as heel height elevation.
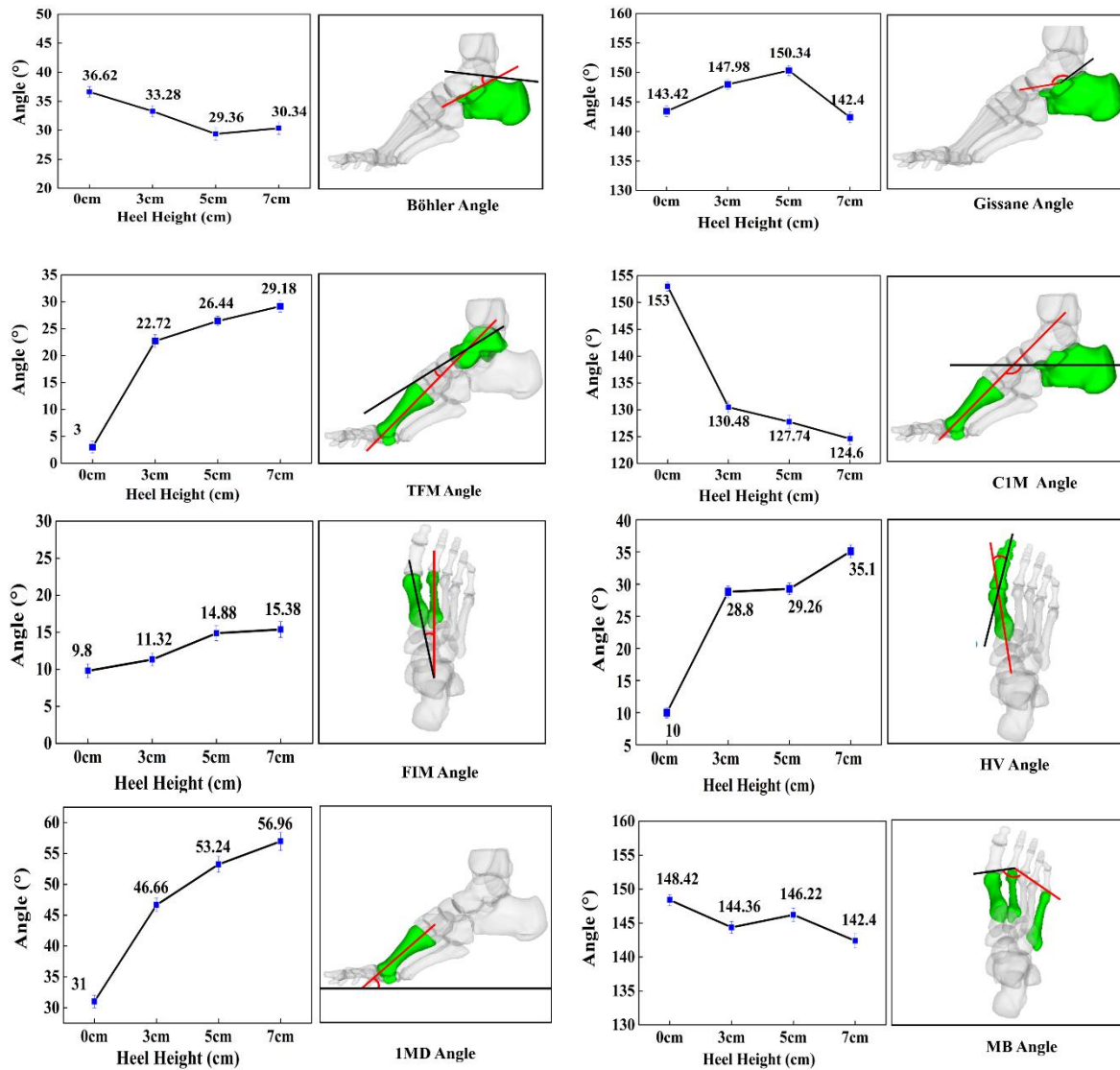
Fig 5.1. 8 specific types of angular change among four heel heights.

Related articles to the second thesis point:

[1] **Wang, M.,** Jiang, C., Fekete, G., Teo, E. C., Gu, Y. (2021). Health view to decrease negative effect of high heels wearing: a systemic review. Applied bionics and biomechanics, 2021, 1-12. **IF: 1.781, Q4**

[2] Zhao, X., **Wang, M.,** Fekete, G., Baker, J. S., Wiltshire, H., Gu, Y. (2018). Analyzing the effect of an arch support functional insole on walking and jogging in young healthy females. Technology and Health Care, 4, 1-11. **IF: 1.35, Q4**

3rd thesis point: I deduced the strain distribution of the plantar fascia during HHS gait at different heel heights by combining FEM, MSM, and motion capture techniques. My scientific results are summarized in four points:

- I calculated an average change of strain (ACS) of 20% between the distal and the middle part when identical heel height was considered during the first and mid-standing phases. The ACS has been deduced for each phase between the 3-5 and 5-7 cm (see Table 5.1). According to Table 5.1, a heel height over 5cm significantly increases the plantar fascia strain, which could increase the prevalence of plantar fasciitis development or heel pain symptom in the HHS population.

Table 5.1. The average change of strain at different heel heights in three gait phases.

Phases	ACS at 3-5 cm [%]	ACS at 5-7 cm [%]
First peak phase	12.1	9.2
Mid-standing phase	5	27.2
Second peak phase	13	42

- By my new method, I proved that the middle and proximal segments of the plantar fascia behave completely the same way in the first and mid-standing phase when identical heel height is considered.

- Based on my calculation, the highest and lowest peak plantar fascia strain occurred on the proximal region and the middle part respectively, in the second peak stance phase when identical heel height is considered.

- I identified a controversial part of my model, which is the simulation of the second-peak phase. The highest average change of strain (ACS) values was found here, but no visible trend could be established.
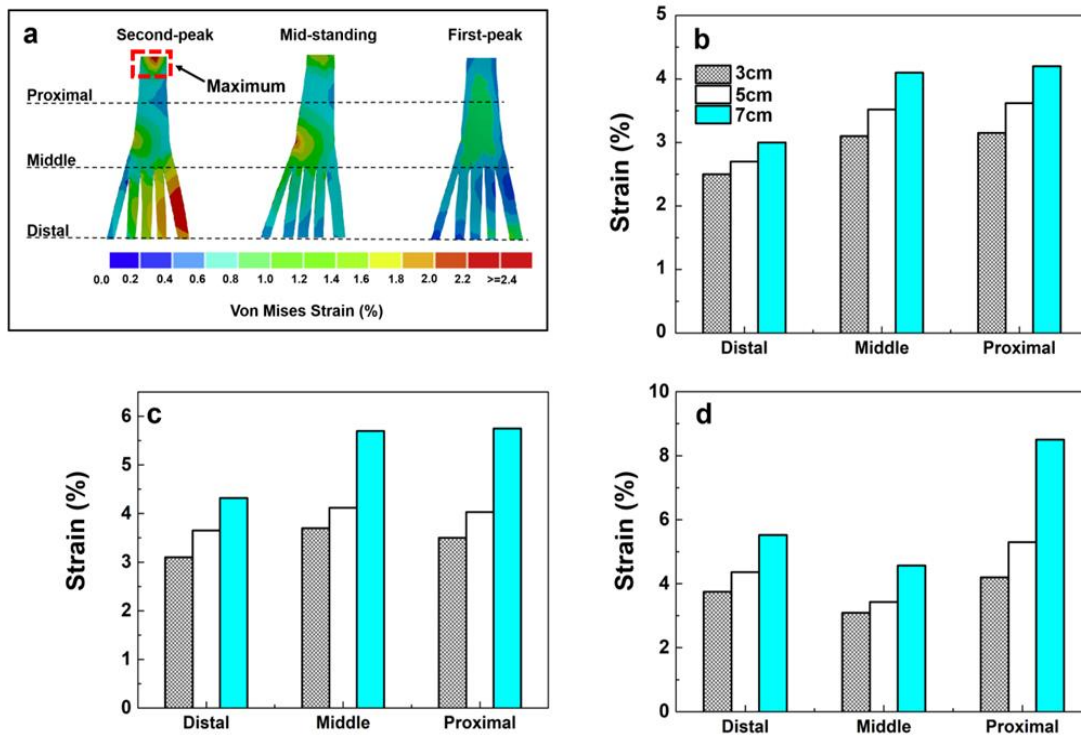
Fig 4.11. The peak 3D fascia strain for three heel heights in three gait events, (b) First-peak phase, (c) mid-standing phase, (d) second-peak phase.

Related articles to the third thesis point*:*

[1] **Wang, M.,** Li, S., Teo, E. C., Fekete, G., Gu, Y. (2021). The influence of heel height on strain variation of plantar fascia during high heel shoes walking-combined musculoskeletal modeling and finite element analysis. Frontiers in Bioengineering and Biotechnology, 9, 1-10. **IF: 5.48, Q1**

List of all publications

1. **Wang, M.,** Li, S., Teo, E. C., Fekete, G., Gu, Y. (2021). The influence of heel height on strain variation of plantar fascia during high heel shoes walking-combined musculoskeletal modeling and finite element analysis. Frontiers in Bioengineering and Biotechnology, 9, 1-10. IF: 5.48

2. **Wang, M.,** Ying, J., Ugbolue, U. C., Buchan, D. S., Gu, Y., Baker, J. S. (2021). Cardio-Metabolic Risk Factors in Scottish South Asian and Caucasian Youth. International Journal of Environmental Research and Public Health, 18, 1-10. IF: 3.39

3. **Wang, M.,** Song, Y., Baker, J. S., Fekete, G., Ugbolue, U. C., Li, S., Gu, Y. (2021). The biomechanical characteristics of a feline distal forelimb: A finite element analysis study. Computers in Biology and Medicine, 129, 1-9. IF: 4.589

4. Zhou, H., Song, Y., **Wang, M.,** Ugbolue, U. C., Gu, Y. (2021). Thermal imaging evaluation of the felines paw pad temperature before and after walking: A pilot study. Veterinární medicína, 66, 393-399. IF: 0.588

5. **Wang, M.,** Jiang, C., Fekete, G., Teo, E. C., Gu, Y. (2021). Health view to decrease negative effect of high heels wearing: a systemic review. Applied bionics and biomechanics, 2021, 1-12. IF: 1.781

6. Thirupathi, A., **Wang, M.,** Lin, J. K., Fekete, G., István, B., Baker, J. S., Gu, Y. (2021). Effect of different exercise modalities on oxidative stress: a systematic review. BioMed Research International, 2021, 1-10. IF:2.583

7. **Wang, M.,** Baker, J. S., Quan, W., Shen, S., Fekete, G., Gu, Y. (2020). A preventive role of exercise across the coronavirus 2 (SARS-CoV-2) pandemic. Frontiers in Physiology, 11, 1-8. IF: 4.134

8. Xu, D., Cen, X., **Wang, M.,** Rong, M., István, B., Baker, J. S., Gu, Y. (2020). Temporal kinematic differences between forward and backward jump-landing. International Journal of Environmental Research and Public Health, 17, 1-9. IF: 3.39

9. Quan, W., **Wang, M.,** Liu, G., Fekete, G., Baker, J. S., Ren, F., Gu, Y. (2020). Comparative Analysis of Lower Limb Kinematics between the Initial and Terminal Phase of 5km Treadmill Running, Journal of Visualized Experiments, 161, 1-10. IF: 1.4

10. Song, Y., Ren, F., Sun, D., **Wang, M.,** Baker, J. S., István, B., Gu, Y. (2020). Benefits of exercise on influenza or pneumonia in older adults: a systematic review. International Journal of Environmental Research and Public Health, 17, 2655. IF: 3.39

11. Song, Y., **Wang, M.,** Baker, J. S., Gu, Y. (2019). The effect of voluntary head movements on postural kinetics in the standing cat. PeerJ, 7, e8186. IF: 2.98

12. Song, Y., **Wang, M.,** Baker, J. S., Gu, Y. (2019). The loading characteristics of landing in cats with different body weights. Veterinární medicína, 64, 497-504. IF: 0.588

13. **Wang, M.**, Song, Y., Valentin, S., Baker, J. S., Gu, Y. (2019). Kinetic analysis of felines landing from different heights. PeerJ, 7, e8007. IF: 2.98

14. Zhao, X., **Wang, M.,** Fekete, G., Baker, J. S., Wiltshire, H., Gu, Y. (2018). Analyzing the effect of an arch support functional insole on walking and jogging in young, healthy females. Technology and Health Care, 4, 1-11. IF: 1.35

15. **Wang, M.,** Song, Y., Baker, J. S., Fekete, G., Gu, Y. (2018). Sitting to standing postural changes: Energy expenditure and a possible mechanism to alleviate sedentary behavior. Physiology International, 105, 157-165. IF: 1.88

16. **Wang, M.,** Gu, Y., Baker, J. S. (2018). Analysis of foot kinematics wearing high heels using the Oxford foot model. Technology and health care, 26, 815-823. IF: 1.308

17. **Wang, M.,** Fu, L., Gu, Y., Mei, Q., Fu, F., Fernandez, J. (2018). Comparative study of kinematics and muscle activity between elite and amateur table tennis players during topspin loop against backspin movements. Journal of Human Kinetics, 64, 25-33.

18. **Wang, M. Z.,** Song, Y., Fekete, G., Gu, Y. D. (2018). The variation of plantar temperature and plantar pressure during shod running with socks or not. In Journal of Biomimetics, Biomaterials and Biomedical Engineering, 35, 1-8. IF: 0.7

19. Zhang, Y., **Wang, M.,** Awrejcewicz, J., Fekete, G., Ren, F., Gu, Y. (2017). Using gold-standard gait analysis methods to assess experience effects on lower-limb mechanics during moderate high-heeled jogging and running. JoVE (Journal of Visualized Experiments), 127, e55714. IF: 1.3

Reference

1. Wang, M., Jiang, C., Fekete, G., Teo, E. C., & Gu, Y. (2021). Health view to decrease negative effect of high heels wearing: a systemic review. Applied bionics and biomechanics, 2021.

2. Broega, A. C., Righetto, M., & Ribeiro, R. (2017, October). Female high heel shoes: a study of comfort. In IOP Conference Series: Materials Science and Engineering (Vol. 254, No. 23, p. 232001). IOP Publishing.

3. Csapo, R., Maganaris, C. N., Seynnes, O. R., & Narici, M. V. (2010). On muscle, tendon and high heels. Journal of Experimental Biology, 213(15), 2582-2588.

4. Barkema, D. D., Derrick, T. R., & Martin, P. E. (2012). Heel height affects lower extremity frontal plane joint moments during walking. Gait & posture, 35(3), 483-488.

5. Blanchette, M. G., Brault, J. R., & Powers, C. M. (2011). The influence of heel height on utilized coefficient of friction during walking. Gait & posture, 34(1), 107-110.

6. Cronin, N. J., Barrett, R. S., & Carty, C. P. (2012). Long-term use of high-heeled shoes alters the neuromechanics of human walking. Journal of applied physiology, 112(6), 1054-1058.

7. Ebbeling, C. J., Hamill, J., & Crussemeyer, J. A. (1994). Lower extremity mechanics and energy cost of walking in high-heeled shoes. Journal of Orthopaedic & Sports Physical Therapy, 19(4), 190-196.

8. Esenyel, M., Walsh, K., Walden, J. G., & Gitter, A. (2003). Kinetics of high-heeled gait. Journal of the American Podiatric Medical Association, 93(1), 27-32.

9. Lee, C. M., Jeong, E. H., & Freivalds, A. (2001). Biomechanical effects of wearing high-heeled shoes. International journal of industrial ergonomics, 28(6), 321-326.

10. Li, J. S., Gu, Y. D., Ren, X. J., Lake, M. J., & Zeng, Y. J. (2010). Biomechanical effects of foam inserts on forefoot load during the high-heeled gait: a pilot study. Journal of mechanics in medicine and biology, 10(04), 667-674.

11. Hong, W. H., Lee, Y. H., Chen, H. C., Pei, Y. C., & Wu, C. Y. (2005). Influence of heel height and shoe insert on comfort perception and biomechanical performance of young female adults during walking. Foot & ankle international, 26(12), 1042-1048.

12. Kerrigan, D. C., Lelas, J. L., & Karvosky, M. E. (2001). Women's shoes and knee

osteoarthritis. The Lancet, 357(9262), 1097-1098.

13. Menant, J. C., Perry, S. D., Steele, J. R., Menz, H. B., Munro, B. J., & Lord, S. R. (2008). Effects of shoe characteristics on dynamic stability when walking on even and uneven surfaces in young and older people. Archives of physical medicine and rehabilitation, 89(10), 1970-1976.

14. Simonsen, E. B., Svendsen, M. B., Nørreslet, A., Baldvinsson, H. K., Heilskov-Hansen, T., Larsen, P. K., ... & Henriksen, M. (2012). Walking on high heels changes muscle activity and the dynamics of human walking significantly. Journal of applied biomechanics, 28(1), 20-28.

15. Mika, A., Oleksy, Ł., Mika, P., Marchewka, A., & Clark, B. C. (2012). The influence of heel height on lower extremity kinematics and leg muscle activity during gait in young and middle-aged women. Gait & posture, 35(4), 677-680.

16. Stefanyshyn, D. J., Nigg, B. M., Fisher, V., O'Flynn, B., & Liu, W. (2000). The influence of HHS on kinematics, kinetics, and muscle EMG of normal female gait. Journal of Applied Biomechanics, 16(3), 309-319.

17. Titchenal, M. R., Asay, J. L., Favre, J., Andriacchi, T. P., & Chu, C. R. (2015). Effects of high heel wear and increased weight on the knee during walking. Journal of Orthopaedic Research, 33(3), 405-411.

18. Yu, J., Wong, D. W. C., Zhang, H., Luo, Z. P., & Zhang, M. (2016). The influence of high-heeled shoes on strain and tension force of the anterior talofibular ligament and plantar fascia during balanced standing and walking. Medical Engineering & Physics, 38(10), 1152-1156.

19. Gray, H. (2015). Gray's anatomy: with original illustrations by Henry Carter. Arcturus Publishing Limited.

20. Nordin, M., & Frankel, V. H. (Eds.). (2001). Basic biomechanics of the musculoskeletal system. Lippincott Williams & Wilkins.

21. Sarrafian, S. K. (1993). Biomechanics of the subtalar joint complex. Clinical orthopaedics and related research, (290), 17-26.

22. Brockett, C. L., & Chapman, G. J. (2016). Biomechanics of the ankle. Orthopaedics and trauma, 30(3), 232-238.

23. Marks, L. J., & Michael, J. W. (2001). Artificial limbs. BMJ, 323(7315), 732-735.

24. Espregueira-Mendes, J. D., & Vieira da Silva, M. (2006). Anatomy of the proximal tibiofibular joint. Knee Surgery, Sports Traumatology, Arthroscopy, 14(3), 241-249.

25. Procter, P., & Paul, J. P. (1982). Ankle joint biomechanics. Journal of biomechanics, 15(9), 627-634.

26. Calhoun, J. H., Li, F., Ledbetter, B. R., & Viegas, S. F. (1994). A comprehensive study of pressure distribution in the ankle joint with inversion and eversion. Foot & ankle international, 15(3), 125-133.

27. Brodsky, J. W., Polo, F. E., Coleman, S. C., & Bruck, N. (2011). Changes in gait following the Scandinavian total ankle replacement. JBJS, 93(20), 1890-1896.

28. Spooner, S. K., & Kirby, K. A. (2006). The subtalar joint axis locator: a preliminary report. Journal of the American Podiatric Medical Association, 96(3), 212-219.

29. Sammarco, V. J. (2004). The talonavicular and calcaneocuboid joints: anatomy, biomechanics, and clinical management of the transverse tarsal joint. Foot and ankle clinics, 9(1), 127-145.

30. Melão, L., Canella, C., Weber, M., Negrao, P., Trudell, D., & Resnick, D. (2009). Ligaments of the transverse tarsal joint complex: MRI–anatomic correlation in cadavers. American Journal of Roentgenology, 193(3), 662-671.

31. Latt, L. D., Glisson, R. R., Adams Jr, S. B., Schuh, R., Narron, J. A., & Easley, M. E. (2015). Biomechanical comparison of external fixation and compression screws for transverse tarsal joint arthrodesis. Foot & Ankle International, 36(10), 1235-1242.

32. Kayano, J. (1986). Dynamic function of medial foot arch. Nihon Seikeigeka Gakkai Zasshi, 60(11), 1147-1156.

33. Kitaoka, H. B., Ahn, T. K., Luo, Z. P., & An, K. N. (1997). Stability of the arch of the foot. Foot & ankle international, 18(10), 644-648.

34. Xiong, S., Goonetilleke, R. S., Witana, C. P., Weerasinghe, T. W., & Au, E. Y. L. (2010). Foot arch characterization a review, a new metric, and a comparison. Journal of the American Podiatric Medical Association, 100(1), 14-24.

35. Asghar, A., & Naaz, S. (2021). The transverse arch in the human feet: A narrative review of its evolution, anatomy, biomechanics and clinical implications. Morphologie.

36. Venkadesan, M., Yawar, A., Eng, C. M., Dias, M. A., Singh, D. K., Tommasini, S. M., ... & Mandre, S. (2020). Stiffness of the human foot and evolution of the transverse arch. Nature, 579(7797), 97-100.

37. Cobb, S. C., Tis, L. L., Johnson, J. T., Geil, M. D., & McCarty, F. A. (2009). The effect of low-mobile foot posture on multi-segment medial foot model gait kinematics. Gait & posture, 30(3), 334-339.

38. Kelikian, A. S., & Sarrafian, S. K. (Eds.). (2011). Sarrafian's anatomy of the foot and ankle: descriptive, topographic, functional. Lippincott Williams & Wilkins.

39. Dedieu, P., Drigeard, C., Gjini, L., Dal Maso, F., & Zanone, P. G. (2013). Effects of foot orthoses on the temporal pattern of muscular activity during walking. Clinical biomechanics, 28(7), 820-824.

40. Kaplan, E. B., & Milford, L. W. (1984). The retinacular system of the hand. Spinner M (Ed) Kaplan's functional and surgical anatomy of the hand, 3nd edn. Philadelphia, JB Lippicott 1984: 245, 79.

41. MANN, R., & INMAN, V. T. (1964). Phasic activity of intrinsic muscles of the foot. JBJS, 46(3), 469-481.

42. Sarrafian, S. K., & Kelikian, A. S. (2011). Retaining systems and compartments. Sarrafian's anatomy of the foot and ankle: descriptive, topographic, functional. 3rd ed. Philadelphia: Lippincott Williams & Wilkins.

43. Gusmão, L. C. B. D., Lima, J. S. B., Duarte, F. H. G., Souto, A. G. D. F., & Couto, B. D. M. V. (2013). Anatomical basis for the use of the fibularis tertius muscle in myocutaneous flaps. Revista Brasileira de Cirurgia Plástica, 28, 191-195.

44. Aquino, A., & Payne, C. (1999). Function of the plantar fascia. The foot, 9(2), 73-78.

45. Buchbinder, R. (2004). Plantar fasciitis. New England Journal of Medicine, 350(21), 2159-2166.

46. Schepsis, A. A., Leach, R. E., & Gorzyca, J. (1991). Plantar fasciitis. Etiology, treatment, surgical results, and review of the literature. Clinical Orthopaedics and Related Research, (266), 185-196.

47. Stecco, C., Corradin, M., Macchi, V., Morra, A., Porzionato, A., Biz, C., & De Caro, R. (2013). Plantar fascia anatomy and its relationship with A chilles tendon and

paratenon. Journal of anatomy, 223(6), 665-676.

48. Rosenbaum, A. J., DiPreta, J. A., & Misener, D. (2014). Plantar heel pain. Medical Clinics, 98(2), 339-352.

49. Hicks, J. H. (1953). The mechanics of the foot: I. The joints. Journal of anatomy, 87(Pt 4), 345.

50. Hicks, J.J.J.o.a., The mechanics of the foot: II. The plantar aponeurosis and the arch. 1954. 88(Pt 1): p. 25.

51. Mann, R. A., & Hagy, J. L. (1979). The function of the toes in walking, jogging and running. Clinical orthopaedics and related research, (142), 24-29.

52. Sarrafian, S. K. (1987). Functional characteristics of the foot and plantar aponeurosis under tibiotalar loading. Foot & ankle, 8(1), 4-18.

53. Bojsen-Møller, F., & Lamoreux, L. (1979). Significance of free dorsiflexion of the toes in walking. Acta Orthopaedica Scandinavica, 50(4), 471-479.

54. Ker, R. F., Bennett, M. B., Bibby, S. R., Kester, R. C., & Alexander, R. (1987). The spring in the arch of the human foot. Nature, 325(6100), 147-149.

56. Brockett, C. L., & Chapman, G. J. (2016). Biomechanics of the ankle. Orthopaedics and trauma, 30(3), 232-238.

57. Donatelli, R. (1985). Normal biomechanics of the foot and ankle. Journal of Orthopaedic & Sports Physical Therapy, 7(3), 91-95.

58. Reeser, L. A., Susman, R. L., & Stern Jr, J. T. (1983). Electromyographic studies of the human foot: experimental approaches to hominid evolution. Foot & ankle, 3(6), 391-407.

59. Lundberg, A. (1990). Patterns of motion of the ankle/foot complex.

60. Castro, M. D. (2002). Ankle biomechanics. Foot and ankle clinics, 7(4), 679-693.

61. Grimston, S. K., Nigg, B. M., Hanley, D. A., & Engsberg, J. R. (1993). Differences in ankle joint complex range of motion as a function of age. Foot & ankle, 14(4), 215-222.

62. Patil, K. M., Braak, L. H., & Huson, A. (1993). Stresses in a simplified two dimensional model of a normal foot—a preliminary analysis. Mechanics research communications, 20(1), 1-7.

63. Fish, D. J., & Nielsen, J. P. (1993). Clinical assessment of human gait. JPO: Journal of Prosthetics and Orthotics, 5(2), 39.

64. Cronin, N. J. (2014). The effects of HHS on female gait: a review. Journal of electromyography and kinesiology, 24(2), 258-263.

65. Pannell, S. L., & MD, U. (2012). The postural and biomechanical effects of high heel shoes: A literature review. Journal of Vascular Surgery.

66. Foster, A., Blanchette, M. G., Chou, Y. C., & Powers, C. M. (2012). The influence of heel height on frontal plane ankle biomechanics: implications for lateral ankle sprains. Foot & ankle international, 33(1), 64-69.

67. Cho, W. H., & Choi, H. (2006, January). Center of pressure (COP) during the postural balance control of high-heeled woman. In 2005 IEEE Engineering in Medicine and Biology 27th Annual Conference (pp. 2761-2764). IEEE.

68. Gerber, S. B., Costa, R. V., Grecco, L. A. C., Pasini, H., Marconi, N. F., & Oliveira, C. S. (2012). Interference of high-heeled shoes in static balance among young women. Human movement science, 31(5), 1247-1252.

69. Hapsari, V. D., & Xiong, S. (2016). Effects of HHS wearing experience and heel height on human standing balance and functional mobility. Ergonomics, 59(2), 249-264.

70. Mika, A., Kielnar, R., & Świerczek, M. (2016). The influence of high-and low-heeled shoes on balance in young women. Acta of bioengineering and biomechanics, 18(3), 97-103.

71. Truszczyńska, A., Trzaskoma, Z., Stypińska, Z., Drzał-Grabiec, J., & Tarnowski, A. (2019). Is static balance affected by using shoes of different height?. Biomedical Human Kinetics, 8(1), 137-144.

72. Wan, F. K., Yick, K. L., & Winnie, W. M. (2019). Effects of heel height and high-heel experience on foot stability during quiet standing. Gait & Posture, 68, 252-257.

73. Mandato, M. G., & Nester, E. (1999). The effects of increasing heel height on forefoot peak pressure. Journal of the American Podiatric Medical Association, 89(2), 75-80.

74. Nyska, M., McCabe, C., Linge, K., & Klenerman, L. (1996). Plantar foot pressures during treadmill walking with high-heel and low-heel shoes. Foot & ankle international, 17(11), 662-666.

75. Speksnijder, C. M., vd Munckhof, R. J., Moonen, S. A., & Walenkamp, G. H. (2005). The higher the heel the higher the forefoot-pressure in ten healthy women. The foot, 15(1), 17-21.

76. Gu, Y., Li, F., Li, J., Feng, N., Lake, M. J., Li, Z., & Ren, J. (2014). Plantar pressure distribution character in young female with mild hallux valgus wearing high-heeled shoes. Journal of Mechanics in Medicine and Biology, 14(01), 1450008.

77. Mickle, K. J., Munro, B. J., Lord, S. R., Menz, H. B., & Steele, J. R. (2011). Gait, balance and plantar pressures in older people with toe deformities. Gait & posture, 34(3), 347-351.

78. Perera, A. M., Mason, L., & Stephens, M. M. (2011). The pathogenesis of hallux valgus. JBJS, 93(17), 1650-1661.

79. Luximon, Y., Cong, Y., Luximon, A., & Zhang, M. (2015). Effects of heel base size, walking speed, and slope angle on center of pressure trajectory and plantar pressure when wearing high-heeled shoes. Human movement science, 41, 307-319.

80. Krebs, D. E., Robbins, C. E., Lavine, L., & Mann, R. W. (1998). Hip biomechanics during gait. Journal of Orthopaedic & Sports Physical Therapy, 28(1), 51-59.

81. Kerrigan, D. C., Todd, M. K., & Riley, P. O. (1998). Knee osteoarthritis and high-heeled shoes. The Lancet, 351(9113), 1399-1401.

82. Snow, R. E., & Williams, K. R. (1994). HHS: their effect on center of mass position, posture, three-dimensional kinematics, hindfoot motion, and ground reaction forces. Archives of physical medicine and rehabilitation, 75(5), 568-576.

83. Joseph, J. (1968). The pattern of activity of some muscles in women walking on high heels. Rheumatology, 9(7), 295-299.

84. DK, M., & EP, W. (1963). ANALYSIS OF OXYGEN COMSUMPTION OF WOMEN WHILE WALKING IN DIFFERENT STYLES OF SHOES. Archives of physical medicine and rehabilitation, 44, 569-571.

85. Gajdosik, R. L., Vander Linden, D. W., & Williams, A. K. (1999). Influence of age on length and passive elastic stiffness characteristics of the calf muscle-tendon unit of women. Physical therapy, 79(9), 827-838.

86. Weppler, C. H., & Magnusson, S. P. (2010). Increasing muscle extensibility: a matter

of increasing length or modifying sensation?. Physical therapy, 90(3), 438-449.

87. Opila-Correia, K. A. (1990). Kinematics of high-heeled gait with consideration for age and experience of wearers. Archives of physical medicine and rehabilitation, 71(11), 905-909.

88. Ho, K. Y., Blanchette, M. G., & Powers, C. M. (2012). The influence of heel height on patellofemoral joint kinetics during walking. Gait & posture, 36(2), 271-275.

89. Chien, H.-L., et al., Kinematic and kinetic adaptations in the lower extremities of experienced wearers during high-heeled gait. 2014. 26(03): p. 1450042.

90. Chien, H. L., Lu, T. W., Liu, M. W., Hong, S. W., & Kuo, C. C. (2014). Kinematic and kinetic adaptations in the lower extremities of experienced wearers during high-heeled gait. Biomedical Engineering: Applications, Basis and Communications, 26(03), 1450042.

91. Mika, A., Oleksy, L. U. K. A. S. Z., Mikołajczyk, E., Marchewka, A., & Mika, P. (2011). Changes of bioelectrical activity in cervical paraspinal muscle during gait in low and high heel shoes. Acta Bioeng Biomech, 13(1), 27-33.

92. Edwards, L., Dixon, J., Kent, J. R., Hodgson, D., & Whittaker, V. J. (2008). Effect of shoe heel height on vastus medialis and vastus lateralis electromyographic activity during sit to stand. Journal of orthopaedic surgery and research, 3(1), 1-7.

93. Reilly, D. T., & Martens, M. (1972). Experimental analysis of the quadriceps muscle force and patello-femoral joint reaction force for various activities. Acta Orthopaedica Scandinavica, 43(2), 126-137.

94. OGATA, K., WHITESEDE, L. A., LESKER, P. A., & SIMMONS, D. J. (1977). The effect of varus stress on the moving rabbit knee joint. Clinical Orthopaedics and Related Research®, (129), 313-318.

95. Basmajian, J. V. (1954). An electromyographic study of certain muscle of the leg and foot in the standing position. Surg Gynec Obstet, 98, 662-666.

96. Gefen, A., Megido-Ravid, M., Itzchak, Y., & Arcan, M. (2002). Analysis of muscular fatigue and foot stability during high-heeled gait. Gait & posture, 15(1), 56-63.

97. de Oliveira Pezzan, P. A., João, S. M. A., Ribeiro, A. P., & Manfio, E. F. (2011). Postural assessment of lumbar lordosis and pelvic alignment angles in adolescent users

and nonusers of high-heeled shoes. Journal of manipulative and physiological therapeutics, 34(9), 614-621.

98. Delp, S. L., Anderson, F. C., Arnold, A. S., Loan, P., Habib, A., John, C. T., ... & Thelen, D. G. (2007). OpenSim: open-source software to create and analyze dynamic simulations of movement. IEEE transactions on biomedical engineering, 54(11), 1940-1950.

99. Pandy, M. G. (2001). Computer modeling and simulation of human movement. Annual review of biomedical engineering, 3(1), 245-273.

100. Lu, T. W., & O'connor, J. J. (1999). Bone position estimation from skin marker co-ordinates using global optimisation with joint constraints. Journal of biomechanics, 32(2), 129-134.

101. Kargo, W. J., & Rome, L. C. (2002). Functional morphology of proximal hindlimb muscles in the frog Rana pipiens. Journal of Experimental Biology, 205(14), 1987-2004.

102. Thelen, D. G., & Anderson, F. C. (2006). Using computed muscle control to generate forward dynamic simulations of human walking from experimental data. Journal of biomechanics, 39(6), 1107-1115.

103. Rajagopal, A., Dembia, C. L., DeMers, M. S., Delp, D. D., Hicks, J. L., & Delp, S. L. (2016). Full-body musculoskeletal model for muscle-driven simulation of human gait. IEEE transactions on biomedical engineering, 63(10), 2068-2079.

104. Millard, M., Uchida, T., Seth, A., & Delp, S. L. (2013). Flexing computational muscle: modeling and simulation of musculotendon dynamics. Journal of biomechanical engineering, 135(2).

105. Lloyd, D. G., & Besier, T. F. (2003). An EMG-driven musculoskeletal model to estimate muscle forces and knee joint moments in vivo. Journal of biomechanics, 36(6), 765-776.

106. Manal, K., & Buchanan, T. S. (2013). An electromyogram-driven musculoskeletal model of the knee to predict in vivo joint contact forces during normal and novel gait patterns. Journal of biomechanical engineering, 135(2).

107. Shao, Q., Bassett, D. N., Manal, K., & Buchanan, T. S. (2009). An EMG-driven model

to estimate muscle forces and joint moments in stroke patients. Computers in biology and medicine, 39(12), 1083-1088.

108. Garner, B. A., & Pandy, M. G. (2001). Musculoskeletal model of the upper limb based on the visible human male dataset. Computer methods in biomechanics and biomedical engineering, 4(2), 93-126.

109. Dao, T. T. (2016). Rigid musculoskeletal models of the human body systems: a review. Journal of Musculoskeletal Research, 19(03), 1630001.

110. Scheys, L., Desloovere, K., Spaepen, A., Suetens, P., & Jonkers, I. (2011). Calculating gait kinematics using MR-based kinematic models. Gait & posture, 33(2), 158-164.

111. Zhu, Z., & Li, G. (2012). An automatic 2D–3D image matching method for reproducing spatial knee joint positions using single or dual fluoroscopic images. Computer methods in biomechanics and biomedical engineering, 15(11), 1245-1256.

112. Scheys, L., Van Campenhout, A., Spaepen, A., Suetens, P., & Jonkers, I. (2008). Personalized MR-based musculoskeletal models compared to rescaled generic models in the presence of increased femoral anteversion: effect on hip moment arm lengths. Gait & posture, 28(3), 358-365.

113. Chen, W. M., Park, J., Park, S. B., Shim, V. P. W., & Lee, T. (2012). Role of gastrocnemius–soleus muscle in forefoot force transmission at heel rise—A 3D finite element analysis. Journal of biomechanics, 45(10), 1783-1789.

114. Colacino, F. M., Emiliano, R., & Mace, B. R. (2012). Subject-specific musculoskeletal parameters of wrist flexors and extensors estimated by an EMG-driven musculoskeletal model. Medical engineering & physics, 34(5), 531-540.

115. Damsgaard, M., Rasmussen, J., Christensen, S. T., Surma, E., & De Zee, M. (2006). Analysis of musculoskeletal systems in the AnyBody Modeling System. Simulation Modelling Practice and Theory, 14(8), 1100-1111.

116. Er, M. S., Verim, O., Altinel, L., & Tasgetiren, S. (2013). Three-dimensional finite element analysis used to compare six different methods of syndesmosis fixation with 3.5-or 4.5-mm titanium screws: a biomechanical study. Journal of the American Podiatric Medical Association, 103(3), 174-180.

117. Brilakis, E., Kaselouris, E., Xypnitos, F., Provatidis, C. G., & Efstathopoulos, N.

(2012). Effects of foot posture on fifth metatarsal fracture healing: a finite element study. The Journal of foot and ankle surgery, 51(6), 720-728.

118. Wang, Y., Wong, D. W. C., & Zhang, M. (2016). Computational models of the foot and ankle for pathomechanics and clinical applications: a review. Annals of biomedical engineering, 44(1), 213-221.

119. Gu, Y. D., Rong, M., Li, Z. Y., Lake, M. J., & Ruan, G. Q. (2012). Finite element analysis of deep transverse metatarsal ligaments mechanical response during landing. In Advanced Materials Research (Vol. 472, pp. 2558-2561). Trans Tech Publications Ltd.

120. Behforootan, S., Chatzistergos, P., Naemi, R., & Chockalingam, N. (2017). Finite element modelling of the foot for clinical application: a systematic review. Medical engineering & physics, 39, 1-11.

121. Actis, R. L., Ventura, L. B., Smith, K. E., Commean, P. K., Lott, D. J., Pilgram, T. K., & Mueller, M. J. (2006). Numerical simulation of the plantar pressure distribution in the diabetic foot during the push-off stance. Medical and biological engineering and computing, 44(8), 653-663.

122. Orlin, M. N., & McPoil, T. G. (2000). Plantar pressure assessment. Physical therapy, 80(4), 399-409.

123. Shimizu, M., & Andrew, P. D. (1999). Effect of heel height on the foot in unilateral standing. Journal of Physical Therapy Science, 11(2), 95-100.

124. Luximon, Y., Luximon, A., Yu, J., & Zhang, M. (2012). Biomechanical evaluation of heel elevation on load transfer—experimental measurement and finite element analysis. Acta Mechanica Sinica, 28(1), 232-240.

125. Fontanella, C. G., Arduino, A., Toniolo, I., Zampieri, C., Bortolan, L., & Carniel, E. L. (2021). Computational methods for the investigation of ski boots ergonomics. Sports Engineering, 24(1), 1-14.

126. Forestiero, A., Raumer, A., Carniel, E. L., & Natali, A. N. (2015). Investigation of the interaction phenomena between foot and insole by means of a numerical approach. Proceedings of the Institution of Mechanical Engineers, Part P: Journal of Sports Engineering and Technology, 229(1), 3-9.

127. Wu, L. (2007). Nonlinear finite element analysis for musculoskeletal biomechanics of medial and lateral plantar longitudinal arch of Virtual Chinese Human after plantar ligamentous structure failures. Clinical Biomechanics, 22(2), 221-229.

128. Isvilanonda, V., Iaquinto, J. M., Pai, S., Mackenzie-Helnwein, P., & Ledoux, W. R. (2016). Hyperelastic compressive mechanical properties of the subcalcaneal soft tissue: An inverse finite element analysis. Journal of Biomechanics, 49(7), 1186-1191.

129. Zhao, Y., Zhang, S., Sun, T., Wang, D., Lian, W., Tan, J., & Zou, D. (2013). Mechanical comparison between lengthened and short sacroiliac screws in sacral fracture fixation: a finite element analysis. Orthopaedics & Traumatology: Surgery & Research, 99(5), 601-606.

130. Halloran, J. P., Sibole, S., Van Donkelaar, C. C., Van Turnhout, M. C., Oomens, C. W. J., Weiss, J. A., & Erdemir, A. (2012). Multiscale mechanics of articular cartilage: potentials and challenges of coupling musculoskeletal, joint, and microscale computational models. Annals of biomedical engineering, 40(11), 2456-2474.

131. Budhabhatti, S. P., Erdemir, A., Petre, M., Sferra, J., Donley, B., & Cavanagh, P. R. (2007). Finite element modeling of the first ray of the foot: a tool for the design of interventions.

132. Scarton, A., Guiotto, A., Malaquias, T., Spolaor, F., Sinigaglia, G., Cobelli, C., & Sawacha, Z. (2018). A methodological framework for detecting ulcers' risk in diabetic foot subjects by combining gait analysis, a new musculoskeletal foot model and a foot finite element model. Gait & Posture, 60, 279-285.

133. Tadepalli, S. C., Erdemir, A., & Cavanagh, P. R. (2011). Comparison of hexahedral and tetrahedral elements in finite element analysis of the foot and footwear. Journal of biomechanics, 44(12), 2337-2343.

134. Fontanella, C. G., Matteoli, S., Carniel, E. L., Wilhjelm, J. E., Virga, A., Corvi, A., & Natali, A. N. (2012). Investigation on the load-displacement curves of a human healthy heel pad: in vivo compression data compared to numerical results. Medical engineering & physics, 34(9), 1253-1259.

135. Chokhandre, S., Halloran, J. P., van den Bogert, A. J., & Erdemir, A. (2012). A three-dimensional inverse finite element analysis of the heel pad. Journal of biomechanical

engineering, 134(3).

136. Li, S., Zhang, Y., Gu, Y., & Ren, J. (2017). Stress distribution of metatarsals during forefoot strike versus hindfoot strike: A finite element study. Computers in Biology and Medicine, 91, 38-46.

137. Gefen, A. (2002). Stress analysis of the standing foot following surgical plantar fascia release. Journal of biomechanics, 35(5), 629-637.

138. Tao, K., Wang, D., Wang, C., Wang, X., Liu, A., Nester, C. J., & Howard, D. (2009). An in vivo experimental validation of a computational model of human foot. Journal of Bionic Engineering, 6(4), 387-397.

139. Yu, J., Cheung, J. T. M., Fan, Y., Zhang, Y., Leung, A. K. L., & Zhang, M. (2008). Development of a finite element model of female foot for high-heeled shoe design. Clinical Biomechanics, 23, S31-S38.

140. Shin, J., Yue, N., & Untaroiu, C. D. (2012). A finite element model of the foot and ankle for automotive impact applications. Annals of biomedical engineering, 40(12), 2519-2531.

141. Telfer, S., Erdemir, A., Woodburn, J., & Cavanagh, P. R. (2014). What has finite element analysis taught us about diabetic foot disease and its management? A systematic review. PLoS One, 9(10), e109994.

142. Carson, M. C., Harrington, M. E., Thompson, N., O'connor, J. J., & Theologis, T. N. (2001). Kinematic analysis of a multi-segment foot model for research and clinical applications: a repeatability analysis. Journal of biomechanics, 34(10), 1299-1307.

143. Grood, E. S., & Suntay, W. J. (1983). A joint coordinate system for the clinical description of three-dimensional motions: application to the knee. Journal of biomechanical engineering, 105(2), 136-144.

144. Curtis, D. J., Bencke, J., Stebbins, J. A., & Stansfield, B. (2009). Intra-rater repeatability of the Oxford foot model in healthy children in different stages of the foot roll over process during gait. Gait & posture, 30(1), 118-121.

145. Stebbins, J., Harrington, M., Thompson, N., Zavatsky, A., & Theologis, T. (2006). Repeatability of a model for measuring multi-segment foot kinematics in children. Gait & posture, 23(4), 401-410.

146. Hösl, M., Böhm, H., Multerer, C., & Döderlein, L. (2014). Does excessive flatfoot deformity affect function? A comparison between symptomatic and asymptomatic flatfeet using the Oxford Foot Model. Gait & posture, 39(1), 23-28.

147. Levinger, P., Murley, G. S., Barton, C. J., Cotchett, M. P., McSweeney, S. R., & Menz, H. B. (2010). A comparison of foot kinematics in people with normal-and flat-arched feet using the Oxford Foot Model. Gait & posture, 32(4), 519-523.

148. Alonso-Vázquez, A., Villarroya, M. A., Franco, M. A., Asín, J., & Calvo, B. (2009). Kinematic assessment of paediatric forefoot varus. Gait & posture, 29(2), 214-219.

149. Cavanagh, P. R., Morag, E., Boulton, A. J. M., Young, M. J., Deffner, K. T., & Pammer, S. E. (1997). The relationship of static foot structure to dynamic foot function. Journal of biomechanics, 30(3), 243-250.

150. Healey, K., & Chen, K. (2010). Plantar fasciitis: current diagnostic modalities and treatments. Clinics in podiatric medicine and surgery, 27(3), 369-380.

151. Dreeben, S., & Mann, R. A. (1996). Advanced hallux valgus deformity: long-term results utilizing the distal soft tissue procedure and proximal metatarsal osteotomy. Foot & ankle international, 17(3), 142-144.

152. Hutton, W. C., & Dhanendran, M. (1981). The mechanics of normal and hallux valgus feet--a quantitative study. Clinical orthopaedics and related research, (157), 7-13.

153. Eustace, S., O'byrne, J., Stack, J., & Stephens, M. M. (1993). Radiographic features that enable assessment of first metatarsal rotation: the role of pronation in hallux valgus. Skeletal radiology, 22(3), 153-156.

154. Cronin, N. J., Peltonen, J., Ishikawa, M., Komi, P. V., Avela, J., Sinkjaer, T., & Voigt, M. (2008). Effects of contraction intensity on muscle fascicle and stretch reflex behavior in the human triceps surae. Journal of Applied Physiology, 105(1), 226-232.

155. Lundberg, A., Goldie, I., Kalin, B. O., & Selvik, G. (1989). Kinematics of the ankle/foot complex: plantarflexion and dorsiflexion. Foot & ankle, 9(4), 194-200.

156. Williams, D. S., McClay, I. S., Hamill, J., & Buchanan, T. S. (2001). Lower extremity kinematic and kinetic differences in runners with high and low arches. Journal of applied biomechanics, 17(2), 153-163.

157. Simonsen, O. H., Revald, P., Kjaer, I. L., Christensen, M., Mølgaard, C., & Lass, P.

(2006). Tibialis posterior tendon dysfunction. An often neglected cause of painful adult flatfoot. Ugeskrift for laeger, 168(39), 3314-3316.

158. McGinley, J. L., Baker, R., Wolfe, R., & Morris, M. E. (2009). The reliability of three-dimensional kinematic gait measurements: a systematic review. Gait & posture, 29(3), 360-369.

159. Frey, C., Thompson, F., Smith, J., Sanders, M., & Horstman, H. (1993). American Orthopaedic Foot and Ankle Society women's shoe survey. Foot & ankle, 14(2), 78-81.

160. Posadzy, M., Desimpel, J., & Vanhoenacker, F. (2018). Cone beam CT of the musculoskeletal system: clinical applications. Insights into imaging, 9(1), 35-45.

161. Saraiva, J., Bilreiro, C., Silva, L., Castro, M. O. E., Santos, B. M. Q., & Soares, C. (2015, June). Radiography of the lower limb–useful measurements for the daily practice. In ESSR 2015 Annual Scientific Meeting.

162. Shereff, M. J., DiGiovanni, L., Bejjani, F. J., Hersh, A., & Kummer, F. J. (1990). A comparison of nonweight-bearing and weight-bearing radiographs of the foot. Foot & Ankle, 10(6), 306-311.

163. Thomas, J. L., Kunkel, M. W., Lopez, R., & Sparks, D. (2006). Radiographic values of the adult foot in a standardized population. The Journal of foot and ankle surgery, 45(1), 3-12.

164. Rak, V., Ira, D., & Masek, M. (2009). Operative treatment of intra-articular calcaneal fractures with calcaneal plates and its complications. Indian journal of orthopaedics, 43(3), 271.

165. Domínguez, G., & Munuera, P. V. (2008). Metatarsus adductus angle in male and female feet: normal values with two measurement techniques. Journal of the American Podiatric Medical Association, 98(5), 364-369.

166. Doty, J. F., Coughlin, M. J., Weil, L., & Nery, C. (2014). Etiology and management of lesser toe metatarsophalangeal joint instability. Foot and ankle clinics, 19(3), 385-405.

167. Espinosa, N., Maceira, E., & Myerson, M. S. (2008). Current concept review: metatarsalgia. Foot & ankle international, 29(8), 871-879.

168. Bouché, R. T., & Heit, E. J. (2008). Combined plantar plate and hammertoe repair with flexor digitorum longus tendon transfer for chronic, severe sagittal plane instability of

the lesser metatarsophalangeal joints: preliminary observations. The Journal of foot and ankle surgery, 47(2), 125-137.

169. Chauhan, D., Bhutta, M. A., & Barrie, J. L. (2011). Does it matter how we measure metatarsal length?. Foot and ankle surgery, 17(3), 124-127.

170. Coughlin, M. J. (1993). Second metatarsophalangeal joint instability in the athlete. Foot & ankle, 14(6), 309-319.

171. Roy, S.J.T.P. and Sportsmedicine, How I manage plantar fasciitis. 1983. 11(10): p. 127-131.

172. Alkenani, N., Alaqil, M., Murshid, A., Alharbi, M., Albahli, O., & Alghnam, S. (2017). Standardized radiological values of foot among Saudi population. Saudi Journal of Sports Medicine, 17(3), 144.

173. Maynou, C., Szymanski, C., & Thiounn, A. (2017). The adult cavus foot. EFORT open reviews, 2(5), 221-229.

174. Parekh, S. (2012). Foot and ankle surgery. JP Medical Ltd.

175. Zhou, Y., Zhou, B., Liu, J., Tan, X., Tao, X., Chen, W., & Tang, K. (2014). A prospective study of midfoot osteotomy combined with adjacent joint sparing internal fixation in treatment of rigid pes cavus deformity. Journal of orthopaedic surgery and research, 9(1), 1-5.

176. Dessouky, R., Heineman, N., Zhang, L., Hummel, J., Skweres, J., Wukich, D., & CHHSabra, A. (2018). Hallux valgus and metatarsus adductus measurements: inter-reader reliability and correlations on radiographs and MRI. Clinical Radiology, 73(12), 1057-e7.

177. Gentili, A., Masih, S., Yao, L., & Seeger, L. L. (1996). Foot axes and angles. the British Journal of radiology, 69(826), 968-974.

178. Karasick, D., & Wapner, K. L. (1990). Hallux valgus deformity: preoperative radiologic assessment. AJR Am j Roentgenol, 155(1), 119-23.

179. Shelton, T., Singh, S., Kreulen, C., & Giza, E. (2018). The influence of percentile weight bearing on foot radiographs. Foot & Ankle Orthopaedics, 3(3), 2473011418S00436.

180. Barnett, C. H. (1962). The normal orientation of the human hallux and the effect of

footwear. Journal of anatomy, 96(Pt 4), 489.

181. Gu, Y., Zhang, Y., & Shen, W. (2013). Lower extremities kinematics variety of young women jogging with different heel height. International Journal of Biomedical Engineering and Technology, 12(3), 240-251.

182. Dayton, P., Feilmeier, M., Hirschi, J., Kauwe, M., & Kauwe, J. S. (2014). Observed changes in radiographic measurements of the first ray after frontal plane rotation of the first metatarsal in a cadaveric foot model. The Journal of Foot and Ankle Surgery, 53(3), 274-278.

183. Lamm, B. M., Stasko, P. A., Gesheff, M. G., & Bhave, A. (2016). Normal foot and ankle radiographic angles, measurements, and reference points. The journal of foot and ankle surgery, 55(5), 991-998.

184. Bouaicha, S., Ehrmann, C., Moor, B. K., Maquieira, G. J., & Espinosa, N. (2010). Radiographic analysis of metatarsus primus elevatus and hallux rigidus. Foot & ankle international, 31(9), 807-814.

185. Coughlin, M. J., & Shurnas, P. S. (2003). Hallux rigidus: grading and long-term results of operative treatment. JBJS, 85(11), 2072-2088.

186. Bryant, A., Tinley, P., & Singer, K. (2000). A comparison of radiographic measurements in normal, hallux valgus, and hallux limitus feet. The Journal of foot and ankle surgery, 39(1), 39-43.

187. Saraiva, J., et al. Radiography of the lower limbвАуuseful measurements for the daily practice. in ESSR 2015 Annual Scientific Meeting. 2015.

188. Saltzman, C. L., Brandser, E. A., Berbaum, K. S., DeGnore, L., Holmes, J. R., Katcherian, D. A., ... & Alexander, I. J. (1994). Reliability of standard foot radiographic measurements. Foot & ankle international, 15(12), 661-665.

189. Hart, D. J., & Hart, T. J. (1985). Iatrogenic metatarsal coalition: a postoperative complication of adjacent V-osteotomies. The Journal of Foot Surgery, 24(3), 205-208.

190. Alonso, C. G., Curiel, M. D., Carranza, F. H., Cano, R. P., & Pérez, A. D. (2000). Femoral bone mineral density, neck-shaft angle and mean femoral neck width as predictors of hip fracture in men and women. Osteoporosis International, 11(8), 714.

191. Arunakul, M., Amendola, A., Gao, Y., Goetz, J. E., Femino, J. E., & Phisitkul, P. (2013).

Tripod index: a new radiographic parameter assessing foot alignment. Foot & ankle international, 34(10), 1411-1420.

192. Brage, M. E., Rockett, M., Vraney, R., Anderson, R., & Toledano, A. (1998). Ankle fracture classification: a comparison of reliability of three X-ray views versus two. Foot & ankle international, 19(8), 555-562.

193. Coughlin, M. J., & Kaz, A. (2009). Correlation of Harris mats, physical exam, pictures, and radiographic measurements in adult flatfoot deformity. Foot & ankle international, 30(7), 604-612.

194. Guenoun, B., Zadegan, F., Aim, F., Hannouche, D., & Nizard, R. (2012). Reliability of a new method for lower-extremity measurements based on stereoradiographic three-dimensional reconstruction. Orthopaedics & Traumatology: Surgery & Research, 98(5), 506-513.

195. Hermans, J. J., Wentink, N., Beumer, A., Hop, W. C. J., Heijboer, M. P., Moonen, A. F., & Ginai, A. Z. (2012). Correlation between radiological assessment of acute ankle fractures and syndesmotic injury on MRI. Skeletal radiology, 41(7), 787-801.

196. Jones, M. T., Sanders, A. E., DaCunha, R. J., Cody, E. A., Sofka, C. M., Nguyen, J., ... & Ellis, S. J. (2019). Assessment of various measurement methods to assess first metatarsal elevation in hallux rigidus. Foot & Ankle Orthopaedics, 4(3), 2473011419875686.

197. Lau, B. C., Allahabadi, S., Palanca, A., & Oji, D. E. (2021). Understanding Radiographic Measurements Used in Foot and Ankle Surgery. JAAOS-Journal of the American Academy of Orthopaedic Surgeons, 10-5435.

198. Chen, Y. N., Chang, C. W., Li, C. T., Chang, C. H., & Lin, C. F. (2015). Finite element analysis of plantar fascia during walking: a quasi-static simulation. Foot & ankle international, 36(1), 90-97.

199. Desouza, C., Salazar, H., Cheong, B., Murgo, J., & Fonseca, V. (2003). Association of hypoglycemia and cardiac ischemia: a study based on continuous monitoring. Diabetes care, 26(5), 1485-1489.

200. Mahowald, S., Legge, B. S., & Grady, J. F. (2011). The correlation between plantar fascia thickness and symptoms of plantar fasciitis. Journal of the American Podiatric

Medical Association, 101(5), 385-389.

201. Wearing, S. C., Smeathers, J. E., Sullivan, P. M., Yates, B., Urry, S. R., & Dubois, P. (2007). Plantar fasciitis: are pain and fascial thickness associated with arch shape and loading?. Physical therapy, 87(8), 1002-1008.

202. Luffy, L., Grosel, J., Thomas, R., & So, E. (2018). Plantar fasciitis: a review of treatments. Journal of the American Academy of PAs, 31(1), 20-24.

203. Trojian, T., & Tucker, A. K. (2019). Plantar fasciitis. American family physician, 99(12), 744-750.

204. López-López, D., Marañon-Medina, J., Losa-Iglesias, M. E., Calvo-Lobo, C., Rodríguez-Sanz, D., Palomo-López, P., & Vallejo, R. B. D. B. (2018). The influence of heel height related on quality of life on the foot in a sample of women. Revista da Associação Médica Brasileira, 64, 324-329.

205. Di Sipio, E., Piccinini, G., Pecchioli, C., Germanotta, M., Iacovelli, C., Simbolotti, C., ... & Padua, L. (2018). Walking variations in healthy women wearing high-heeled shoes: Shoe size and heel height effects. Gait & Posture, 63, 195-201.

206. Wiedemeijer, M. M., & Otten, E. (2018). Effects of HHS on gait. A review. Gait & posture, 61, 423-430.

207. Sun, D., Gu, Y., Mei, Q., Shao, Y., Sun, J., & Fernandez, J. (2017). Effect of heel heights on female postural control during standing on a dynamic support surface with sinusoidal oscillations. Journal of Motor Behavior, 49(3), 281-287.

208. Khodair, S. A. Z., & Younes, R. L. (2019). Wearing high heels and plantar fasciitis; MRI evaluation. Imaging, 8(1), 1-5.

209. Kogler, G. F., Veer, F. B., Verhulst, S. J., Solomonidis, S. E., & Paul, J. P. (2001). The effect of heel elevation on strain within the plantar aponeurosis: in vitro study. Foot & ankle international, 22(5), 433-439.

210. Marshall, P. (1988). The rehabilitation of overuse foot injuries in athletes and dancers. Clinics in Sports Medicine, 7(1), 175-191.

211. Kainz, H., Modenese, L., Lloyd, D. G., Maine, S., Walsh, H. P. J., & Carty, C. P. (2016). Joint kinematic calculation based on clinical direct kinematic versus inverse kinematic gait models. Journal of biomechanics, 49(9), 1658-1669.

212. Hwang, S. J., Choi, H. S., Choi, H. H., Kim, H. S., & Kim, Y. H. (2006). The evaluation of the lower extremity joint moments and muscle force during various high-heel walking. In Key Engineering Materials (Vol. 326, pp. 755-758). Trans Tech Publications Ltd.

213. Hedrick, M. R. (1996). The plantar aponeurosis. Foot & ankle international, 17(10), 646-649.

214. Lemmon, D., Shiang, T. Y., Hashmi, A., Ulbrecht, J. S., & Cavanagh, P. R. (1997). The effect of insoles in therapeutic footwear—a finite element approach. Journal of biomechanics, 30(6), 615-620.

215. Gu, Y., Li, J., Ren, X., Lake, M. J., & Zeng, Y. (2010). Heel skin stiffness effect on the hindfoot biomechanics during heel strike. Skin Research and Technology, 16(3), 291-296.

216. Pailler-Mattei, C., Bec, S., & Zahouani, H. (2008). In vivo measurements of the elastic mechanical properties of human skin by indentation tests. Medical engineering & physics, 30(5), 599-606.

217. Siegler, S., Block, J., & Schneck, C. D. (1988). The mechanical characteristics of the collateral ligaments of the human ankle joint. Foot & ankle, 8(5), 234-242.

218. Yu, J., Cheung, J. T. M., Wong, D. W. C., Cong, Y., & Zhang, M. (2013). Biomechanical simulation of high-heeled shoe donning and walking. Journal of biomechanics, 46(12), 2067-2074.

219. Taylor, R. (1990). Interpretation of the correlation coefficient: a basic review. Journal of diagnostic medical sonography, 6(1), 35-39.

220. Son, J., Choi, H., & Kim, Y. (2008, May). Analysis of Changes in Muscle Length of Lower Limbs during High-heeled Walking Based on the Musculoskeletal Model. In 2008 International Conference on BioMedical Engineering and Informatics (Vol. 2, pp. 809-812). IEEE.

221. Lieber, R. L., & Fridén, J. (2000). Functional and clinical significance of skeletal muscle architecture. Muscle & Nerve: Official Journal of the American Association of Electrodiagnostic Medicine, 23(11), 1647-1666.

222. Narici, M. (1999). Human skeletal muscle architecture studied in vivo by non-invasive

imaging techniques: functional significance and applications. Journal of Electromyography and Kinesiology, 9(2), 97-103.

223. Zajac, F. E. (1989). Muscle and tendon: properties, models, scaling, and application to biomechanics and motor control. Critical reviews in biomedical engineering, 17(4), 359-411. 224. Ito, M., Kawakami, Y., Ichinose, Y., Fukashiro, S., & Fukunaga, T. (1998). Nonisometric behavior of fascicles during isometric contractions of a human muscle. Journal of applied physiology.

225. Herzog, W., Guimaraes, A. C., Anton, M. G., & Carter-Erdman, K. A. (1991). Moment-length relations of rectus femoris muscles of speed skaters/cyclists and runners. Medicine and Science in Sports and Exercise, 23(11), 1289-1296.

226. Peng, Y., Wong, D. W. C., Wang, Y., Chen, T. L. W., Zhang, G., Yan, F., & Zhang, M. (2021). Computational models of flatfoot with three-dimensional fascia and bulk soft tissue interaction for orthosis design. Medicine in Novel Technology and Devices, 9, 100050.

227. Alexander, I. J., Chao, E. Y., & Johnson, K. A. (1990). The assessment of dynamic foot-to-ground contact forces and plantar pressure distribution: a review of the evolution of current techniques and clinical applications. Foot & ankle, 11(3), 152-167.

228. Chevalier, T. L., Hodgins, H., & Chockalingam, N. (2010). Plantar pressure measurements using an in-shoe system and a pressure platform: A comparison. Gait & posture, 31(3), 397-399.

229. Mika, A., Oleksy, L. U. K. A. S. Z., Mikołajczyk, E., Marchewka, A., & Mika, P. (2011). Changes of bioelectrical activity in cervical paraspinal muscle during gait in low and high heel shoes. Acta Bioeng Biomech, 13(1), 27-33.

230. Erdemir, A., Hamel, A. J., Fauth, A. R., Piazza, S. J., & Sharkey, N. A. (2004). Dynamic loading of the plantar aponeurosis in walking. JBJS, 86(3), 546-552.

ABBREVATION

1D: one-dimensional

1MD: first metatarsal declination

2D: two-dimensional

3D: three dimensional

APMA: American Podiatric Medical Association

AT: tibial anterior

BF: barefoot

BW: body weight

C1M: calcaneal-1st metatarsal

CMC: computed muscle control

COM: center of mass

COP: center of pressure

COP: center of pressure

CT: computed tomography

COP: center of pressure

DOF: degrees of freedom

EDL: extensor digitorum longus

EHL: extensor hallucis longus

EMG: Electromyography

EW: experience wearers

FEM: finite element model

FIM: First intermetatarsal

GC: gastrocnemius

GRF: ground reaction force

HHS: high heel shoes

HV: hallux valgus

IEW: inexperience wearers

IK: inverse kinematics

MB: metatarsal break

MPJ: metatarsophalangeal joint

MSM: musculoskeletal modeling

MRI: magnetic resonance imaging

OA: osteoarthritis

OFM: Oxford foot model

PT: peroneus tertius

RACA: Posterior calcaneus proximal

RASI: Anterior Superior illiac Spine

RCPG: Posterior end of the calcaneus

RD1M: 1st metatarsal distal medial

RD5M :5st metatarsal, distal lateral

RHEE: Heel

RHFB: Later head of fibula

RHLX: Hallux

RKNE: Standard lateral knee

RLCA: Lateral calcaneus

RMMA: Medial Malleoli

ROM: range of motion

RP1M: 1st metatarsal proximal dorsal

RP5M: 5st metatarsal, proximal lateral

RPSI: Posterior Superior iliac Spine

RRA: residual reduction algorithm

RSHN: Anterior aspect of the skin

RSTL: Sustaniculum tail

RTIB: Tibia marker

RTUB: Tibia tuberosity;

RTOE: Toe

SACR: Posterior Superior iliac Spine

SL: soleus

STL: Stereolithography

TCJ: talocalcaneal joint

TJ: tibiotalar joint

TFM: talus-first metatarsal

TTJ: transverse tarsal joint

V3D: Visual 3D

LIST OF TABLES

LIST OF FUGURES

110

linear truss element of Achilles tendon, ligament and muscle.

Fig 4.6. HHS model in three different heel height.

Fig 4.7. Stress-strain curve for bulk soft tissue.

Fig 4.8. loading and boundary condition of the foot on the high heel sole (present in 3cm heel height).

Fig 4.9. Muscle activation between estimate and EMG signals during HHS gait in different heel height; (a) shows 3cm heel height gait; (b) shows the 5cm heel height gait; (c) shows the 7cm heel height gait. Fig 4.10. (a) the different stance phase of HHS gait, (b) FEM predicted, (c) plantar contact pressure in experimental measurement.

Fig 4.11. The peak 3D fascia strain for three heel heights in three gait events, (b) First-peak phase, (c) mid-standing phase, (d) second-peak phase.

Fig 5.1. The strain variation on the plantar fascia under HHS in three gait phases.